THE SURFACE IMPEDANCE OF METALS AT 24,000 MC/SEC

W. B. NOWAK

TECHNICAL REPORT NO. 97

MAY 27, 1949

RESEARCH LABORATORY OF ELECTRONICS
MASSACHUSETTS INSTITUTE OF TECHNOLOGY

The research reported in this document was made possible through support extended the Massachusetts Institute of Technology, Research Laboratory of Electronics, jointly by the Army Signal Corps, the Navy Department (Office of Naval Research) and the Air Force (Air Materiel Command), under Signal Corps Contract No. W36-039-sc-32037, Project No. 102B; Department of the Army Project No. 3-99-10-022.

MASSACHUSETTS INSTITUTE OF TECHNOLOGY
Research Laboratory of Electronics

Technical Report No. 97 May 27, 1949

THE SURFACE IMPEDANCE OF METALS AT 24,000 MC/SEC*

W. B. Nowak

Abstract

The surface conductivity of copper, silver, tin and lead at 24,000 Mc/sec has been measured as a function of temperature over the interval 300°K to 4°K by means of resonant cavity techniques. Only the normal (non-superconducting) state has been investigated. The influence of surface roughness on the impedance has been determined qualitatively for copper. It is shown that this influence becomes greater at low temperatures than at room temperatures. No essential disagreement with the Reuter and Sondheimer theory of the surface impedance is found that is not explicable by surface roughness. The frequency dependence predicted by the theory is verified in the case of tin (the smoothest surface obtained) by comparison with results of Simon at 9000 Mc/sec.

A brief summary of the Reuter and Sondheimer theory is given, with emphasis on the assumptions involved and conclusions reached. Values of n, the number of free electrons per atom, are estimated from the data using the theory, and are found to be low compared to values deduced from other types of measurements, but comparable or higher than any previously reported values for this type of measurement.

A brief account is given of Morgan's theory of the influence of surface roughness on surface losses, and an approximate "correction" to the data is applied on the basis of this theory with some additional assumptions. This raises the computed values of n.

Some discussion is given of the measurement techniques, and the surface preparation.

It is concluded that the microwave method for determining n, at least at 24,000 Mc/sec, is not the most advantageous because of the small skin depth (large influence of surface roughness), and because of the sensitivity of n to the measured impedance, i.e., impedance to the 4.5 power.

---

* This report is identical with a thesis of the same title submitted by the author in partial fulfillment of the requirements for the degree of Doctor of Science in Electrical Engineering at the Massachusetts Institute of Technology.

ERRATA

Page 7: Omit "π" in numerator of second term in Eq.(12).

Page 13, line 12:

$$C_1 = 2.682 \times 10^{-9}$$

Page 32, line 2:

Replace the word "identical" with the word "mirror-image".

Page 47, line 4:

Replace the word "acetone" with the words "carbon tetrachloride".

I. INTRODUCTION

Since November 1945, the Research Laboratory of Electronics at M.I.T. has had a group working in the field of low-temperature physics. Part of the program of this group has been the study of the electrical conductivity of metals at high frequencies. Garrison (1) and Maxwell (2) have investigated lead and tin, respectively, at 24,000 Mc/sec in both the normal and the superconducting states. They obtained the result, in agreement with London (3) and Pippard (4), that the r-f losses at low temperatures (approximately 20°K) were larger than was to be expected from the d-c conductivity, and that these losses reached an asymptotic value (for the normal state) independent of the d-c conductivity change with temperature.

Pippard (4) has used a frequency of about 1200 Mc/sec and has investigated silver, gold, tin, mercury, copper and aluminum, all of which exhibit the anomalous behaviour.

Recently, Reuter and Sondheimer (5) have published a theory of this anomalous effect, based on the free-electron model. Points of interest in the theory are the frequency dependence of the asymptotic r-f conductivity and the number of free electrons per atom, which can be obtained by matching experiment to theory.

During the war, it was often noted that even at room temperatures, where classical theory applies, the attenuation in microwave cavities and wave guides was considerably higher than expected from the d-c conductivity. In particular, the variation of attenuation at 24,000 Mc/sec with machining, or other surface

fabrication, was reported by Maxwell (6). This extra loss has been attributed to the surface roughness, which is comparable to the r-f skin depth (in copper, about 17 microinches or 4250 angstroms). Since the skin depth decreases with decreasing temperature, it is to be expected that this roughness will become more important at low temperatures. Such proves to be the case. Morgan (7) has calculated the extra losses due to various types of roughness as a function of the ratio of rms roughness to skin depth at room temperatures. This theory may be applied as an approximate correction in the cases where smooth surfaces were not obtainable.

The purposes of the present research were:

a. to determine the surface impedance of several metals as a function of temperature from 300°K to 4.2°K at 24,000 Mc/sec;

b. to ascertain the role played by surface roughness on the surface impedance;

c. to check the Reuter and Sondheimer theory; and, if the theory is valid,

d. to obtain n, the number of free electrons per atom.

The number of free electrons per atom is necessary in computing the penetration depths of metals in the superconducting state (2). The values of n can be compared with those derivable from other measurements, such as the Hall effect, the specific heat at low temperature, and optical dispersion.

The first part of this report is a summary of the classical and the Reuter and Sondheimer theories, and outlines the assumptions and results of these theories. The remainder of the report is devoted to a discussion of experimental techniques and results.

II. THEORY

2.1 Classical and Anomalous Surface Impedance

In this section, a brief review is given of the assumptions and results of the theory of the skin effect in metals. Both classical theory and its extension by Reuter and Sondheimer are treated.*

The theory of the behaviour of electromagnetic radiation in metals is developed as follows:

a. Maxwell's equations, plus the supplementary relations $D = \epsilon E$ and $B = \mu H$, are assumed, where ϵ and μ are assumed equal to ϵ_o and μ_o, respectively. Only non-magnetic metals are considered here.

b. The form of the electromagnetic wave, i.e., TEM, TE, TM, or a mixture, is decided, and the coordinate system appropriate to the problem is set up.

c. Some functional relationship is derived or assumed between the current density J and the electric field E, introducing parameters characteristic of the metal, viz., the conductivity σ, and the relaxation time .

d. Maxwell's equations are solved for E and H.

e. Boundary conditions are imposed.

The functional relationship between J and E is the crucial point wherein the classical theory fails to depict adequately the high-frequency behaviour of metals at low temperatures. The classical theory rests upon the Ohm's law conductivity equation $J = \sigma E$, where σ could be complex. This simple proportionality states that the current at any point in the metal is determined by the value of the electric field <u>at that point</u>. This is true if the electric

* Gaussian units are used in this section

field is constant over the mean free path of an electron, which condition is met either with a constant field or with a mean free path approaching zero as a limit. When the mean free path is long and the field varies along the mean free path, the current is a more complicated function of the field, i.e., $J = f(E,x,y,z)$. Not only is the average velocity gained by the electron altered, but the current at any point is the sum of contributions from electrons that have come from other regions where the field has a value different from that at the point in question.

The assumption of $J = \sigma E$ leads to a solution in the metal for a simple harmonic electric field which is exponentially damped in the propagation direction. When the mean free path is short compared to this penetration depth, Ohm's law is valid, and the solution is a consistent one. At high enough temperatures, this condition is met at all frequencies. At any temperature, if the frequency is high enough, the distance travelled by an electron during one cycle of the field is small compared with the penetration depth, and thus, regardless of the mean free path, the field may be thought of as spatially constant, and classical theory obtains. The intermediate cases are those not describable by the relation $J = \sigma E$.

The fields E and H need not be found explicitly. It is necessary only to compute the surface impedance Z of the metal, since it can be related to all measurable quantities. Below are listed a few definitions and relations showing the connection between Z in the different systems of units and the complex index of refraction, n. The index n has physical meaning only in the classical theory where the fields are exponentially damped in the metal. Of course,

n must be independent of units, since it is a pure number.

$$n = \frac{\gamma}{\gamma_o} = \frac{\text{complex propagation constant of metal}}{\text{propagation constant of free space}} \quad . \qquad (1)$$

$$E = E_o\, e^{-\gamma x} \quad , \qquad E' = -\gamma E \quad . \qquad (2)$$

$$\gamma_o = \frac{2\pi j}{\lambda_o} = \frac{j\omega}{c} \quad .$$

$$n = \frac{\gamma c}{j\omega} \quad . \qquad (3)$$

$$Z = \frac{E(0)}{H(0)} = -\frac{j\mu\omega E(0)}{E'(0)} = \frac{j\mu\omega}{\gamma} = \frac{\mu c}{n} \qquad \text{(MKS)}, \qquad (4)$$

$$Z = -\frac{j\omega E(0)}{c\, E'(0)} = \frac{j\omega}{c\gamma} = \frac{1}{n} \qquad \text{(Gaussian)} \quad , \qquad (5)$$

$$Z = \frac{4\pi E(0)}{cH(0)} = \frac{4\pi j\omega}{c^2\gamma} = \frac{4\pi}{cn} \qquad \text{(Reuter and Sondheimer).} \qquad (6)$$

Reuter and Sondheimer have obtained a general solution for the current density J in terms of a definite integral over the entire electric field in the metal. They have solved the integro-differential equation obtained by combining this with Maxwell's equations.

The following assumptions have been made in obtaining the expression for J:

a. The electric field is propagated normal to the surface of the metal.

b. The metal is semi-infinite in extent and has a plane surface. The linear dimensions of the specimen are large compared to the field penetration depth.

c. The electrons are quasi-free. That is, the energy is proportional to the square of the momentum; the effective mass of the electron in the metal need not be equal to the electronic rest mass. This implies no dependence of the equilibrium distribution function on direction.

d. A mean free path ℓ (or a relaxation time τ) may always be ascribed to the collision process. This mean free path is that computed from the d-c conductivity. A relaxation time is really justifiable only at very high and very low

temperatures, where an electron at each collision, loses an amount of energy that is small compared to kT.

e. A fraction p of the electrons arriving at the surface are scattered specularly, while the remainder (1 - p) are diffusely scattered. The fraction p is assumed independent of the direction of motion of the electron.

Assumption (d) is necessary in order to transform the Boltzmann transport equation, into a differential equation. This relaxation time relates the rate of change of the electronic distribution function to its departure from the equilibrium distribution, i.e., $df/dt = -(f-f_o)/\tau$.

The surface of the metal is in the xy plane, and the positive z direction is towards the interior of the metal. The fields are

$$E = E_x(z)\ e^{j\omega t} \quad , \tag{7a}$$

$$H = H_y(z)\ e^{j\omega t} \quad . \tag{7b}$$

Maxwell's equations are then

$$-\frac{dH}{dz} = \frac{j\omega}{c} E + \frac{4\pi}{c} J \quad , \tag{8}$$

$$\frac{dE}{dz} = -\frac{j\omega}{c} H \quad . \tag{9}$$

Eliminating H, the relation between E and J is

$$\frac{d^2E}{dz^2} + \frac{\omega^2}{c^2} E = \frac{4\pi j\omega}{c^2} J \quad . \tag{10}$$

The procedure is to apply the Boltzmann equation to the distribution function, f, of the electrons,

$$f = f_o + f_1(\underline{v},z) \quad , \tag{11}$$

where

$$f_o = \frac{1}{e^{\left[\frac{E - \zeta}{kT}\right]} + 1}$$

and f_1 is to be determined. f is a function of the velocity-vector $\underline{v}$ and the space-vector $\underline{r}$. τ depends only on $|v|$. The Boltzmann equation is

$$\frac{\partial f}{\partial t} - \frac{\pi e}{m}\left[\underline{E} + \frac{\underline{v} \times \underline{H}}{c}\right] \cdot \operatorname{grad}_v f + \underline{v} \cdot \operatorname{grad}_r f = -\frac{(f - f_o)}{\tau} \quad . \tag{12}$$

Putting Eq. (11) into (12), neglecting the products of E with f_1, and remembering that f_o is independent of direction, one finds that the linear terms in H cancel and f_1 satisfies the relation

$$\frac{\partial f_1}{\partial z} + \frac{1 + j\omega\tau}{\tau v_z} f_1 = \frac{e}{m v_z} \frac{\partial f_o}{\partial v_x} E(z) \quad . \tag{13}$$

The solution of this equation is, for $v_z < 0$

$$f_1^{(1)} = -\frac{e}{m v_z} \frac{\partial f_o}{\partial v_x} e^{-\frac{(1 + j\omega\tau)z}{\tau v_z}} \int_z^{\infty} E(t) e^{\frac{(1 + j\omega\tau)t}{\tau v_z}} dt, \tag{14a}$$

and for $v_z > 0$

$$f_1^{(2)} = \frac{e}{m v_z} \frac{\partial f_o}{\partial v_x} e^{-\frac{(1 + j\omega\tau)z}{\tau v_z}} \left[p \int_{-\infty}^{z} E(t) e^{\frac{(1 + j\omega\tau)t}{\tau v_z}} dt + (1 - p) \int_o^z E(t) e^{\frac{(1 + j\omega\tau)t}{\tau v_z}} dt \right] . \tag{14b}$$

The current density is then found from the generalized expression

for $J = nev$

$$J(z) = -\,2e\left(\frac{m}{h}\right)^3 \iiint v_x f \, dv_x \, dv_y \, dv_z \quad . \tag{15}$$

The general relation between J and E replacing Ohm's law is given by Reuter and Sondheimer as

$$J(z) = \frac{2\pi e^2 m^2 \bar{v}^2}{h^3}\left[p\int_{-\infty}^{\infty} k_a\left(\frac{z-t}{\ell}\right)E(t)\,dt + (1-p)\int_{0}^{\infty} k_a\left(\frac{z-t}{\ell}\right)E(t)\,dt\right] , \tag{16}$$

where $a = \omega\tau$, $\ell = \bar{v}\tau$ ($\bar{v}$ corresponds to the top of the Fermi band), and

$$k_a(u) = Ei_1\left[(1+ja)\,|u|\right] - Ei_3\left[(1+ja)\,|u|\right] ,$$

$$Ei_n(u) = \int_1^{\infty} \frac{e^{-su}}{s^n}\,ds \qquad (\mathcal{R}u > 0) \quad .$$

Combining (10) and (16), the general expression for the field E is

$$\frac{d^2E}{dz^2} + \frac{\omega^2}{c^2}E = \frac{8\pi^2 j\omega e^2 m^2 \bar{v}^2}{c^2 h^3}\left[p\int_{-\infty}^{\infty} k_a\left(\frac{z-t}{\ell}\right)E(t)\,dt + (1-p)\int_{0}^{\infty} k_a\left(\frac{z-t}{\ell}\right)E(t)\,dt\right] . \tag{17}$$

It is convenient to introduce the dimensionless parameter α ,

$$\alpha = \frac{8\pi^2\omega e^2 m^2 \bar{v}^2 \ell^3}{c^2 h^3} = \frac{3}{2}\left(\frac{\ell}{\delta}\right)^2 , \tag{18}$$

where $\delta = c/\sqrt{2\pi\omega\sigma}$ is the classical skin depth, and use is made of the expressions

$$n = \frac{8\pi}{3}\left(\frac{mv}{h}\right)^3 , \qquad \sigma = \frac{ne^2\ell}{m\bar{v}} \quad .$$

The importance of α will appear subsequently.

Reuter and Sondheimer have not evaluated the electric field in detail, since it is not needed to calculate the surface impedance. They have, however, considered the simplest case of $p = 1$ and $\omega\tau \ll 1$ in order to see the general behaviour. They have expressed the field as the sum of two terms. The first term is the classical exponential decay with depth of penetration, while the second term is very complicated, and has been given in asymptotic form, being

$$\frac{2j\alpha}{(1-2j\alpha)^2}\ \frac{e^{-x}}{x^2} \qquad \text{as } x \to \infty \quad .$$

The first term is predominant when $\alpha < \alpha_o$, while the second term (which never approximates a true exponential wave) predominates when $\alpha > \alpha_o$, where $\alpha_o = 2.63$. α_o occurs as the result of a characteristic equation $s^2 - j\alpha K(s) = 0$ possessing roots or not in certain regions depending upon whether $\alpha > \alpha_o$ or $\alpha < \alpha_o$. The interpretation of this is that the field in the metal is describable classically until the skin depth δ is approximately equal to the mean free path ℓ . When $\ell > \delta$, the field is no longer exponential, and may perhaps be thought of as decaying rapidly near the surface, and then diminishing at a slower rate, behaving as e^{-x}/x^2 for distances large compared to ℓ .

The classical formula for the field may be obtained from (17) by regarding E as a constant. Perhaps an easier method is to note that the first term in (13) is neglected in the classical treatment. When the resultant expression for f_1 is put into Eq. (14), the relation between current and field is found to be

$$J = \frac{\sigma E}{1 + j\omega\tau} \quad . \tag{19}$$

Inserting (19) into (10), and neglecting the displacement current term ω^2/c^2, the electric field is

$$E(z) = E(0)\, e^{-\frac{z}{\delta\sqrt{1 + j\omega\tau}}(1+j)} \quad . \tag{20}$$

It will be noted that for high frequencies, i.e., $\omega\tau \gg 1$, the penetration depth becomes $\delta\sqrt{\omega\tau}$.

The surface impedance integrals have been evaluated to give explicit formulae for Z in the two limits of classical ($\alpha \to 0$) and extreme non-classical ($\alpha \to \infty$) behaviour, in the two cases of $p = 0$ and $p = 1$. In these expressions, the parameter ξ arises.

$$\xi = \frac{j\alpha}{(1 + j\omega\tau)^3} \quad . \tag{21}$$

When $|\xi| \ll 1$, the behaviour is classical, and when $|\xi| \gg 1$, the behaviour is extremely non-classical.

For $|\xi| \ll 1$, $\ell/\delta \ll (1+\omega^2\tau^2)^{3/4}$. This occurs when $\ell \ll \delta$ if $\omega\tau \ll 1$ (low frequencies) and $|v|/\omega \ll \delta\sqrt{\omega\tau}$ if $\omega\tau \gg 1$ (high frequencies). This agrees with the previous statements that classical theory is valid only when the mean free path or the distance an electron traverses in one cycle of the field is small compared to the penetration depth. The displacement-current term $\omega^2 \ell^2/c^2(1 + j\omega\tau)^2$ occurring in the integrals for Z is negligible except when $|\xi| \ll 1$. Thus displacement current is only appreciable at high frequencies where the behaviour is classical, and this term is omitted in the evaluation of the integrals for the non-classical case.

For $|\xi| \gg 1$, the asymptotic expressions for Z turn out to be independent of τ , although derived without restriction, and are

identical with expressions obtained by neglecting $\omega\tau$ compared with unity. Other interesting features of these asymptotic expressions are, that they vary as $\omega^{2/3}$ (while the classical impedance varies as $\omega^{1/2}$), that the value of Z for p = 0 is 9/8 of the value for p = 1, and that the reactance is $\sqrt{3}$ times the resistance (whereas, classically, the reactance equals the resistance).

For convenience, the various impedance formulae in the limiting cases are listed below. Another parameter, A, has been defined so that, at a constant frequency, Z is a function of α only.

$$A = \sqrt{6}\left(\frac{\pi\omega}{ec^2}\right)^{2/3}\left(\frac{m\bar{v}}{3n}\right)^{1/3} . \qquad (22)$$

Classical: p = 0 and p = 1,

$$Z_{cl} = R_{cl} + jX_{cl} = \frac{4\pi\omega\ell}{c^2}\left[\frac{\omega^2\ell^2}{c^2} - \frac{4}{3}\frac{j\alpha}{(1 + j\omega\tau)}\right]^{-1/2} . \qquad (23)$$

For $\omega\tau \ll 1$ and $\omega^2\ell^2/c^2 \ll \alpha$ (at 300°K, wavelengths $\gg 10^{-2}$cm; at 4°K, wavelengths > 10 cm) :

$$R_{cl} = X_{cl} = \frac{\pi\omega\ell}{c^2}\sqrt{\left(\frac{6}{\alpha}\right)} = \sqrt{\frac{2\pi\omega}{c^2\sigma}} , \qquad (24a)$$

or

$$Z_{cl} = A\alpha^{-1/6}(1 + j) , \qquad (24b)$$

$$\frac{A}{R} = \frac{A}{X} = \alpha^{1/6} .$$

For $\omega\tau \sim 1$, and $\omega^2\ell^2/c^2 \ll \alpha$:

$$R_{cl} = \sqrt{\frac{2\pi\omega}{c^2\sigma}}\left[\sqrt{1 + \omega^2\tau^2} - \omega\tau\right]^{1/2} , \qquad (25a)$$

$$X_{cl} = \sqrt{\frac{2\pi\omega}{c^2\sigma}} \left[\sqrt{1 + \omega^2\tau^2} + \omega\tau\right]^{1/2} \quad . \qquad (25b)$$

For $\omega\tau \gg 1$, and $\omega^2 \ell^2/c^2 \ll \alpha$:

$$R_{cl} = \sqrt{\frac{\pi}{c^2\tau\sigma}} \quad , \qquad (26a)$$

$$X_{cl} = 2\pi\tau\sqrt{\frac{\pi}{c^2\tau\sigma}} \quad . \qquad (26b)$$

For $\omega\tau \gg 1$, and $\omega^2 \ell^2/c^2 > \alpha$ $(\omega^2 > 4\pi\sigma/\tau)$ the dielectric constant becomes zero and the metal becomes transparent. At very high frequencies, R goes to $4\pi/c$ and X goes to zero.

Extreme non-classical:

$$Z_\infty = \frac{4\sqrt{2}}{9(\pi)^{1/3}} A(1 + j\sqrt{3}) \qquad (27a)$$

$$(p = 1) \quad .$$

$$\frac{A}{R}_\infty = 2.330 \quad , \frac{A}{X}_\infty = 1.345 \qquad (27b)$$

$$Z_\infty = \frac{A}{2\pi^{1/3}} (1 + j\sqrt{3}) \qquad (28a)$$

$$(p = 0) \quad .$$

$$\frac{A}{R}_\infty = 2.071 \quad , \frac{A}{X}_\infty = 1.196 \qquad (28b)$$

It has been mentioned above that the asymptotic non-classical values of Z are rigorously independent of $\omega\tau$. At room temperatures, where classical behaviour is valid, $\omega\tau$ is negligible for wavelengths greater than about 1 mm. Reuter and Sondheimer have therefore omitted terms in $\omega\tau$ compared to unity in their numerical integration for Z. They have tabulated values of $E(0)/E'(0)$ for $p = 1$ and $p = 0$ for nine values of α. The results of this theory

and these computations are expressed in Figure 1, which plots A/R and A/X *versus* $\alpha^{1/6}$. The classical theory is a 45° line. One may show that

$$\alpha^{1/6} = c_2 n^{-2/9} \sigma^{1/2} \quad ,$$

and

$$A = c_1 n^{-2/9} \quad ,$$

where the constants are given by

$$c_2 = \left(\frac{3}{2}\right)^{1/6} \left(\frac{3}{8\pi}\right)^{1/9} \frac{h^{1/3}}{e^{2/3}} \left(\frac{2\pi\omega}{c^2}\right)^{1/6} \quad ,$$

$$c_1 = 6 \left(\frac{\pi\omega}{ec^2}\right)^{2/3} 3^{-2/9} \left(\frac{1}{8\pi}\right)^{1/9} h^{1/3} \quad .$$

For 24,000 Mc/sec, these constants are, in Gaussian units,

$$c_2 = 8.255 \times 10^{-5} \quad ,$$

$$c_2 = 2.682 \times 10^{-9} \quad .$$

Reuter and Sondheimer have investigated the restriction that the field is incident normally upon the metal, and have found that the results for Z hold unchanged for oblique incidence. The new terms introduced in the integral for $E(0)/E'(0)$ because of the oblique incidence are negligible in the region of anomalous behaviour.

2.2 Surface Roughness

Even at room temperature, the surface impedance of a cavity

resonating at 24,000 Mc/sec is greater than would be expected from the d-c conductivity. This increase is attributed to the roughness of the surface. When special precautions are taken to insure an order of surface roughness smaller than that of the penetration depth, the losses may be brought to those predicted from d-c measurements. Inasmuch as the behaviour is classical, with the mean free path much smaller than the skin depth, the effect of the roughness will be to invalidate the solutions for the field and the current based on plane-surface boundary conditions, and to require new solutions of Maxwell's equations, taking explicit account of an hypothesized surface configuration. In the low-temperature limit, where the mean free path is long compared to the skin depth, an additional complication is present. Not only must Maxwell's equations be solved for the rough contours, but the assumption of Ohm's law must be discarded. This latter case has not as yet been analyzed.

Morgan (7) has evaluated, by numerical methods, the effect on surface losses (in the classical case) of several types of roughness for various values of the ratio of root-mean-square roughness to skin depth. Two cases are at once evident: (a) current flow transverse to the grooves, and (b) current flow parallel to the grooves. These two cases are both treated two-dimensionally, i.e., the grooves are infinitely long and parallel. The overall curvature of the metal surface is assumed to be small compared to the reciprocal of the groove width, d.

For the transverse case, the magnetic field is impressed along the grooves, and it is assumed that the field outside the metal is

the same as it would be if the conductivity were infinite. Since the grooves are small compared to the free-space wavelength, the field is assumed constant over the surface. Morgan has examined the problem for square, rectangular, and equilateral-triangular grooves, all of the same period, d. The dimensions of these were chosen so that the total surface area is the same for each and is twice that of a plane surface.

Subject to these various boundaries, Maxwell's equation $\nabla^2 \underline{H} = j\omega\mu\sigma \underline{H}$ (MKS) is solved by a "relaxation" method. Once the field has been found, the power loss per unit volume in the metal is evaluated. The usual formula for the losses which involves the integral of the tangential H over the surface is not applicable here because the field in the metal is not a simple damped exponential.

Figures 2 and 3 are reproduced from Morgan's report, and plot P/P_0 versus Δ/δ, where Δ is the rms deviation from the mean value of the roughness. It is evident that the curves are approaching $P/P_0 = 2.00$ as Δ/δ increases. This must be so, since, for small penetration depths, the roughness merely adds extra surface area.

For the case of current flow parallel to the grooves, the problem is much more difficult. The only case Morgan has examined explicitly is the one of square grooves which are large compared to the skin depth. Results of his calculation show that the limit of P/P_0 is 1.360 as compared to 2.00 for the transverse case.

The exact character of the roughness of the surfaces employed in the measurements to be described here is not known. An order-of-magnitude correction will be applied, using curve III, Figure 3.

This correction will also be applied (at low temperatures), ignoring the possible effects of mean-free-path limitation at the extra boundaries, in order to obtain estimates of the surface impedance and of the number of free electrons per atom. Details of this correction are discussed in a later section.

III. EXPERIMENTAL TECHNIQUES

3.1 General

Garrison and Maxwell have described many of the experimental techniques useful in the pursuit of low-temperature research at 24,000 Mc/sec. Inasmuch as the surface impedance of metals has become substantially constant by 4.2°K (in most cases by 20°K), no efforts were made, except in the one instance of lead, to go below the liquid-helium point and, indeed, in a few runs, only 7°K was reached because of cryostat difficulties. In the present work, emphasis was placed on obtaining more accurate data over the temperature interval 300°K to 4.2°K and on greater care in the surface treatment of the specimen.

In general, only two electrical parameters are measurable: impedance and frequency. The real part of the impedance is related to the losses in the system, while the imaginary part is related to the electrical energy stored in the system per cycle. The frequency may be related to the dimensions of the specimen, if a resonant structure is used, and perturbations of the frequency are related to the imaginary part of the impedance. In actual practise, the specimen is in the form of a resonant structure, so that the measured impedance is mostly that due to the specimen rather than that due to the connecting transmission lines.

It can be readily shown from Eq. III.59 of Reference (11) that

$$\frac{1}{Q_o} + 2j\,\frac{\omega_a - \omega_o}{\omega_a} = \frac{2}{\omega_a \mu_o G}\,(R + jX) = \frac{2R}{\omega_a \mu_o G} + j\,\frac{X}{Q_o R}\quad , \qquad (30)$$

where Q_o = unloaded Q of the resonant structure , ω_a = unperturbed resonant frequency, ω_o = perturbed resonant frequency, R + jX = impedance of the structure, G = a constant depending on the geometry of the structure, and $Q_o = \omega_o \mu_o G/2R$.

The real part of the impedance is obtained by evaluating the unloaded Q of a cavity from measurements of the loaded Q, and of the voltage-standing wave ratio (VSWR), β_o, on resonance. Discussions of these and related quantities may be found in References (1), (2), (6) and (11).

For the present investigation, the imaginary part of the impedance is not useful. The change in the reactive part of the impedance as a function of temperature must be separated from the effects of thermal expansion, since both produce a change in the measured resonant frequency. The thermal-expansion shift is about 100 Mc/sec over the interval of 300°, while the reactive shift is only about 5 Mc/sec. Therefore, the thermal expansion would have to be known more accurately than it is at present in order to make the correction which is necessary to detect the reactive shift. Thermal contraction virtually ceases at 15°K, insofar as the resolution and frequency stability of the microwave equipment is concerned, so that it is possible to measure reactance shifts below this temperature, i.e., in the superconducting state. However, in the normal state, the reactance as well as the resistance reach asymptotic values at about 20°K. Therefore, only the losses in the cavity, and R and Q_o, are useful.

The procedure used here is to measure the loaded Q, Q_L, of the cavity at one or two fixed-temperature points, and to measure the

relative unloaded Q, $(Q_o)_{300}/(Q_o)_T$, at all other temperatures by observing the power-reflection coefficient on resonance, r_o^2 . The cavities are of the reflection type, i.e., only one coupling window. Pertinent relations among the quantities are

$$\beta_o = \frac{1 + r_o}{1 - r_o} \quad , \tag{31}$$

$$\beta_o = \frac{Q_w}{Q_o} \text{ (undercoupled)}, \quad \beta_o = \frac{Q_o}{Q_w} \text{ (overcoupled)} \ , \tag{32}$$

$$\frac{1}{Q_L} = \frac{1}{Q_w} + \frac{1}{Q_o} \quad , \tag{33}$$

where Q_w = Q of coupling window (and was checked over the temperature range to be constant to within about one per cent). The cavities employed were always undercoupled, so that the phase of the reflected wave was the same on and off resonance. This minimizes errors in connection with the unbalanced impedance bridge used in this work.

3.2 Cryogenics

Following the practise in this Laboratory at the onset of this research, the experiments were performed with the cavity inside the Collins cryostat (13), rather than in another set of Dewars into which helium is transferred from the Collins machine. Disadvantages of this procedure are:

a. vibration of the machine while running makes measurements very difficult, and

b. the heat leak of the waveguides into the cryostat slows down the operation of the machine.

Advantages are:

a. a larger experimental volume is available than in the usual glass Dewars, i.e., a 4-inch diameter cylinder, 4 inches long, and

b. temperatures of 6° or 7° K may be obtained even though the machine may not be capable of liquefying any helium for transfer purposes because of temporary difficulties, i.e., frozen Joule-Thompson valve, excessive engine friction, vacuum leaks, etc.

Measurements were not taken while the temperature was falling because, even with no precooling, the rate of temperature fall was too fast for the cavity to follow over the range 80° to 20° K. If precooling was used, the machine reached 80° from room temperature in about 20 minutes. Temperature differences as large as 10° were recorded when the rate of cooling was about three degrees per minute. More time was saved by using precooling, and by taking the data as the cryostat warmed up. It should be remembered that in the Collins cryostat, the experimental chamber is filled with helium at about an atmosphere pressure, and that the cavity is therefore in fairly good thermal contact with the inner Dewar wall. The diffusion pump on the cryostat Dewar was shut off simultaneously with the machine to enable the temperature to rise faster. The deterioration of the vacuum between the Dewar walls permitted a small amount of air and/or helium to enter. Under these conditions, the temperature rises at a rate of 1.0° to 0.5°K/minute from 4.2° to 20°. The rate is about 0.3° to 0.2°K/minute from 20° to 60°. After 60°K, helium from a pressure tank is fed judiciously into the Dewar wall space. Either a constant rate of 0.5°/minute may be maintained, or, if fewer points are desired, a large sudden rise followed by a short wait for equilibrium will boost the average rate. Some sporadic attempts were made to put heaters inside the cryostat. These did

not work out so well or so conveniently as the exchange-gas method, because the low temperature reduced the resistance of the heaters, necessitating large currents, and because the electrical wattage necessary to heat up the mass of metal Dewars is quite large.

3.3 Temperature Measurement

The Collins cryostat is equipped with a constant-volume helium gas thermometer using a Bourdon gauge for an indicator. The bulb for the gauge is located some distance away from the bottom of the cryostat where the cavity is placed. During cooling, when the engines are running, a convection current of helium is maintained in the cryostat, and the gas thermometer is found to read nearly the same as the temperature of the cavity. At 77°K, there is an error of 3°. When the cryostat was taken apart for repairs, the helium gas thermometer bulb was immersed in liquid nitrogen, and the Bourdon gauge was observed to read 86°K. On warming up, there is no convection, and the helium gas becomes stratified. The gas thermometer may then read 20° higher than the cavity over the range 40° to 300°K, even though a slow rate of warming is maintained. For this reason, the cryostat thermometer was not used except for very rough purposes.

The resonant frequency of the cavity may be used for temperature measurement. To use this method, the thermal expansion of copper (of which the cavity rim is made) must be known as a function of temperature. Figure 4 is a curve of the linear thermal-expansion coefficient, α, of copper versus the absolute temperature.

Since α changes markedly over the large temperature interval required, no simple algebraic expression of α as a function of T was found. Instead, a mechanical integration of Figure 4 was performed, from which is plotted, Figure 5, a curve of frequency shift, δ, from the room-temperature resonant frequency, versus temperature. This method suffers from the insufficient precision of the absorption wavemeters used, particularly for temperatures below $60^{\circ}K$.

The frequency method checks within two degrees with the gold resistance thermometer which furnished the actual temperature data for the copper measurements. This resistance thermometer is made from 0.002-inch diameter high-purity gold wire wound on a mica form as shown in Figure 6. The ends of the gold wire are mechanically clamped in two brass fittings, and the current and potential leads are soldered to these fittings. The thermometer was annealed for one hour at $400^{\circ}C$. In use, it was placed in a small cellophane bag and held next to the cavity by scotch drafting tape. The helium gas in the cryostat provides thermal contact. The resistance is measured by reading, on a type K potentiometer (Leeds and Northrup), the potential across the thermometer, and across a ten-ohm standard resistor (at $300^{\circ}K$), connected in series with the thermometer. Figure 7 shows the resistance versus temperature curve of this thermometer. In actual use, the temperature is obtained from expanded plots of this graph. The calibration was obtained by comparison with a helium gas thermometer and mercury manometer, shown in Figure 8. The bulb is made from two copper spinnings hard-soldered together, has a volume of 188.9 cc, and

approximates the mass of the cavity to be used in the microwave work. A 0.040-inch diameter cupronickel capillary tube connected the bulb with the mercury manometer. The manometer is 1/8-inch bore of the open-end type, necessitating knowledge of the atmospheric pressure, but reducing the length of manometer required. The manometer tubing is mounted on lucite to which millimeter graph paper is affixed. The lucite is held rigid by an aluminum angle along one edge. The aluminum also serves as a mounting to the cryostat. A long flourescent light, placed behind the lucite, affords soft illumination. Cylindrical lenses of polished lucite are mounted on sliders to magnify the meniscus and graph paper. Lines were drawn front and back on the lenses to be aligned with the meniscus as a means of avoiding parallax. The thermometer was filled with helium to about one-atmosphere pressure at room temperature. The change in volumes with temperature of the bulb, the capillary, and the manometer are negligible. The expression used for the temperature is

$$T = \frac{V_o T_o P}{P_o(V_o + v_o) - P v_o - \frac{A}{2\rho g}(P_o - P)} \quad , \qquad (34)$$

where V_o = bulb volume, v_o = volume of metal capillary + manometer at T_o, T_o = temperature of filling with helium, ρ = density of mercury, $g = 981$ cm/sec^2, A = area of manometer tube, P_o = pressure of helium at T_o. The actual computational formula was

$$T = \frac{1835}{\frac{10^4}{P} - 0.2945} \quad ,$$

where P is in mm, and T in degrees Kelvin. Accuracy of absolute

calibration is estimated at about 0.3°K.

Temperature data on tin, silver, and lead were taken with a copper-constantan thermocouple soft-soldered to the cavity-sealing diaphragm. The advantage of this over the resistance thermometer is convenience. Since the r-f impedance becomes independent of temperature at about 20°K, the fact that the thermal emf becomes unmeasurable below 24°K is not too detrimental. The cryostat thermometer was sufficiently accurate from 24° to 4.2°K.

3.4 Resonator

The cavity chosen was a right-circular cylinder of diameter-to-axial-length ratio 9.742, operating in a TM_{050} mode, and whose two flat sides were removable in part. Advantages of this type of cavity are:

a. it is readily demountable for change of specimen (the two flat sides);

b. the specimen has flat surfaces for easy polishing and examination (although it has been subsequently shown that small wire surfaces are also good);

c. it is easily made vacuum-tight;

d. it contains no dielectric supports;

e. it contains no joints except along current nodes;

f. it is easily fabricated, and

g. its electrical constants are readily calculated.

Some disadvantages are:

a. the curved and adjacent flat sections constituting the "base" of the cavity are not readily polished;

b. the r-f losses in the flat-side specimens are obtained by subtraction of curved-section losses from total

cavity losses;

c. all the currents are perpendicular to machining marks and hence maximize surface-roughness losses.

Not being able to polish the base is a disadvantage only when the highest possible Q is desired. The errors introduced by the subtraction process are minimized by selecting the largest possible ratio of specimen to base area.

The cavity diameter was made as large as the cryostat would permit, hence the high mode number. The break in the walls is circular and occurs at the outermost current node (approximately λ_o /4 from the cylindrical wall). Great care was exercised in fitting the specimens into the cavity, and measurements indicated that the gap between specimen and base of cavity was 0.0005 to 0.001 inches. To further insure against any effects due to the gap, the shoulder which terminates the gap and on which the specimen rests was made at approximately λ_o /4 from the inner surface. Thus the gap becomes, in essence, a choke. The magnitude of the losses in this gap are computed to be less than one per cent (cf. Reference (7)).

Coupling to the cavity is provided by means of a hole in the circumference which connects to the end of a waveguide. This guide is so oriented that its E field is parallel to that of the cavity, i.e., along the cavity axis. The size of the coupling hole was determined experimentally for the desired range of standing-wave ratios.

Except for a 1-3/4-inch piece of copper guide, specially made and permanently hard-soldered to the cavity, all waveguide is

0.500 x 0.250-inch O.D. x 0.040-inch wall coin silver.

Figure 9 is a scale drawing of the cavity.

It is important in a higher-mode cavity that the various modes be identifiable in order to be sure of operating in the correct one. A convenient method of plotting the mode frequencies for different cavity proportions is shown in Figure 10. This method is described in Reference (14). The equation of any line on this plot is

$$(fa)^2 = \left(\frac{cr}{\pi}\right)^2 + \left(\frac{cn}{2}\right)^2\left(\frac{a}{z}\right)^2 = A + Bn^2\left(\frac{a}{z}\right)^2 \quad , \qquad (35)$$

$$(n > 0 \text{ for TE modes}),$$

where c = velocity of light in free space; for $TM_{\ell mn}$ modes, $r = r_{\ell m} = m^{th}$ root of $J_\ell (r_{\ell m}) = 0$; for $TE_{\ell mn}$ modes, $r = r_{\ell m} = m^{th}$ root of $J'_\ell (r_{\ell m}) = 0$, a = diameter of cavity, z = axial length of cavity. TE_{0mn} and TM_{1mn} modes are intrinsically degenerate, while other degeneracies exist when mode lines intersect. Since experimental and theoretical absolute-Q values for the cavity must be compared, the desired resonant mode is identified by measuring the cavity dimensions and the frequencies of the modes in range, and matching the resulting points to the mode chart. Each frequency will then be identified with its mode. For $TM_{\ell m0}$ modes, only the cavity diameter need be known, and measurements using a swept oscillator and ordinary wavemeter proved sufficiently precise to detect an error of 0.005 inches out of 2.338 inches in the cavity diameter.

The electric and magnetic fields for the cylindrical cavity are obtained from Maxwell's equations with appropriate boundary conditions. To solve Maxwell's equations for the fields E and H

in cylindrical coordinates (see Figure 11), in the case of no angular

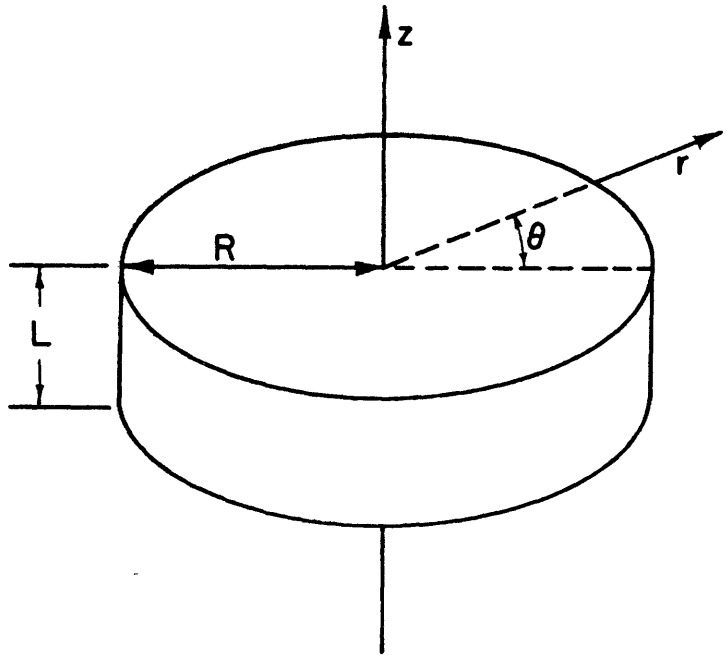

Fig 11. Cylindrical coordinate system for cavity.

nodes ($\ell = 0$) or axial nodes ($n = 0$), it is advantageous to put these conditions into the original differential equations. Assuming E and H vary as $e^{j\omega t}$,

$$\left.\begin{aligned} -j\mu\omega H_r &= 0 \\ -j\mu\omega H_\theta &= -\frac{\partial E_z}{\partial r} \\ -j\mu\omega H_z &= \frac{1}{r}\frac{\partial (rE\theta)}{\partial r} \end{aligned}\right\} \quad \nabla \times E = -\dot{B} \quad , \qquad (36)$$

$$\left.\begin{aligned} (j\epsilon\omega+\sigma)E_r &= 0 \\ (j\epsilon\omega+\sigma)E_\theta &= -\frac{\partial H_z}{\partial r} \\ (j\epsilon\omega+\sigma)E_z &= \frac{1}{r}\frac{\partial (rH_\theta)}{\partial r} \end{aligned}\right\} \quad \nabla \times H = J + \dot{D} \quad , \qquad (37)$$

$$\frac{1}{r}\frac{\partial(rE_r)}{\partial r} = 0 \quad , \qquad \nabla\cdot D = \rho = 0 \quad ,$$
$$\frac{1}{r}\frac{\partial(rH_r)}{\partial r} = 0 \quad , \qquad \nabla\cdot B = 0 \quad . \tag{38}$$

For the TM_{0m0} mode, $E_r = E_\theta = H_r = H_z = 0$. For the space inside the cavity $\sigma = 0$. The actual fields inside the cavity are assumed to be those of a cavity with perfectly conducting walls. Therefore $E_z = 0$ at $R = r$. Letting $k = 2\pi/\lambda_o = r_{0m}/R$, where r_{0m} is the m^{th} root of $J_0(r_{0m}) = 0$,

$$E_z = -j\sqrt{\frac{\mu}{\epsilon}}\, J_0\left(\frac{r_{0m}}{R}\, r\right)\, e^{j\omega t} \quad , \tag{39}$$

$$H_\theta = J_1\left(\frac{r_{0m}}{R}\, r\right)\, e^{j\omega t} \quad . \tag{40}$$

To calculate the Q of the cavity, one may use the expression (11)

$$Q = 2\pi\, \frac{\text{energy stored}}{\text{energy lost/cycle}} = \omega\, \frac{\text{energy stored}}{\text{energy lost/sec}} \quad . \tag{41}$$

The energy stored = E_s = maximum value of energy in the magnetic (or electric) field.

$$E_s = (1/2)\int \mu\, H_{max}^2\, dV \quad ,$$
$$E_s = 1/2 \iiint J_1^2(kr)r\, d\theta\, dz\, dr = \pi\mu L \int_o^R J_1^2(kr)r\, dr \quad ,$$
$$E_s = \frac{\pi\mu L R^2}{2}\, J_1^2(kR) \quad . \tag{42}$$

The energy lost (in the cavity walls) per second = $E_L = 1/2\int \mathrm{Re}(E\times H^*)dA$,

$$E_L = 1/2 \int \mathrm{Re}(Z)\, H_t^2\, dA \quad ,$$

where Re(Z) = real part of the surface impedance, H_t = component of H tangential to the walls.

The cavity is divided into three parts along nodal circles on the two flat sides of the cylinder. The radii of these circles are $r_n = (1/k)r'_{Om'}$, where $r'_{Om'}$ is the m'^{th} root of $J_1(r'_{Om'}) = 0$, i.e., these are circles at current nodes. Let the surface impedance of the area enclosed by the circles be Z_s (specimen), and the surface impedance of the remainder of the areas be Z_b (base). Then

$$E_L(\text{lids}) = \text{Re}(Z_s)\int_0^{2\pi}\int_0^{r_n} J_1^2(kr)r\,dr\,d\theta$$

$$= \pi r_n^2\ \text{Re}(Z_s)J_0^2(kr_n) \quad , \tag{43}$$

$$E_L(\text{base}) = \text{Re}(Z_b)\int_0^{2\pi}\int_{r_n}^{R} J_1^2(kr)r\,dr\,d\theta$$

$$+ 1/2\text{Re}(Z_b)\int_0^{L}\int_0^{2\pi} J_1^2(kR)R\,d\theta\,dz$$

$$= \pi\text{Re}(Z_b)\left[R^2J_1^2(kR) - r_n^2J_0^2(kr_n)\right]$$

$$+ \pi LR\ \text{Re}(Z_b)\ J_1^2(kR) \quad . \tag{44}$$

Letting

$$K = \frac{r_n}{R}\ \frac{J_0(kr_n)}{J_1(kR)} \quad ,$$

$$Q = \frac{\omega\mu L/2}{K^2\text{Re}(Z_s) + \left[1 + \frac{L}{R} - K^2\ \ \text{Re}(Z_b)\right]} \quad . \tag{45}$$

If $\text{Re}(Z_s) = \text{Re}(Z_b)$,

$$Q_{s=b} = \frac{\omega\mu L}{2(1 + \frac{L}{R})\ \text{Re}(Z_b)} \quad . \tag{46}$$

For the cavity design used, R = 1.169 inches, r_n = 1.043 inches, L = 0.240 inches, r_{05} = 14.9309, $r'_{04'}$ = 13.3237. Therefore,

$$K^2 = \left(\frac{1.043}{1.169}\right)^2 \left(\frac{0.2184}{0.2065}\right)^2 = 0.8904 \quad .$$

$$\omega = 2\pi f = 2\pi(2.4 \times 10^{10}) \quad \text{cycles/sec} \quad ,$$

$$\mu = \mu_0 = 4\pi \times 10^{-7} \quad \text{henries/meter} \quad .$$

$$Q = \frac{638.5}{\mathrm{Re}(Z_s) + 0.3536\ \mathrm{Re}(Z_b)} \quad , \tag{47}$$

$$Q_{s=b} = \frac{471.7}{\mathrm{Re}(Z)} \quad , \tag{48}$$

$$\mathrm{Re}(Z_s) = \frac{1}{\Sigma_s} = \frac{638.5}{Q} - \frac{0.3536}{\Sigma_b} \quad \text{ohms} \quad . \tag{49}$$

To calculate the Q of the cavity for the case of copper at $300^{\circ}K$, the classical formula for Z is valid, and we have $\mathrm{Re}(Z) = (\mu\omega\rho/2)^{1/2}$. From d-c measurements, $\rho_{300} = 1.693 \times 10^{-8}$ ohm-meters. Therefore,

$$\mathrm{Re}(Z) = 0.04002 \text{ ohms}; \quad \Sigma = 24.99 \text{ mhos};$$

$$Q_{s=b} = 11{,}790$$

3.5 Microwave Techniques

From considerations fully documented elsewhere, References (1), (2), (16), the best and most convenient method for measuring the Q's of magnitude here involved, i.e., 5000 to 36,000, is the observation of the voltage-reflection coefficient, r, or the voltage-standing-wave ratio, β. This may be done in any of three ways: (1) β, by a standing-wave detector; (2) β or r, by a balanced bridge; (3) r, by an unbalanced bridge. The last method has been chosen for the

present work because it has the advantages of great speed in recording the data, of a wide range of VSWR which may be covered with good accuracy, and of an inherent correction for transmission-line attenuation (so that the VSWR both on and off resonance need not be measured). It suffers the disadvantages of having to obtain the power-response law of the system (never exactly square), of having to insure a matched-as well as symmetrized-impedance bridge, and of never being able to measure directly the output which would result from replacing the cavity by a short circuit. This last difficulty is the most serious one.

Experience has shown that the practical realization of a well-matched and symmetrized, "magic" impedance bridge at 24,000 Mc/sec is very difficult. The fabrication of a waveguide E and H plane side-outlet "magic" T is particularly hard, and supplementary tuning screws must be placed in the matched-load arm and in the output arm for final balancing (1). The net result is that the bridge usually has the insufficient bandwidth of about 50 Mc/sec for a phase VSWR under 1.05, although its discrimination against direct coupling from input to output arms is high (about 40 to 50 db) over a large band. Because the overall change of resonant frequency of the cavity with temperature is about 80 Mc/sec, and because the phase VSWR increases very rapidly near the edges of the effective band-width, another type of impedance bridge is used in these measurements, i.e., the waveguide "rat race" (16). Two brass models of this bridge were built and tested. Figures 12 and 13 are scale drawings of the models, and Figures 14 and 15 show their performance characteristics. Rat race II is the one actually used in the low-temperature work.

The rat race is more readily made than the T, and is fabricated on a milling machine in two identical halves which are then soft-soldered together. The various waveguide arms are soft-soldered into the bridge block and auxiliary tuning screws are added in the waveguides. These tuning screws are also soft-soldered in place for vacuum purposes to make sure that they will not shift in adjustment under vibration.

Inasmuch as the rat race is a bridge which depends upon wave cancellation instead of upon symmetry for its properties, it might be expected that its frequency behaviour is inferior to that of the T. This is, in fact, the case for the discrimination, but not the case for the phase VSWR and the input VSWR. The input VSWR of the rat race is low over a wide frequency band by appropriate choice of the ring-waveguide dimensions. The addition of the screws in the matched-load arm can increase the discrimination, and 40 db is the figure found for rat race II used in this work. Under this condition, the phase VSWR bandwidth, after adjusting output-arm screws, decreases to about 100 Mc/sec. The phase VSWR at the resonant frequency at 300°K was 1.01. The waveguide bends machined into the bridge block, as well as the positions of the junctions, also contribute to the effective bandwidth. A polyiron load of VSWR about 1.05 is clamped into the load arm and sealed up with soft solder.

If the impedance bridge is not perfectly balanced, and a length of several feet of waveguide separate cavity from bridge, large output variations with frequency are noted over small frequency ranges. To reduce this long-line effect, caused by the large phase shift at the bridge of the reflected wave with a small frequency

shift, the rat race is placed in the cryostat with 3.94 inches of waveguide between bridge and cavity. Both input and output arms run the full length of the cryostat, so that the crystal, its fixed 10-db bakelite attenuating pad, and its flexible isolating waveguide, are outside at room temperature. This procedure has the additional advantage that the necessary bandwidth of the bridge is reduced, since the dimensions of the bridge, the tuning screws, and the resonant cavity all change with temperature to effect some compensation. Because the rat race is two-dimensional instead of three-dimensional (as a T is), the geometry and the facility in obtaining vacuum tightness aid this method. No objectionable behaviour with temperature of the polyiron load was expected or observed.

The phase VSWR and approximate power output of the bridge was checked as constant over the temperature interval 300°K to 179°K, and at 78°K. This was done by substituting for the cavity a precision, milled, 180° bend, shown in Figure 16. The transmission line was brought out of the Dewar to a mica vacuum seal and to a variable shorting plunger.

3.6 Electronic Techniques

For obtaining the relative unloaded Q as a function of temperature, while the temperature is slowly changing, r_o^2 is measured and use is made of Eqs. (31) and (32). For obtaining the unloaded Q at a fixed temperature, r^2 is measured as a function of the frequency deviation from resonance and the result plotted as the best straight line of $(1 + r^2)/(1 - r^2)$ *versus* $(\omega - \omega_o)^2$. The slope and intercept

at $\omega = \omega_o$ are used with the following equation, cf. Reference (6), to find Q_o and β_o (VSWR on resonance):

$$(2\delta Q_o)^2 \ \beta_o + \left(\beta_o + \frac{1}{\beta_o} \right) = 2 \frac{1 + r^2}{1 - r^2} \quad , \tag{50}$$

where $\delta = (\omega - \omega_o)/\omega_o$; the above equation holds for the case of undercoupling.

For the relative-Q data, a 2K33 klystron oscillator, whose repellor is sinusoidally modulated at 60 cps, provides the r-f power source. A 1N26 (Sylvania) crystal is the detector, and a battery-operated wide-band preamplifier plus a Dumont 208B oscilloscope constitutes the data-presentation equipment. The oscilloscope has a 5LP11 short persistent screen tube with a blue phosphor which gives a finer trace than the ordinary green phosphor (5LP1). This also permits shorter exposure times when the screen is photographed (1/25 second as compared to bulb). The oscilloscope pattern appears as in Figure 17, where the power reflected from the cavity is plotted as a function of frequency with the addition of a zero base line. The bell shape is the characteristic mode of the klystron power output versus frequency as the reflector voltage is varied, while the sharp dip is due to the cavity resonance. The cavity dip always removes the section of pattern which would be present if the cavity were replaced by a short circuit at the coupling hole. However, the total height of the pattern must be known in order to compute the ratio h/H which is equal to r_o^2, the power-reflection coefficient. If H were constant with frequency as the klystron is manually tuned, the dip could be swept off to the side, and the

height recorded. This is almost never the case because of residual frequency-sensitive errors in the matching of the impedance bridge, and because of klystron power-output variation. These bridge errors are not systematic, as a phase sensitivity error might be (cf. Reference (1) and Appendix II), since the reflected power is compared to a short circuit at the resonant frequency rather than to reflected power at other frequencies.

The height H of the mode pattern is estimated from the photographs, taken at each temperature, to a precision of 2 per cent or better. This is the method finally adopted.

For rough purposes, visual data was taken with the photographs; the dip was moved to each side of the mode, alternately, and the average mode height obtained. This procedure is accurate so long as the height H varies linearly with frequency. Such is not usually the case, and errors of 10 per cent in H may be easily introduced.

Two other methods have been found for measuring H. These were not used in practise because they were either as sensitive to impedance bridge mismatches as the other techniques, or were rather critical in adjustment.

In the first method, the klystron is operated CW, and the manual tuning knob is replaced by a shaft mounted in ball bearings. An eccentric disc is fixed to the shaft and a ball bearing is fixed to the disc such that its outer race bears against the klystron tuning strut. When the shaft is rotated, the motion of the strut is equivalent to that obtained by manual tuning. The resultant output, with impedance bridge and cavity, appears on an oscilloscope as in Figure 18. A small commutator on the shaft provides the

synchronized base line. It was found that speeds of about 10 to 30 cps were optimum, using a long persistent oscilloscope tube. Faster speeds caused microphonic jitter, and higher harmonics appeared on the trace. No deleterious effects were noted on klystron life after 200 hours of running time. The center frequency can be manually shifted by the tuning screw on the klystron. Total sweeps of 200 Mc/sec have been obtained.

In the second method, use is made of the fact that the focus grid voltage, which controls the beam current, slightly shifts the klystron frequency. A 60-cps sine wave is placed on the reflector in the usual manner, and a 60-cps sine wave is introduced on the focus grid by the circuit shown in Figure 20. No base line is provided for the oscilloscope trace, because the two mode patterns are desired (one on each sweep, forward and return). Zero reference is made from the no-output portions of the mode pattern. If the amplitude and phase of the focus grid modulation are correctly adjusted, the oscilloscope pattern is similar to Figure 19. One of the mode patterns is shifted in frequency from the other because the klystron oscillates with different focus grid voltages at each mode. This may be understood by reference to Figure 21. As the reflector voltage is modulated, the klystron oscillates between the voltages V_a and V_b. The source of the two mode patterns is now evident. Figure 22 is in correct juxtaposition with respect to Figure 21, and shows that the focus grid modulation should be about 90° out of phase with the reflector modulation. The procedure for using this method is to tune the klystron manually so that both cavity dips are off the modes. The cathode current and reflector voltage are then

adjusted until both mode patterns have the same height. This adjustment is checked by tuning the dips off the modes to the other side. Usually the heights of the modes will vary together, always remaining equal to each other.

To facilitate measurement of the distances h and H visually, it is convenient to have the base line on the scope fixed for small variations of H. This is accomplished by adding a clamping crystal as shown in Figure 23. The effect on the 60-cycle response is not harmful.

For obtaining the absolute unloaded Q of the cavity, a "master" and "slave" oscillator arrangement, which has been adequately described by Maxwell (2), is used. For the convenience of the reader, Figures 24 and 25 are reproduced here from Maxwell's thesis. Some improvements of this technique have been the use of wider-band crystal mounts, adequate fan cooling of the klystrons and the power supplies to prevent drifting in the 2K33 circuits, and the use of a Ballantine VTVM instead of an oscilloscope at the output. This particular master-and-slave technique is not recommended for further use unless an adequate supply, or a replacement, is found for the 2K50 thermally tuned klystron. The objections to the use of this tube are that the supply is limited, with no further production, and the tube becomes gassy and non-oscillating after a relatively short life of about 100 hours. This should not be interpreted as a criticism of the manufacturer, for it is the author's understanding that the tube was designed for guided-missile work, and has an adequate lifetime for this purpose. It may be possible to salvage the gassy tubes by repumping them and reactivating their cathodes.

3.7 Vacuum Seals

In the majority of measurements, the rubber gasket-mica seal with the asymmetrical metal-foil matching iris described by Maxwell (2 is used. The seals are permanently affixed to the input and output waveguides, thereby eliminating the necessity of a vacuum joint of Apiezon "Q". The loss in flexibility for testing the r-f mismatch of the seal is not significant. It was found that after tightening the seal, the metal foil was so firmly pressed against the brass flanges that, with care, the seal could be taken apart, the mica cleaned, the gasket re-treated with vacuum wax, and the seal reassembled without disturbing the matching adjustment, which is made for a VSWR $\leq$ 1.01 over the band.

Another useful seal has been developed. This seal is composed of two mica windows of identical thickness, only one of which need hold vacuum, spaced apart by approximately $\lambda_g/4$. Thus one window cancels the mismatch introduced by the other. Although inherently more frequency-sensitive than the metal-foil seal, the bandwidth is more than adequate, being, at the very least, with no padding, 150 Mc/sec for a VSWR less than 1.02, using 0.002-inch thickness of mica spaced 0.139 inch apart in a choke flange coupling with an especially long outer member. Mica thickness is not critical to within 0.0005 inch, at least. The advantage of this type of seal is that, once the dimensions have been established, it may be readily dis- and reassembled at will with no trial-and-error foil adjustments. More seals may be made with the above-mentioned dimensions, and they will perform as well, without individual foil adjustments,

providing the chokes used are not mismatched greater than the average of VSWR = 1.05.

The impedance bridge and its tuning screws are rendered vacuum-tight by soft soldering as mentioned in Section 3.5.

The cavity is sealed for vacuum in a manner which drastically reduces the heating, and resultant oxidation, of the cavity, and eliminates all danger of flux entering into the cavity. The following description of this seal may be understood with reference to Figures 26 and 27, illustrating a sealed cavity and an unsealed cavity (VIII), respectively. A wide copper hoop is soldered to a brass tube. The cavity and its coupled waveguide fits into this, and the brass tube is soldered to a flange which is itself soldered to the waveguide. There is a space of about 1/16 inch between the cavity and the hoop, and the only metallic thermal contact between outer-hoop assembly and cavity is through the flange on the waveguide. The inside surface of the hoop, near the edge, is tinned with soft solder. Two copper diaphragms are then spun, and are shown at the right in Figure 27. The outer cylindrical surface of the diaphragm cups are also tinned. The lids of the cavity are fitted into place, and the diaphragms are pressed into the hoop to bear lightly upon the back surface of the cavity lids. A brass plate, having a circular trough of mean diameter equal to that of the hoop, is heated and the trough filled with molten soft solder. The outer rims of the hoop assembly are then dipped, in turn, into the solder trough for a few seconds, the assembly being cooled after each rim-dipping by partial immersion in a water bath. This technique is almost 100 per cent successful in vacuum tightness, the very few

leaks which appear being due to lack of clean solder; these are easily repaired with a soldering iron. When the cavity is evacuated, the diaphragms collapse, holding the lids firmly in place and providing additional thermal contact with the outside atmosphere.

To remove the cavity lids, the diaphragms are cut off along an outer ridge in a milling machine. The remaining portion is then unsoldered by use of a torch, protecting the hoop from excessive heat, and localizing the applied heat, by judicious application of wet asbestos. New cups are, of course, spun for each sealing operation.

3.8 D-C Measurements

The d-c conductivity of copper has been measured, using standards four-terminal potentiometer techniques and a Leeds and Northrup type K potentiometer. A 48-foot length of 0.015-inch diameter wire, drawn from the same stock as the cavity by the Union Plate and Wire Co., Attleboro, Massachusetts, was wound on a mica cross (Figure 28). Care was taken to avoid undue heating of the copper by the current; currents of less than 800 milliamperes were used. Measurements of the conductivity as a function of temperature were made with the wire in the "as wound" stressed state, and after a half-hour anneal at 400°K in a hydrogen atmosphere.

Values for the d-c conductivity of lead are taken from Reference (1), of tin from Reference (2), and of silver from computations using Gruneisen's formula (17).

3.9 Specimen Fabrication

The base, or outer rim, of cavity IV was turned on the lathe, as smooth as possible, with a sharp carboloy tool bit. The copper was oxygen-free high-conductivity (OFHC) stock. The copper lids for this cavity were similarly fabricated. Measurements were made on the cavity in this state after degreasing in acetone, trichlorethylene, and alcohol. The cavity was then annealed in the hydrogen furnace for 15 minutes at 900°C and remeasured.

The base of cavity VIII was turned from solid-rod stock of vacuum-cast copper. This copper is purer than the so-called "spectroscopic" copper and was procured from the National Research Corporation in Cambridge, Massachusetts. Despite the high density reported for this pure copper, a few small blow holes (perhaps 0.005 inch in diameter) were noted during the machining. The inside dimensions of the rim were bored to within a few thousandths of an inch of the nominal values. The final finishing operations was to push a polished steel burnishing tool of the correct dimensions into the reentrant portion. A specially milled OFHC copper waveguide was hard-soldered to the cavity in a hydrogen furnace. It was found that the coin-silver waveguide, used everywhere else in these measurements, could not be reliably passed through the hydrogen furnace without "bubbling" the surface very severely.

The copper lids for cavity VIII were machined from the vacuum-cast rod stock. The final machining operation was to obtain, by use of a smooth worn file, a finish having some mirror-like properties. Measurements were made on these lids after the usual degreasing.

The cavity and lids were then annealed together, without breaking open the vacuum seal again, for 24 hours at 143°C in a vacuum of about 10^{-5} mm Hg, using an oil diffusion pump, (untrapped). R-f measurements were again made. The lids were then taken out and passed through the hydrogen furnace for 15 minutes at 900°C. However, a great deal of moisture collected on the specimen while in the cooling chamber, and some oxidation was noted. The lids were therefore repassed through the furnace as before, with more satisfactory results. No degreasing is necessary after this treatment, and the lids were again measured. The same lids were next electropolished as described below.

The lids were fitted into an OFHC copper guard-ring assembly to prevent excessive loss of metal at the corners of the specimen. Six liters of an orthophosphoric acid solution, with a specific gravity of 1.520 at 34.5°C (about 70 per cent by volume) were mixed in a glass tank 11-1/2 x 8 x 8 inches. The specimen and guard ring were held vertically at one end and a stainless steel cathode was hung vertically at the other end of the tank, 11 inches away. It was not found possible to polish these large areas with small anode-cathode spacings of a few inches in small tanks as is usually reported in the literature. The bath temperature was 30°C, and steady-state polishing conditions prevailed at 3.3 to 3.5 amperes and 3.9 to 3.5 volts, with no agitation. This corresponds to a current density of about 0.27 amperes per square inch. Early efforts showed that agitation produced better polishing, but the correct degree of turbulence over these large flat areas was not obtainable. A streamline flow of electrolyte merely succeeds in

forming flow marks on the specimen because of differential polishing. Rods about 1/4 inch in diameter and 6 inches long are well-polished to a glassy surface, free from pits, by rapidly rotating them in the bath with a stirring motor.

After one hour of polishing, the circular tool marks made during the original machining were still visible. One copper lid exhibited an "etched" appearance. On microscopic examination this turned out to be preferential loss of material on grain boundaries. Each grain appeared as a sort of step, being highly polished on its own surface, the step edges being very rounded and smooth. The other copper lid did not have an "etch" pattern to such a marked extent. The guard ring, after two hours of polishing, still had circular machine marks, but never exhibited any "etched" appearance. The latter copper lid, in contradistinction to the first lid, showed vertical flow marks, due probably to convection currents in the electrolyte as it changed density (the bath becomes blue around the anode).

After removal from the phosphoric acid, the samples were washed quickly with distilled water, and were swabbed with cotton to remove the viscous electrolyte. The lids were then dismounted from the guard ring under alcohol, swabbed with cotton in clean alcohol, rinsed in another alcohol bath, and dried quickly in a hot-air blast. No visible oxide was formed using this technique. Figures 29a, 29b, 29c, and 29d, are photomicrographs of the electropolished lids taken after the measurements were completed.

Polishing procedures involving the use of rouge or grits were avoided because of the tendency for the specimen to load up with

the abrasive, and because of the oxidation attendant with these methods.

All specimens investigated in this work were kept under at least a rough forepump vacuum unless they were actually being manipulated during surface preparation or cavity sealing.

The silver lids were prepared by melting down some 99.98 per cent pure pellets in a graphite crucible mold of dimensions somewhat larger than those of the final lids. This melting was done in air in a muffle furnace. The castings seemed sound and free of any porosity, and were composed of a few large grains. These castings were machined to dimensions, and passed through the hydrogen furnace at 600°C for forty-five minutes for annealing. They emerged with slightly bubbled surfaces, thus indicating the presence of some dissolved oxygen, picked up, perhaps, during the casting. The cavity surfaces of these lids were then hammered down to enable remachining to the correct diameter, and to true the surface perpendicular with the cavity axis. The surface was further polished with the fine silver "wool" removed on the finish cut. The lids were taken to Arthur D. Little, Inc., Cambridge, Massachusetts, for electropolishing. The resulting surfaces were very mirror-like, but some of the original machine marks were still visible. After the electropolishing, the lids were annealed for two hours at 280°C under a vacuum of about 10^{-5} mm, and their r-f properties measured. Photomicrographs of the silver lids are shown in Figures 30a, 30b, 30c and 30d.

The tin specimens were made by casting chemically pure tin (99.95 per cent) in a brass mold against a smooth glass surface. The apparatus is illustrated schematically in Figure 31. A clean porcelain crucible was used to melt the tin, and the pouring was done

in air at atmospheric pressure. Attempts to cast in a vacuum proved fruitless because of the many voids which appeared in the metal. The brass mold was weighted sufficiently to prevent it from floating and allowing the tin to flow out between the brass and glass. The re-entrant groove in the mold is to prevent any movement of the tin in the cavity as the temperature is lowered, i.e., the tin contracts onto the brass. Both brass and glass were degreased before casting, the latter in a dichromate solution. Just prior to pouring, the brass was heated to about 180°C (melting-solder temperature) and the glass was also warmed a little beyond the point necessary to drive off moisture. If the glass were not heated, moisture bubbles formed many pits on the surface of the tin. The casting was allowed to cool in air and the rate of cooling was such that the tin solidified in about one minute. No alloying of tin with brass was encountered; the tin could be remelted away completely from the mold; this is due to oxidation of the brass. After casting, the glass plate is stripped away from the tin, leaving a very smooth, clean, mirror-like surface with only a few scattered pits and bits of tin oxide. The tin is composed of perhaps a dozen large long grains arranged radially. The specimen is then machined to the correct diameter and depth along the dotted lines shown in Figure 31.

Considerable difficulty was encountered in stripping the glass from the tin. Initial efforts using optically polished pyrex were unsuccessful. The metal appears to bond in many places to the glass. Commercial pyrex plate glass, which was smooth but not optically flat, could be stripped using mechanical force. Various methods of stripping by differential thermal expansion were not successful,

and it was deemed better not to touch the tin surface with any liquid after stripping. All attempts to aid the parting of tin and glass by dilute greasing agents in very thin layers resulted in easy stripping and in a myriad of tiny bubble holes in the surface, contributing an estimated 10 per cent increase in surface area. Photomicrographs of the two tin lids are shown in Figures 32a, 32b, 32c and 32d.

The lead specimens were cast in brass molds, shown schematically in Figure 33. The lead used was Johnson-Matthey spectroscopic, batch number 1932, and the casting was done in air at atmospheric pressure. The mold was preheated. The lead was in the molten state for about two minutes in the mold, and, after solidifying, was composed of a few very large grains. After casting, the lead and brass were machined to dimensions along the dashed lines shown in Figure 33. An unsuccessful effort was made to prepare a very smooth surface by pressing, in the mold, an optically polished tool-steel piston at 75 tons force, on a conically machined lead surface. The surface thus prepared still showed tool marks from the turning operation, although otherwise appearing smooth, and having dull, mirror-like oxide layer. Kerosene was used on this specimen as a lubricant, and it was supposed that it could be removed by the degreasing procedures previously mentioned. Low-temperature measurements indicated an extremely high residual resistance which was attributed to either very deep oxide layers or insufficient removal of kerosene. The following technique was then utilized with fairly satisfactory results. The same lead specimens described above were remachined on the lathe using soap and water as a lubricant and using a very fine cross feed with a medium-slow spindle speed, so that about half an

hour was necessary to make the one-inch radius cut. A very sharp pointed tool bit was used and the final chip was 0.0005 inch thick. The use of a lubricant is imperative, since lead will pit and tear if turned dry. Acetone proved very bad indeed as a lubricant, the damage it caused extending at least 0.010 inch into the metal. The lead surface prepared in this way was bright (little oxidation) and had some faint mirror-like properties. Immediately after machining, the specimen was put under a heavy stream of hot water for about seven minutes to rinse the soap, and was then washed in two alcohol baths and dried quickly in a hot-air blast. The surface oxidation was much less intense than that encountered during the pressing method. The lead, like all the other specimens, was immediately stored under a forepump vacuum, and was exposed to air only during the sealing of the cavity. It is felt that although the surfaces may not have been as smooth as those pressed out by Garrison, they were considerably more free of flux and of oxide (not having been heated while sealing).

IV. EXPERIMENTAL RESULTS

4.1 D-C Resistivities

Copper. The square root of the relative d-c resistivity versus temperature is presented in Figures 34a and 34b. Figure 34a is for the coil in a stressed, as wound, condition, whereas Figure 34b is after a half-hour anneal at 400°C in a hydrogen atmosphere. The large residual resistance is due to either insufficient annealing or insufficient purity. If the residual resistance, ρ_o, is subtracted from the resistance at each temperature, the "ideal" curve shown in Figure 35 is obtained. For comparison, values from the International Critical Tables are also plotted for polycrystalline and single crystal samples. It should be noted that the Critical Tables are normalized to 273°K, whereas the curve is normalized to 298°K. Values on the curve have been compared with those derived from Gruneisen's formula (17) and good agreement was found. The value for the resistivity at 300°K is 1.693×10^{-6} ohm-cm. This is the measured value, and is also that given in the Metals Handbook (1948).

Silver. The temperature variation of the d-c resistivity has been computed from Gruneisen's formula, and the values thus found check down to 35°K with those given in the Critical Tables. The actual values used for plotting against the r-f results are those from Gruneisen's formula. The resistivity of silver at 300°K is taken as 1.59×10^{-6} ohm-cm from the Metals Handbook.

Tin. The temperature variation of the d-c resistivity is taken from Reference (2). The resistivity at 300°K is taken as 11.5×10^{-6}

ohm-cm.

Lead. The temperature variation of the d-c resistivity is taken from Reference (1). The resistivity at 300°K is taken as 21.5 x 10^{-6} ohm-cm.

All four metals have room-temperature resistivities higher than those reported in Reference (17).

Values for the relative conductivities and for $\alpha^{1/6} n^{2/9} = c_2 \sqrt{\sigma}\, \Omega^{2/9}$ are given for convenient temperatures in Tables I - IV; c_2 is given in Section 2.1 as 8.255 x 10^{-5}, while Ω is the reciprocal of the number of atoms per cm^3, and has the values:

Copper:	1.182 x 10^{-23}	cm^3/atom
Silver:	1.707 x 10^{-23}	
Tin:	2.701 x 10^{-23}	
Lead:	3.032 x 10^{-23}	

4.2 Surface Impedance

For all the metals— copper, tin, silver and lead— data were taken every five degrees while the cryostat was warming up. To put all this data, and more from several runs, on the final curves would not be practical, so except in Figure 45, the graphs are given with no experimental points plotted. In Figure 45, the experimental points of a typical run are given. The table of results for each metal has entries for only fourteen temperatures. These were picked so that, if plotted on a logarithmic temperature scale, they will give approximately equally spaced points for easy curve drawing and interpolation.

Copper. Cavity IV, after machining and annealing in H_2 for fifteen minutes at 900°C, had a Q_o = 11,590 at 300°K. One low-

temperature run was made which was discarded because of inaccurate temperature data. The asymptotic value of the relative Q_o, (Q_{300}/Q_T), is good, however, and is 0.250. Later, while checking the constancy of the window Q, Q_w, at 77°K, the pumping line on the forepump slipped off, allowing air to rush in and condense in the cavity for about 15 seconds before the situation was corrected. The cavity was at once brought to room temperature. The Q_o was then remeasured as 10,900.

Low-temperature data were then taken on this cavity. The second column in Table V is the relative Q_o obtained as an average of four runs and is plotted as shown in Figure 36. The third column is the skin conductivity. Because the Q_o was lowered after the accident, it is supposed that a thin layer of lossy dielectric material was deposited on the cavity walls, and that this layer constitutes a constant shunt conductance in the equivalent circuit. In other words, it is supposed that the losses in this layer are independent of temperature. A correction may then be applied to the data as follows:

$$\frac{1}{Q'_o} = \frac{1}{Q_o} + \frac{1}{Q_s} \quad ,$$

where Q'_o= measured Q, Q_o = true Q, and Q_s = "Q" of spurious lossy material.

$$\Sigma' = KQ'_o \quad ; \quad \Sigma = KQ_o \quad ,$$

$$\frac{K}{\Sigma'} = \frac{K}{\Sigma} + \frac{1}{Q_s} = \frac{K}{\Sigma} + \alpha \quad ; \quad \alpha \neq \alpha(T) \quad .$$

Therefore, the true skin conductivity is given by

$$\Sigma = \Sigma' \left(\frac{1}{1 - \frac{\alpha}{K} \Sigma'} \right) \quad . \tag{51}$$

In the present case, if Σ is in mhos, $K = 471.7$, and $\alpha = 0.053 \times 10^{-4}$. When this correction is made, the values of Σ appear as in column four, Table V. It should be noted that the asymptotic value of the ratio Σ_{300}/Σ_T is 0.262, in satisfactory agreement with the value 0.250 previously found. The four per cent difference might be experimental error, or a real increase due to additional oxidation, etc., of the walls with time. These amended values of Σ are used to compute column five, Table V, and to plot Figure 37, in the manner of Reuter and Sondheimer.

A "correction" for surface roughness may be applied to the values in column four. This correction is made as follows. Knowing, at 300°K, the ratio of Q_o expected from the d-c conductivity to that actually measured, a value of Δ/δ (the ratio of the root-mean-square roughness to the skin depth) may be found from one of Morgan's curves, reproduced here as Figures 2 and 3. Curve III has been used in these corrections. Then, with the values of an effective δ found from the actual measured Q_o, assuming classical theory, the value of Δ/δ is found at any other temperature. It is assumed that Δ remains constant with temperature. For cavity IV, $\Delta \sim 1.5$ micro-inches ~ 380 A.U.

$$\left(\frac{\Delta}{\delta}\right)_T = \left(\frac{\Delta}{\delta}\right)_{300} \left(\frac{\delta_{300}}{\delta_T} \right) = \left(\frac{\Delta}{\delta}\right)_{300} \left(\frac{Q_T}{Q_{300}} \right) \quad .$$

A value of P/P_o corresponding to $(\Delta/\delta)_T$ is found from curve III, Figure 3, and is multiplied into the value of Σ for this temperature.

The results are expressed in columns six and seven, Table V. Figure 38 represents this last column in a Reuter and Sondheimer plot.

Values for n, the number of free electrons per atom, may be found by matching the experimental and theoretical asymptotes at low temperatures. From the data, as measured, it appears that n = 0.13 or n = 0.22 depending upon whether p = 1 or p = 0 asymptotes, respectively, are used. From the data corrected for the extra lossy material, n = 0.33 (p = 1) and n = 0.55 (p = 0). Using the fully corrected data, n = 0.51 (p = 1) and n = 0.87 (p = 0). Assuming that the experimental curve (Figure 38) fits the theoretical curve for p = 1, at least as far as the break from classical behaviour at $\ell = \delta$ (i.e., $\alpha = 1.5$), the apparent value of n derived by comparing the points of departure is 0.88.

Were curve II, Figure 2, used for the roughness correction, values of n 10 per cent higher would have been computed.

Cavity VIII data is summarized in Tables VI through IX, and in Figures 39 through 44. Skin conductivities for the base of cavity VIII were deduced from the residual losses using the lead lids, superconducting at 2°K. This temperature was obtained by pumping with the compressor on four and a half liters of helium in the cryostat (to insure covering the cavity). The lead then had negligible losses compared to the copper. The skin conductivity for the copper base at 2°K was thus found to be 64.2 mhos. If the cavity were all of material like the base, the asymptotic low-temperature Q_o would be 30,300. The composite cavity with electropolished lids gives an asymptotic Q_o of 29,300. The ratios of Σ_{300}/Σ_T for the base were therefore identified with the ratios

of Q_{300}/Q_T given by the electropolished-lids cavity. Since the cavity base affects the calculated surface impedance as a relatively small subtractive term, this procedure is sufficiently precise.

The second column in Tables VI through IX gives the measured relative Q_o for the composite cavity as a whole. By application of Equation (49), the skin conductivities for the sample are obtained, and appear in column three. The very high skin conductivities observed with cavity IV were never realized with cavity VIII.

The Q_o of cavity VIII was lower after annealing in vacuo at 143°C for 24 hours than before annealing. The explanation of this is not clear. It may be the diffusion of thin oxide layers into the metal which increases the losses, or it could be that in the stress-annealing at this low temperature, fissures and peaks are opened up and produced as the strains relax; some small centers of incipient recrystallization might even occur in the highly stressed surface layer at this temperature (average bulk-metal recrystallization temperature is about 180°C, depending on the extent of cold work).

Annealing the copper in hydrogen for 15 minutes at 900°C not only removes thin surface layers of oxide and grease, but apparently reduces the roughness, thus increasing the skin conductivity. For cavity IV, the Q_o at 300°K was raised from about 7,000 to 11,590 by this treatment. For cavity VIII, the magnitude of a similar, although smaller, effect may be seen from the Tables VI, VII, and VIII. It would seem that perhaps surface tension is smoothing out some of the roughness because of the greater mobility of the atoms, or the lower resistance to plastic flow at this

temperature. Furthermore, in all probability, the effective melting temperature of the surface is lower than the bulk melting point of 1083°C.

Electropolishing the copper further increased the cavity Q_o and the skin conductivities. It was not found possible on these large flat specimens to bring the room-temperature Q_o up to theoretical by the electropolishing procedures used.

Computed values for n are summarized in Table XIII.

This series of experiments on copper shows that the low values commonly found for Σ and apparent n are largely due to surface roughness, rather than to surface cold work, oxide layers, etc., although these may be contributory. A few per cent difference between the experimental Σ at 300°K of different surface finishes becomes a ten or twenty per cent difference at 10°K. The smoothest surfaces obtained yield computed values for n which are higher than any reported thus far for this type of measurement. A surface-roughness-correction factor, derived on a semi-theoretical basis, may be applied to the skin conductivity to bring the values for n closer to the order of unity.

Since it is not possible to measure the effective d-c conductivity, σ, of that portion of the metal in which the r-f electromagnetic waves are confined (approximately the skin depth), there is some question as to the correct values of σ to use in calculating $\alpha\ ^{1/6}n^{2/9}$. For the well-annealed samples, perhaps the best which can be done is to use the highest, and most nearly ideal, σ obtainable from tables, etc. For the cases of the stressed and the 143°C-annealed copper, which are plotted in Figure 43 using an ideal σ,

it is interesting to see the results (Figure 44) using the σ of stressed and of 400°C-annealed copper, respectively. The lower values of σ shift the curves to the left by amounts which increase as the temperature decreases. The asymptotic value of Σ is, of course, independent of σ.

In Figures 43 and 44 it can be seen that the curves do not follow a 45° line in the classical region. This deviation is too great to be explained on the possible basis of the curves following the case $p = 0$ rather than $p = 1$ (see Figure 1). The deviation is, however, characteristic of that produced by a source of loss whose importance increases with decreasing temperature. Lossy surface layers and surface roughness are both loss sources of this type. Existence of this deviation, together with a Q_o at 300°K which is lower than theoretical, is probably evidence that the measured values of Σ and the computed values of n are not characteristic of the true crystalline metal. In the case of cavity IV (Figures 37 and 38), the deviation is much smaller, and, correspondingly, Σ and n are larger.

Silver. Results for the silver lids are summarized in Table X and Figures 45 and 46. Although electropolished, the surface still showed scratches and pits. It is not clear whether the pits come from an imperfect casting, from machining, or from electropolishing. The pits are visible only microscopically (see Figures 30a, 30b, 30c and 30d).

Because n is smaller, after "correction" on the basis of curve III, than after equivalent corrections for copper, it might be supposed that a different character of roughness is present.

Tin. Results for the tin lids are summarized in Table XI and Figures 47 and 48. No correction is needed for roughness, Σ_{300} being 4 percent higher than theoretical. This is within the experimental error, although there is some possibility that the effect is real. Simon (18) has measured spectroscopic tin wires, cast in glass in vacuo, from 300°K to 4.2°K at 9090 Mc/sec using a "hairpin" resonator. Matching the room-temperature skin conductivity arbitrarily to the theoretical value, he finds that the asymptotic low-temperature value is 132 mhos. This gives n = 0.21 (p= 1) and n = 0.38 (p = 0), as compared with the author's values, at 24,000 Mc/sec, of n = 0.19 (p = 1) and n = 0.31 (p = 0). Multiplying Simon's skin conductivity of 132 mhos by the ratio of frequencies to the two-thirds power, $(9{,}000/24{,}000)^{2/3}$, the value 68.8 mhos is obtained, as compared with the author's value of 68.4 mhos. Thus it seems, for surfaces sufficiently smooth, the frequency dependence of the theory is correct.

The large bowing of the curve over the classical 45° line is also evidenced by Simon's data. The reason for this is not clear.

Lead. Results for the lead lids are summarized in Table XII and Figures 49 and 50. The skin conductivity at low temperatures is smaller than that observed by Garrison. This is not too surprising, since the sample preparation is different. Because of the large cavity size in relation to the cryostat, it was not possible to arrange for a magnetic field of sufficient magnitude to destroy superconductivity in the lead, even at 4°K. For this reason, Figures 49 and 50 stop just short of clearly exhibiting the asymptotic r-f behavior. The slightly higher value for Σ_{300} obtained

in this work is not too significant, being well within experimental error.

No results can be obtained on the residual losses in the lead at 2°K, because of the much larger losses in the copper base. Instead, the reverse information was procured. The transition point of the lead was observed, and the cavity Q_o increased by a factor of 4.8 from 7.5°K to 2°K.

Roughness corrections, computed in the same manner as for copper, result in raising the apparent values n = 0.04 (p = 1) and n = 0.06 (p = 0) to n = 1.06 (p = 1) and n = 1.81 (p = 0).

Computed values for n for all four metals are collected in Table XIII.

No corrections are necessary for the relaxation time of the electrons, compared with the period of the field. Reuter and Sondheimer have given the first correction term to the asymptotic value of A/R as

$$\Delta \left(\frac{A}{R}\right) = \frac{3\sqrt{2}}{\pi\alpha^{1/3}}\,\gamma \quad , \tag{52}$$

where $\gamma = \omega\tau$. Equation (52) is independent of τ. This correction has the following values for 24,000 Mc/sec, assuming n = 1.0 for copper and silver, n = 0.25 for tin, and n = 0.16 for lead:

Copper:	0.00346
Silver:	0.00423
Tin:	0.0118
Lead:	0.0161

Clearly, these are negligible in comparison with experimental errors.

4.3 Errors

The errors in the d-c resistivity of copper are principally in the length and diameter measurements of the sample. The accuracy of ρ_{298} is estimated at 1.2 per cent. The errors in the d-c resistivity of the other metals is probably of the order of one to two per cent.

The average temperature of the cavity is probably accurate to better than 0.5°K down to 25°K when using a thermocouple, and down to 8°K when using the gold-resistance thermometer. (The latter was used only for the copper measurements.) Below 25°K, when using a thermocouple, the cryostat dial was used, and an accuracy of 2°K was obtained. This is of small moment, however, since the surface impedance has usually reached its asymptotic value before this temperature. Serious errors can be introduced if the rate of change of temperature is too great. For the mass of cavity used here, a rate of 3°K/minute may produce a 20° error. A rate of 1°K/minute is satisfactory, and average rates of about 0.5°K/minute were generally used.

Considerable discussion of the errors arising from an unbalanced-bridge r-f technique has been given in References (1) and (2).

Errors in the relative Q_o may arise from:

a. system response law not exactly square. These errors tend to cancel out for the relative Q data;

b. systematic bridge misadjustments;

c. random errors in data reading. Use of photography enables distances on the oscilloscope screen to be read to an accuracy of better than 1 per cent;

d. extra mismatches in transmission line between cavity and bridge.

Item (b.) is minimized by always using undercoupled cavities, by balancing and matching the bridge using the exact plumbing employed in the measurements, and by matching input and output. (See Appendix II for more complete bridge mismatch equations than appear in References (1) and (16).) If the mode height H (see Section 3.5) varies with frequency, and H is obtained by averaging heights as the dip is swept off the mode, errors as large as 5 per cent may be made in H, resulting in 10 per cent errors in VSWR for VSWR $\simeq$ 10. By photographing the scope and measuring H by approximating the shape of the mode, errors in H were reduced to less than 2 per cent.

The extra mismatch in item (d.) would not be the vacuum seal, as in the case of Garrison, since there was no seal between bridge and cavity. However, there were two soldered junctions between bridge and cavity: one where the waveguide cavity arm joined the bridge block, (never unsoldered), and the other where the cavity waveguide was butt-soldered to the waveguide cavity arm. This latter joint, being taken apart often, is susceptible to the inclusion of small amounts of solder. The distance from coupling hole to this butt joint is 2-3/8 inches, and the distance from the butt joint to the bridge junction is 1-9/16 inches. It will be shown below that if a small mismatch were to occur at the bridge junction, its phase relative to that of the cavity mismatch would not change appreciably over the 300° temperature interval, and thus the small mismatch would not be detectable as an approximately sinusoidal deviation from a mean value of the relative Q_o *versus* temperature. This small mismatch would not change the measured

absolute Q_o, but would change the window Q, Q_w, and the VSWR on resonance, β_o. Using large values of β_o (order of 8) and assuming small junction mismatches, the effect on the relative Q_o will be small.

Let the linear distance between sources of mismatch be ℓ. Then the phase angle, θ, between these mismatches, assuming the mismatches themselves are of the same phase, is

$$\theta = \frac{4\pi \ell}{\lambda_g} \qquad \text{in radians,}$$

where λ_g = the wavelength in the guide. Since the total frequency shift of the cavity in going from 300°K to 4°K is about 80 Mc/sec,

$$\frac{\Delta \ell}{\ell} = \frac{\Delta \lambda}{\lambda} = \frac{\Delta f}{f} = \frac{80}{24{,}000} = 0.00333 \quad ,$$

$$\frac{d\lambda_g}{\lambda_g} = \left(\frac{\lambda_g}{\lambda_o}\right)^2 \frac{d\lambda_o}{\lambda_o} = \left(\frac{0.606}{0.492}\right)^2 \left(\frac{80}{24{,}000}\right) = 0.005 \quad ,$$

$$\frac{d\theta}{\theta} = \frac{d\ell}{\ell} - \frac{d\lambda_g}{\lambda_g} = -0.003 + 0.005 = 0.002 \quad ,$$

$$\theta = 4\pi \frac{(1.568 + 2.375)}{0.606} \times \frac{180}{\pi} = 4680^\circ \quad ,$$

$$d\theta = 0.002 \times 4680 \simeq 10^\circ \quad .$$

Therefore, the largest phase change with temperature between mismatches is about 10°. Figure 51 gives the per cent error in the voltage-reflection coefficient, r, as a function of VSWR, β, for various values of the per cent error in β as a parameter. This graph has been slightly overextended, considering the use of the differential relationships, but it is still useful. Figure 52 gives

the minimum VSWR, β_2, (for the small extra junction mismatch) needed to produce a given error in β_1, the cavity VSWR, as a function of β_1. This assumes that r_2 adds in phase with r_1. From the lengths of the lines from cavity to junctions, it may be seen that this is very nearly the case.

Most relative Q_o curves have a precision of better than 5 per cent. An exception is lead near the superconducting transition point, where the cavity went through a match (VSWR = 1). The accuracy of the relative Q_o curve is probably no better than 5 per cent. The window Q was checked as invariant with temperature to within 2 per cent.

Errors in the absolute Q_o may arise from:

a. system response law. This is measured and correction made for it.

b. bridge errors. This is minimized as mentioned previously.

c. klystron output-power variation with frequency. This may amount to 10 per cent over the band necessary to cover the Q curve plus some "off" resonance frequencies, i.e., about 7 times the bandwidth. Allowance is made for this.

d. klystron output-power variation with time. This is virtually eliminated by taking the measurements rapidly; about 5 minutes is average time for a Q curve.

e. frequency drift. Over the 5-minute interval required for taking the data, the zero is stable to within 0.05 Mc/sec. Frequency differences are accurate to about 1 per cent.

f. random VTVM readings. These are accurate to 1 per cent.

Precision based on reproducibility and on fitting straight lines to the data is about 2 per cent. An accuracy is very difficult to estimate, but is probably around 6 per cent. Some checks were made by measuring Q_o at 77^oK, and these agreed with the Q_o measured at

300°K and the relative Q_o curve.

Errors in the skin conductivity, Σ, where no subtraction for a cavity base is necessary (cavity IV) are the same percentage as the errors in Q_o. At 300°K, where Q_o is measured, errors in Q_o are 5 per cent, so errors in Σ are 5 per cent. At other temperatures, Q_o is given by the expression, for undercoupled cavities,

$$Q_o = (Q_o)_{300} \frac{\beta_{300}}{\beta} \quad .$$

The fractional error in Q_o, and in Σ, is the square root of the sum of the squares of the fractional errors in Q_{300} and in the relative VSWR (taken from the smoothed curve of relative VSWR versus temperature). Therefore, Σ at temperatures other than 300°K is accurate only to 7 per cent. This means the number of free electrons per atom is accurate to only about 35 per cent.

Errors in Σ are slightly larger when the subtractive technique is used. Equation (49) is repeated here:

$$\frac{1}{\Sigma} = \frac{638.5}{Q} - \frac{0.3536}{\Sigma_b} \quad . \qquad (49)$$

The square of the absolute value of the probable error in $1/\Sigma$ equals the square of the absolute value of the probable error in $638.5/Q$ plus the square of the absolute value of the probable error in $0.3536/\Sigma_b$. The greatest probable error in $638.5/Q$ will occur for the largest Q, at a given per cent error in Q, i.e., near room temperature. The maximum value of $638.5/Q$ is about 0.12. At a 7 per cent error, the absolute error is therefore 0.0084. The corresponding value of $0.3536/\Sigma_b$ is 0.015, and at a 5 per cent error, its absolute error is 0.00075. Therefore, the absolute error in $1/\Sigma$ is still

about 0.0084 (the square of 0.00075 being small compared to the square of 0.0084). This corresponds to a per cent error of 8.4 per cent in Σ.

In another limiting case, where the two terms to be subtracted are more comparable in magnitude (tin and lead at low temperatures), $638.5/Q \simeq 4.2(0.3536/\Sigma_b)$. At these temperatures, $0.3536/\Sigma_b \simeq 0.0055$, and the absolute error in this term (5 per cent) is 0.00027. The square of the absolute error in $1/\Sigma$ is then

$$(4.2^2 + 1)\ (0.00027) = 1.37 \times 10^{-6} \quad .$$

Thus the absolute value of the probable error in $1/\Sigma$ is 0.00117 for this case, the per cent error being about 0.117/0.019 = 6.2 per cent.

Therefore it may be said that the final smoothed values of skin conductivity are accurate to at least 7 per cent, in the case of lead and tin perhaps to only 8.5 per cent.

V. CONCLUSIONS

It is concluded from the measurements presented here that, for the most ideal conditions obtained, the Reuter and Sondheimer theory gives the correct frequency dependence of the surface impedance and gives the correct number of free electrons per atom (at least for the quasi-free electron case). Discrepancies from the expected values of the impedance and the number of free electrons appear to arise chiefly from surface roughness, rather than from a failure of the Reuter and Sondheimer theory, providing, of course, the surface is reasonably clean.

Pippard's assumption, that the effect of surface irregularities is to increase the r-f resistivity by a constant proportion independent of temperature, is shown to be unwarranted. From the data on copper reported here, it may be seen that small differences in the surface impedance at room temperature result in large differences in the asymptotic low-temperature impedance, and in the apparent n. The consistent trend of the data shows that, as the surface becomes smoother, and as the room-temperature Σ becomes closer to the theoretical value, the low-temperature Σ increases very much, and the computed n approaches the order of unity.

The smoothest surfaces obtained were those of tin, and the r-f results are in very good agreement with those of Simon, thus checking the frequency dependence of the theory. These results are in disagreement with those of Pippard, whose asymptotic conductivity seems 34 per cent high. It is difficult to draw the conclusion that Pippard's data is wrong, since his other results seem to be on the

low side, and since it is usual to assume that the highest values of conductivity are the most nearly correct, a systematic error may perhaps be the explanation.

The values of n for the fairly smooth surfaces of the electropolished copper and silver are in excellent agreement with each other, and are in good agreement with Pippard's value for copper, but not silver. However, the values for n are still low. Pippard has assumed his room-temperature Σ to be that calculated from the d-c conductivity. Since his Σ_{300} may have been 5 per cent low, his values for n would be reduced by 20 per cent.

The data indicate that the low computed values of n are due to the effects of surface roughness, rather than to surface cold-working, oxide or grease layers, etc., although the latter especially, if present in large amounts, will be a major contributor towards a low apparent n. A "correction" for surface roughness brought about a value of n near unity in only one case, but this is not too surprising in view of the arbitrary assumptions used for the character of roughness and for the applicability of Morgan's curves in the non-classical region. Suppose one were to assume that the portion of curve III, Figure 3, near $P/P_0 = 1.0$ (high temperature) is substantially independent of the character of the roughness, and then determine the values of P/P_0 that would amend the low-temperature data to produce a value of n equal to unity (assuming δ_{eff} varies as the reciprocal of the relative Q_o). The results of this computation are plotted in Figure 53. The similarity of this to Morgan's curves is at once evident. Whether the extra loss at low temperature is due to a different roughness configuration that that assumed, or to a

limitation of the mean free path by the extra boundaries and consequent extra loss, is not known.

Unless a satisfactory roughness correction is found, the theoretical frequency dependence of the extreme non-classical skin conductivity can be checked only for smooth surfaces which give reasonable values of n. Unless smooth, the same sample at different frequencies may not even be expected to give an adequate check, because the roughness will be in different proportion to the skin depth, and also because, if the character of roughness changes over the specimen, a portion will be exposed to different relative field intensities when the frequency changes, thus further modifying the observed losses. This last possibility appears very real, because, in an attempt to verify Morgan's theory at room temperature, Bell Telephone Laboratories (19) have been unable to correlate the losses at 9000 Mc/sec on the basis of inferring a value of Δ for one frequency and using Morgan's curves for predicting the losses at another frequency. At the moment, they ascribe this difficulty to an unknown probability distribution of Δ over the surface.

Further work in this field should first be in the production of very smooth surfaces. In the case of tin, this may be already achieved; Bell laboratories have apparently accomplished this for copper wires, and perhaps for other metals. More definitive checks of the Reuter and Sondheimer theory may then be made, and measurements extended to higher frequencies for observation of relaxation effects. The study of the influence on r-f losses of different roughness configurations is of interest, but at the present time the use of an electron microscope is necessary to tie down the character

of the roughness.

It is concluded that the microwave method of evaluating n is not the most advantageous, because Σ is very sensitive to the surface configuration and n is very sensitive to Σ, depending upon Σ to the 4.5 power.

Appendix I

Frequency Pulling

In locating the frequencies of the cavity resonances, it is not always possible to obtain a clear-cut fitting to the mode chart. The frequency of the modes may be pulled by finite surface reactance, by extra objects in the cavity, and by boundary perturbations such as the coupling hole, cavity deformations, or an improperly placed break in the cavity walls. Frequency pulling may occur for some modes and not for others because, for example, the break in the cavity wall is not properly placed for modes other than the TM_{050} in its vicinity. Frequency pulling which is due to surface reactance may be found from Equation (30).

Pulling may be due to a bowing of the flat walls when the cavity is evacuated. For the sturdy cavity employed in this work, very little bowing, if any, can be expected. It is interesting, however, to compute the magnitudes involved. This may be done by using Equation III.89 in Reference (11). This equation expresses the perturbed frequency ω, resulting from a mode of resonant unperturbed frequency ω_a, in terms of an integral of the normalized fields over the volume of the resonant cavity which is <u>removed</u> by the boundary perturbations:

$$\omega^2 = \omega_a^2\left(1 + \int (H_a^2 - E_a^2)\, dv\right) \quad . \tag{A1}$$

The first step is to compute the normalized fields H_a and E_a, which are defined by the conditions

$$\int E_a^2 \, dv = 1 \quad , \qquad \int H_a^2 \, dv = 1 \quad . \tag{A2}$$

From Section 3.4,

$$E_z = -J \sqrt{\frac{\mu}{\epsilon}} \; J_0(kr) \quad , \tag{A3}$$

$$H_\theta = J_1(kr) \quad , \tag{A4}$$

where $k = 2\pi/\lambda_0 = \omega_a/c$.

Putting Equations (A3) and (A4) into (A2) and performing the integrations over the volume of the cylindrical cavity, the constants are obtained which multiply E_z and H_θ to convert them to E_{za} and $H_{\theta a}$.

$$E_{za} = \frac{1}{R\sqrt{\pi L}} \; \frac{J_0(kr)}{J_1(kR)} \quad , \tag{A5}$$

$$H_{\theta a} = \frac{1}{R\sqrt{\pi L}} \; \frac{J_1(kr)}{J_1(kR)} \quad . \tag{A6}$$

The second step is to fix the nature of the perturbation. It should be noted that Eq. (A1) is strictly correct only for an infinitesimal distortion of the surface. However, if the perturbation does not distort the field at large distances, Eq. (A1) may be used. If the perturbation does alter the configuration of the field lines drastically, the computation still may be carried through, providing the fields used in Eq. (A1) are found by solving the electrostatic problem involving the distortion. It is assumed here that one of the flat sides of the cylindrical resonator is bowed inward parabolically. The radius of curvature of the parabola will be assumed so large that the electric field is substantially unaltered, and

Eq. (A1) may be applied with Eqs. (A5) and (A6).

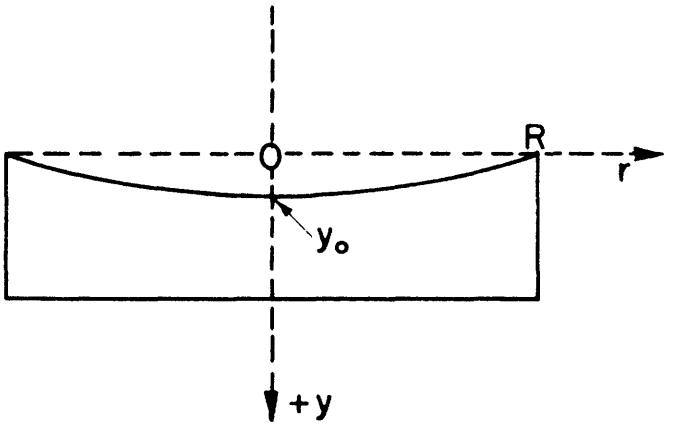

Fig 54. Coordinates of cavity with deformed wall.

The coordinates are set up in Figure 54. The parabola is given by the equation

$$y = y_o \left[1 - \left(\frac{r}{R}\right)^2\right] \quad . \tag{A7}$$

Therefore

$$\int (H_a^2 - E_a^2)\, dv = \frac{2y_o}{LR^2 J_1^2(kR)} \int_0^R \left[J_1^2(kr) - J_0^2(kr)\right] \left[1 - \left(\frac{r}{R}\right)^2\right] r\, dr. \tag{A8}$$

It is at once evident that integrals of the following type must be evaluated:

$$\int J_1^2(x) x^3\, dx, \quad \int J_0^2(x) x^3\, dx, \quad \int J_1^2(x) x\, dx, \quad \int J_0^2(x) x\, dx .$$

$$\int J_0^2(x) x\, dx = \frac{x^2}{2}\left[J_0^2(x) + J_1^2(x)\right] \quad , \tag{A9a}$$

$$\int J_1^2(x) x\, dx = \frac{x^2}{2}\left[J_0^2(x) + J_1^2(x) - \frac{2}{x} J_0(x) J_1(x)\right] \quad , \tag{A9b}$$

$$\int J_1^2(x)x^3\,dx = \frac{x^4}{6}\left[J_1^2(x) + J_2^2(x)\right] \quad , \tag{A9c}$$

$$\int J_0^2(x)x^3\,dx = \frac{x^4}{6}\left[\left(2 + \frac{1}{x^2}\right) J_0^2(x) - \left(\frac{2}{x^2} - 1\right) J_1^2(x) + \frac{2}{x} J_0(x)J_1(x)\right] \quad . \tag{A9d}$$

The last two integrations were performed from the following formula obtained from Watson's "Bessel Functions":

$$(\mu+2)\int z^{\mu+2}\zeta_\upsilon^2(z)\,dz = (\mu+1)\left[\upsilon^2 - \frac{1}{4}(\mu+1)^2\right]\int z^\mu \zeta_\upsilon^2(z)\,dz + \frac{1}{2} z^{\mu+1}\left\{z\zeta'_\upsilon(z) - \frac{1}{2}(\mu+1)\zeta_\upsilon(z)\right\}^2 + \frac{1}{2} z^{\mu+1}\left\{z^2 - \upsilon^2 + \frac{1}{4}(\mu+1)^2\right\}\zeta_\upsilon^2(z) \quad .$$

It is the difference between Eqs. (A9a) and (A9b) which appears in Eq. (A8), and for the limits of integration involved this is zero, (since $J_0(kR) = 0$). Use of formula (A9) with limits of integration over the deformed volume results in

$$\int (H_a^2 - E_a^2)\,dv = -\frac{2y_o}{L(kR)^2} \quad . \tag{A10}$$

Therefore

$$\omega^2 = \omega_a^2 - \frac{2y_o c^2}{LR^2} \quad . \tag{A11}$$

Since the last term in Eq. (A11) is small,

$$\omega - \omega_a = \frac{y_o c^2}{LR^2\omega_a} \quad . \tag{A12}$$

$\omega_a = 2.4 \times 10^{10}$ cps, $y_o = 0.002$ inch, $c = 1.18 \times 10^{10}$ inches/sec,

$L = 0.240$ inch, $R = 2.338$ inches.

$$\omega - \omega_a = - 8.8 \times 10^6 = - 8.8 \text{ Mc/sec} \quad .$$

If both walls were bowed in, the frequency would be decreased by 17.6 Mc/sec. The frequency would be expected to decrease because the maximum deformation occurs where the electric, rather than the magnetic, field is large.

Appendix II

Unbalanced-Impedance-Bridge Equations

Figure 55 is a schematic drawing of an unbalanced impedance bridge of the side-outlet T or rat-race variety, with the input arm 4 (the E arm), the output arm 3 (the H arm), the matched load arm 2, and the test cavity arm 1. Slater (15) has given a general expression for the ratio of power flow in the arms of such a bridge in terms of the admittances and conductances looking out of the various arms, and in terms of certain constants of the bridge relating to its match and symmetry (see Equations 25 and 26 of Reference 15). A more restricted and approximate treatment, based on traveling waves, is given here to aid in seeing the roles played by various small misadjustments from the matched and symmetrized "magic" conditions.

Using the conditions of symmetry and reciprocity, the scattering matrix (16) of the bridge may be written as

$$\begin{pmatrix} S_{11} & S_{12} & S_{13} & S_{14} \\ S_{12} & S_{22} & -S_{13} & S_{14} \\ S_{13} & -S_{13} & S_{33} & S_{34} \\ S_{14} & S_{14} & S_{43} & S_{44} \end{pmatrix}$$

The columns correspond to the total incoming wave fields E_{11}, E_{12}, E_{13}, E_{14}. The rows correspond to the total outgoing wave fields

E_{o1}, E_{o2}, E_{o3}, E_{o4}.

The bridge is easily balanced by tuning screws in arm 2 for symmetry such that $|S_{34}| = |S_{43}| = 0$, or the direct coupling from input to output arms is zero. (In practise, the direct coupling is 30 to 40 db below the minimum output signal used.) What is now desired is E_{o3} in terms of E_{i4}:

$$E_{o3} = S_{13}(E_{i1} - E_{i2}) + S_{33}E_{i3} \quad ,$$

$$E_{i3} = r_3 E_{o3} \quad ,$$

where r_1, r_2, r_3, r_4, are the voltage-reflection coefficients of the individual arms, considering each connected to a matched generator at the bridge. The r's, E's, and S's are all vector quantities.

$$E_{o3} = \frac{S_{13}}{1 - S_{33}r_3} \quad (E_{i1} - E_{i2}) \quad .$$

Similar equations may be deduced for E_{o1}, E_{o2}, and E_{o3}. One may obtain, by simple manipulations, the following three simultaneous equations:

$$\frac{1 - S_{11}r_1 - S_{12}r_1}{r_1} E_{i1} + \frac{1 - S_{22}r_2 - S_{12}r_2}{r_2} E_{i2} = 2S_{14}E_{i4} \quad ,$$

$$\frac{S_{13}}{1 - S_{33}r_3} E_{i1} - \frac{S_{13}}{1 - S_{33}r_3} E_{i2} - E_{o3} = 0 \quad ,$$

$$\frac{1 - S_{11}r_1}{r_1} E_{i1} - S_{12}E_{i2} - S_{13}r_3E_{o3} = S_{14}E_{i4} \quad .$$

E_{o3} may now be found in terms of E_{i4} by determinants, and, after

simplication, is

$$E_{o3} = \frac{r_1 - r_2 - (S_{22} - S_{11})r_1 r_2}{1 - S_{11}r_1 - S_{22}r_2 - (S_{12}^2 - S_{11}S_{22})r_1 r_2} \times$$

$$\frac{S_{13}\, S_{14}}{(1 - S_{13}r_3)(1 - S_{33}r_3)} E_{14} .$$

Ignoring products Sr above the third order,

$$E_{o3} = \frac{(r_1 - r_2)\, S_{13}\, S_{14}}{1 - S_{11}r_1 - S_{22}r_2 - (S_{33} + S_{13})r_3} E_{14} .$$

E_{14} depends upon r_4 and S_{44}. To find this relation, consider the equivalent circuit shown in Figure 56.

$$E = E_o \frac{Z_L}{Z_L + Z_S} .$$

The relations are then recognized as

$$r_4 = \frac{1 - Z_S}{1 + Z_S} , \qquad Z_S = \frac{1 - r_4}{1 + r_4} ,$$

$$S_{44} = \frac{1 - Z_L}{1 + Z_L} , \qquad Z_L = \frac{1 - S_{44}}{1 + S_{44}} .$$

Therefore,

$$E_{14} = \frac{E_o}{2} \frac{1 - S_{44} + r_4 - S_{44}r_4}{1 - S_{44}r_4} ,$$

$$E_{o3} = \frac{(r_1 - r_2)(1 - S_{44} + r_4)\, S_{13}\, S_{14}}{1 - S_{11}r_1 - S_{22}r_2 - (S_{33} + S_{13})r_3 - S_{44}r_4} \frac{E_o}{2} .$$

If the generator, load, and arm 2 are all matched, so that $r_2 = r_3 = r_4 = 0$,

$$E_{o3} = \frac{r_1(1 - S_{44})\, S_{13}\, S_{14}}{1 - S_{11} r_1} \frac{E_o}{2} \quad .$$

Thus, the output of the bridge is proportional to r_1, as it should be, only if S_{11} is zero, or the product $S_{11} r_1$ is constant. The latter is never so. S_{11} is rendered small by placing tuning screws in arm 3, adjusted for zero fluctuation in E_{o3} as a short, $r_1 = 1$, is moved back and forth in arm 1. These tuning screws will change r_3 from zero, if it was so originally, to some other unknown value. Then

$$E_{o3} = \frac{r_1(1 - S_{44} + r_4)\, S_{13}\, S_{14}}{1 - (S_{33} - S_{13})\, r_3} \frac{E_o}{2} \quad .$$

If S_{44}, S_{14}, S_{13}, S_{33}, r_4, and r_3 are of constant magnitude and phase over the frequencies covered by the resonant cavity from 300°K to 4.2°K, E_{o3} will be proportional to r_1. This condition is usually met in practice.

Appendix III

Effect of Cold-Working

The effects of cold-working on the d-c conductivity, σ, are known to be of the order of only a few per cent. In the case of copper, the author has found that the conductivity falls by 2 per cent after some drawing operations. These operations did not, however, put in the maximum possible amount of cold-work the metal would support.

In the region where the surface impedance, Z, is related to the d-c conductivity by classical theory, a 2 per cent change in σ results in only a 1 per cent change in Z. In the anomalous region, the asymptotic value of the impedance is independent of σ. On these grounds, it might be argued that cold-working would not effect the surface impedance appreciably. However, the surface impedance is not a property of the whole volume of the metal specimen, but is a property of that portion of the sample lying within the penetration depth of the surface. This surface layer could have a larger impedance than the bulk metal because it is known that the surfaces of metals may be cold-worked to a much greater degree than the volume as a whole.

The work of Lees (12) has shown that if a surface of copper is mechanically polished (not electropolished) the metal may be distorted and broken up to the point of being amorphous to a depth of probably not over 30 A.U. It may be severely broken up in fragments of about 90 A.U. on a side to a depth of not over about 500 A.U.

Beyond this depth, cold-working is more characteristic of the bulk material, and is small enough not to produce any crystal orientation effects. From this it is seen that the drastically altered material is located within a region small compared to the skin depth of 4250 A.U. for copper at 300°K.

It may be shown that for layers thin compared to the skin depth, the extra losses due to reduction of conductivity are negligible.

The metal may be regarded (see Figure 57) as a transmission line of impedance Z_1, and length $\ell_1 - \ell_2$, joined to another line of impedance Z_2 and length ℓ_2, which is terminated in the impedance Z_3 (bulk metal). The impedance at $-\ell_2$, looking into the metal, is given by the well-known equation

$$Z' = Z_2 \frac{Z_3 \cosh \gamma_2 \ell_2 + Z_2 \sinh \gamma_2 \ell_2}{Z_2 \cosh \gamma_2 \ell_2 + Z_3 \sinh \gamma_2 \ell_2} , \qquad (A1)$$

and then the surface impedance, as seen from free space, is

$$Z = Z_1 \frac{Z' \cosh \gamma_1(\ell_1 - \ell_2) + Z_1 \sinh \gamma_1(\ell_1 - \ell_2)}{Z_1 \cosh \gamma_1(\ell_1 - \ell_2) + Z' \sinh \gamma_1(\ell_1 - \ell_2)} . \qquad (A2)$$

Assuming that $\sigma_3 : \sigma_2 : \sigma_1 = 16:4:1$ and $\ell_2 = 500$ A.U., then $\ell_2/\delta_2 = 500/8500 = 0.059$. The cosh's may be set equal to unity, and the sinh's may be replaced by their arguments. Equations (A1) and (A2) then reduce to

$$Z' = Z_2 \frac{Z_3 + Z_2 \gamma_2 \ell_2}{Z_2 + Z_3 \gamma_2 \ell_2} = \frac{\sqrt{\frac{\sigma_2}{\sigma_3}} + \frac{\ell 2}{\delta_2}(1 + j)}{1 + \sqrt{\frac{\sigma_2}{\sigma_3}} \frac{\ell 2}{\delta_2}(1+j)} Z_2 \sim \sqrt{\frac{\sigma_2}{\sigma_3}} Z_2, \qquad (A3)$$

Table I

Copper: D-C Conductivity

I, stressed; II, annealed; III, ideal

T (°K)	$\left(\frac{\sigma}{\sigma_{300}}\right)^{1/2}_{I}$	$\left(\frac{\sigma}{\sigma_{300}}\right)^{1/2}_{II}$	$\left(\frac{\sigma}{\sigma_{300}}\right)^{1/2}_{III}$	I $c_2\sqrt{\sigma\omega}^{2/9}$	II $c_2\sqrt{\sigma\omega}^{2/9}$	III $c_2\sqrt{\sigma\omega}^{2/9}$
300	1	1	1	0.4789	0.4837	0.4893
250	1.115	1.100	1.103	0.5340	0.5320	0.5397
200	1.290	1.260	1.270	0.6177	0.6095	0.6214
160	1.481	1.473	1.495	0.7091	0.7130	0.7316
130	1.672	1.730	1.770	0.8006	0.8372	0.8654
100	1.992	2.110	2.208	0.9538	1.020	1.081
80	2.375	2.591	2.786	1.137	1.253	1.363
60	2.950	3.509	4.098	1.413	1.696	2.006
50	3.322	4.219	5.495	1.591	2.042	2.689
40	3.731	5.081	8.065	1.786	2.458	3.946
30	4.000	5.995	15.17	1.916	2.900	7.422
20	4.310	6.464	48.54	2.064	3.126	23.74
10	4.310	6.521	- - -	2.064	3.154	- - -
6	4.310	6.521	- - -	2.064	3.154	- - -

$$Z = Z_1 \frac{\sqrt{\frac{\sigma_1}{\sigma_3}} + \frac{\ell_1 - \ell_2}{\delta_1}(1 + j)}{1 + \sqrt{\frac{\sigma_1}{\sigma_3}} \frac{(\ell_1 - \ell_2)}{\delta_1}(1 + j)} \sim \sqrt{\frac{\sigma_1}{\sigma_3}}\, Z_1 \quad , \quad \text{(A4)}$$

$$\frac{Z}{Z_3} = \sqrt{\frac{\sigma_1}{\sigma_3}}\, \frac{Z_1}{Z_3} = 1 \quad . \quad \text{(A5)}$$

Equation (A5) indicates that, to a first approximation, the surface impedance will be that of the bulk metal.

Another way to view this situation is to replace each layer by an equivalent T section. Because the layers are thin and the cosh x and the sinh x are replaced by 1 and x respectively, the equivalent T reduces to simply a shunt impedance. The equivalent circuit for the metal then appears in Figure 58.

Table II

Silver: D-C Conductivity

T (^{o}K)	$\left(\frac{\sigma}{\sigma_{300}}\right)^{1/2}$	$c_2 \sqrt{\sigma}\,\Omega^{2/9}$
300	1	0.5413
250	1.104	0.5976
200	1.247	0.6750
160	1.420	0.7686
130	1.618	0.8758
100	1.938	1.049
80	2.331	1.262
60	3.086	1.670
50	3.861	2.090
40	5.291	2.864
30	8.850	4.791
20	21.41	11.59
10	116.8	63.22
6	431.0	233.3

Table III

Tin: D-C Conductivity *

T (^{o}K)	$\left(\frac{\sigma}{\sigma_{300}}\right)^{1/2}$	$c_2 \sqrt{\sigma}\, \Omega^{2/9}$
300	1	0.2228
250	1.107	0.2466
200	1.235	0.2752
160	1.410	0.3141
130	1.638	0.3649
100	1.953	0.4351
80	2.299	0.5122
60	2.914	0.6492
50	3.460	0.7709
40	4.292	0.9563
30	5.952	1.326
20	10.99	2.449
10	35.59	7.929
4.2	57.80	12.88

* Reference (2)

Table IV

Lead: D-C Conductivity *

T (σ_K)	$\left(\frac{\sigma}{\sigma_{300}}\right)^{1/2}$	$c_2 \sqrt{\sigma}\, \Omega^{2/9}$
300	1	0.1672
250	1.134	0.1896
200	1.292	0.2160
160	1.460	0.2441
130	1.621	0.2710
100	1.812	0.3030
80	2.070	0.3461
60	2.488	0.4160
50	2.762	0.4618
40	3.165	0.5292
30	4.255	0.7114
20	7.299	1.220
10	21.05	3.520
8	28.41	4.750

* Reference (1)

Table V

Copper: Cavity IV

$\Sigma_{300}(d-c)$ = 25.0 mhos, Δ $\sim$ 1.5 microinches

T (^{o}K)	$\frac{Q_{300}}{Q}$	Σ' (mhos)	Σ (mhos)	$c_1 \Sigma\, \Omega^{2/9}$ (e.s.u.)	Σ corr. (mhos)	$c_1 \Sigma$ corr. $\Omega^{2/9}$ (e.s.u.)
300	1	23.1	24.5	0.475	25.0	0.483
250	0.925	25.0	26.6	0.516	27.2	0.528
200	0.805	28.7	30.9	0.600	31.7	0.614
160	0.688	33.6	36.7	0.711	37.8	0.733
130	0.596	38.8	42.9	0.833	44.3	0.860
100	0.490	47.2	53.4	1.04	55.8	1.083
80	0.417	55.4	64.3	1.25	67.9	1.317
60	0.348	66.4	79.5	1.54	85.7	1.663
50	0.325	71.1	86.6	1.68	94.4	1.830
40	0.312	74.1	90.7	1.76	100	1.939
30	0.305	75.8	93.5	1.81	103	2.005
20	0.305	75.8	93.5	1.81	103	2.005
10	0.305	75.8	93.5	1.81	103	2.005
6	0.305	75.8	93.5	1.81	103	2.005

Table VI

Copper: Cavity VIII

Stressed lids, $\Delta \sim 8.4$ microinches

T (^{o}K)	$\frac{Q_{300}}{Q}$	Σ (mhos)	$c_1 \Sigma \Omega^{2/9}$ (e.s.u.)
300	1	20.4	0.396
250	0.914	22.3	0.432
200	0.806	25.4	0.492
160	0.717	28.5	0.553
130	0.647	31.6	0.612
100	0.576	35.2	0.683
80	0.528	38.2	0.741
60	0.479	41.9	0.813
50	0.462	43.2	0.838
40	0.450	43.9	0.852
30	0.445	44.1	0.855
20	0.445	43.9	0.852
10	0.445	43.9	0.852
8	0.445	43.9	0.852

Table VII

Copper: Cavity VIII

143°C-annealed lids, $\Delta \sim 10.7$ microinches

T (°K)	$\frac{Q_{300}}{Q}$	Σ (mhos)	$c_1 \Sigma \Omega^{2/9}$ (e.s.u.)
300	1	18.8	0.365
250	0.908	20.7	0.402
200	0.801	23.6	0.457
160	0.710	26.6	0.516
130	0.640	29.5	0.572
100	0.570	32.9	0.638
80	0.525	35.5	0.688
60	0.485	38.1	0.738
50	0.467	39.3	0.763
40	0.455	40.0	0.777
30	0.445	40.7	0.790
20	0.437	41.6	0.806
10	0.432	42.1	0.817
5	0.430	42.4	0.822

Table VIII

Copper: Cavity VIII

900°C-annealed lids $\Delta \sim 5.6$ microinches

T (°K)	$\frac{Q_{300}}{Q}$	Σ (mhos)	$c_1 \Sigma \Omega^{2/9}$ (e.s.u.)
300	1	22.7	0.441
250	0.913	24.9	0.482
200	0.814	27.9	0.541
160	0.725	31.3	0.607
130	0.642	35.5	0.689
100	0.555	41.1	0.798
80	0.505	45.1	0.874
60	0.462	48.8	0.947
50	0.444	50.5	0.980
40	0.430	51.7	1.004
30	0.420	52.6	1.021
20	0.416	53.1	1.030
10	0.416	53.1	1.030
5.5	0.416	53.1	1.030

Table IX

Copper: Cavity VIII

electropolished lids, $\Delta \sim 4.7$ microinches

T (^{o}K)	$\frac{Q_{300}}{Q}$	Σ (mhos)	$c_1 \Sigma \Omega^{2/9}$ (e.s.u.)
300	1	23.3	0.452
250	0.907	25.7	0.499
200	0.810	28.8	0.559
160	0.720	32.4	0.629
130	0.645	36.2	0.702
100	0.561	41.6	0.807
80	0.505	46.0	0.892
60	0.450	51.9	1.007
50	0.425	54.9	1.065
40	0.400	58.3	1.131
30	0.383	60.9	1.181
20	0.378	61.8	1.245
10	0.378	61.8	1.245
8	0.378	61.8	1.245

Table X

Silver: Cavity VIII

electropolished silver lids, $\Sigma_{300}(d-c) = 25.8$ inches, $\Delta \sim 3.6$ microinches

T ($^{\circ}K$)	$\frac{Q_{300}}{Q}$	Σ (mhos)	$c_1 \Sigma \Omega^{2/9}$ (e.s.u.)
300	1	24.6	0.518
250	0.914	26.9	0.565
200	0.823	29.8	0.626
160	0.744	32.8	0.689
130	0.677	35.8	0.753
100	0.598	40.3	0.848
80	0.537	44.9	0.945
60	0.475	50.9	1.072
50	0.450	53.7	1.130
40	0.430	55.9	1.177
30	0.415	57.8	1.216
20	0.406	59.2	1.246
10	0.404	59.6	1.255
7	0.403	59.8	1.259

Table XI

Tin: Cavity VIII

cast tin lids, $\Sigma_{300}(d-c) = 9.58$ inches

T (^{o}K)	$\frac{Q_{300}}{Q}$	Σ (mhos)	$c_1 \Sigma \Omega^{2/9}$ (e.s.u.)	$\Sigma_{Maxwell}$ (mhos)
300	1	9.96	0.232	8.22
250	0.882	11.34	0.264	9.14
200	0.760	13.23	0.308	10.05
160	0.657	15.37	0.358	11.67
130	0.576	17.59	0.410	13.29
100	0.490	20.8	0.484	15.72
80	0.425	24.1	0.561	18.80
60	0.357	29.0	0.676	23.8
50	0.318	32.9	0.767	27.9
40	0.275	38.8	0.904	34.1
30	0.232	47.4	1.105	44.1
20	0.195	59.1	1.378	55.6
10	0.175	68.4	1.594	57.1
5.5	0.175	68.4	1.594	57.1

Table XII

Lead: Cavity VIII

lead lids, $\Sigma_{300}(d-c) = 7.00$ mhos

T (^{o}K)	$\frac{Q_{300}}{Q}$	Σ (mhos)	$c_1 \Sigma \Omega^{2/9}$ (e.s.u.)	$\Sigma_{Garrison}$ (mhos)
300	1	6.52	0.1559	6.45
250	0.887	7.36	0.1760	7.14
200	0.775	8.45	0.202	7.87
160	0.687	9.53	0.228	9.01
130	0.620	10.5	0.252	9.62
100	0.553	11.80	0.282	11.12
80	0.505	12.90	0.308	12.66
60	0.455	14.31	0.342	15.31
50	0.427	15.26	0.365	16.53
40	0.390	16.75	0.401	19.80
30	0.330	20.0	0.478	24.6
20	0.260	26.2	0.626	34.0
10	0.175	41.8	0.999	56.5
7.5	0.161	46.5	1.110	60.1

Table XIII

Summary of Number of Free Electrons Per Atom, n

		n(p=1)	n(p=o)
Pippard:	(1200 Mc/sec)		
	Silver annealed	0.038	0.065
	unannealed		
	Tin	0.67	1.14
	Copper	0.066	0.11
Garrison:	(24,000 Mc/sec)		
	Lead (Hilger or C.P.)	0.12	0.20
Maxwell:	(24,000 Mc/sec)		
	Tin (Johnson-Matthey)	0.08	0.14
Nowak:	(24,000 Mc/sec)		
	Copper (vacuum cast) IV	0.33	0.55
	corrected for roughness	0.51	0.87
	Copper (vacuum cast) VIII, stressed	0.011	0.018
	corrected for roughness	0.10	0.18
	143°C-annealed	0.0092	0.016
	corrected for roughness	0.12	0.20
	900°C-annealed	0.026	0.044
	corrected for roughness	0.15	0.25
	electropolished	0.059	0.10
	corrected for roughness	0.32	0.54
	Silver (99.98%) electropolished	0.063	0.11
	corrected for roughness	0.16	0.29
	Tin (C.P.) cast against glass	0.19	0.31
	Lead (Johnson-Matthey) machined	0.030	0.060
	corrected for roughness	1.06	1.81

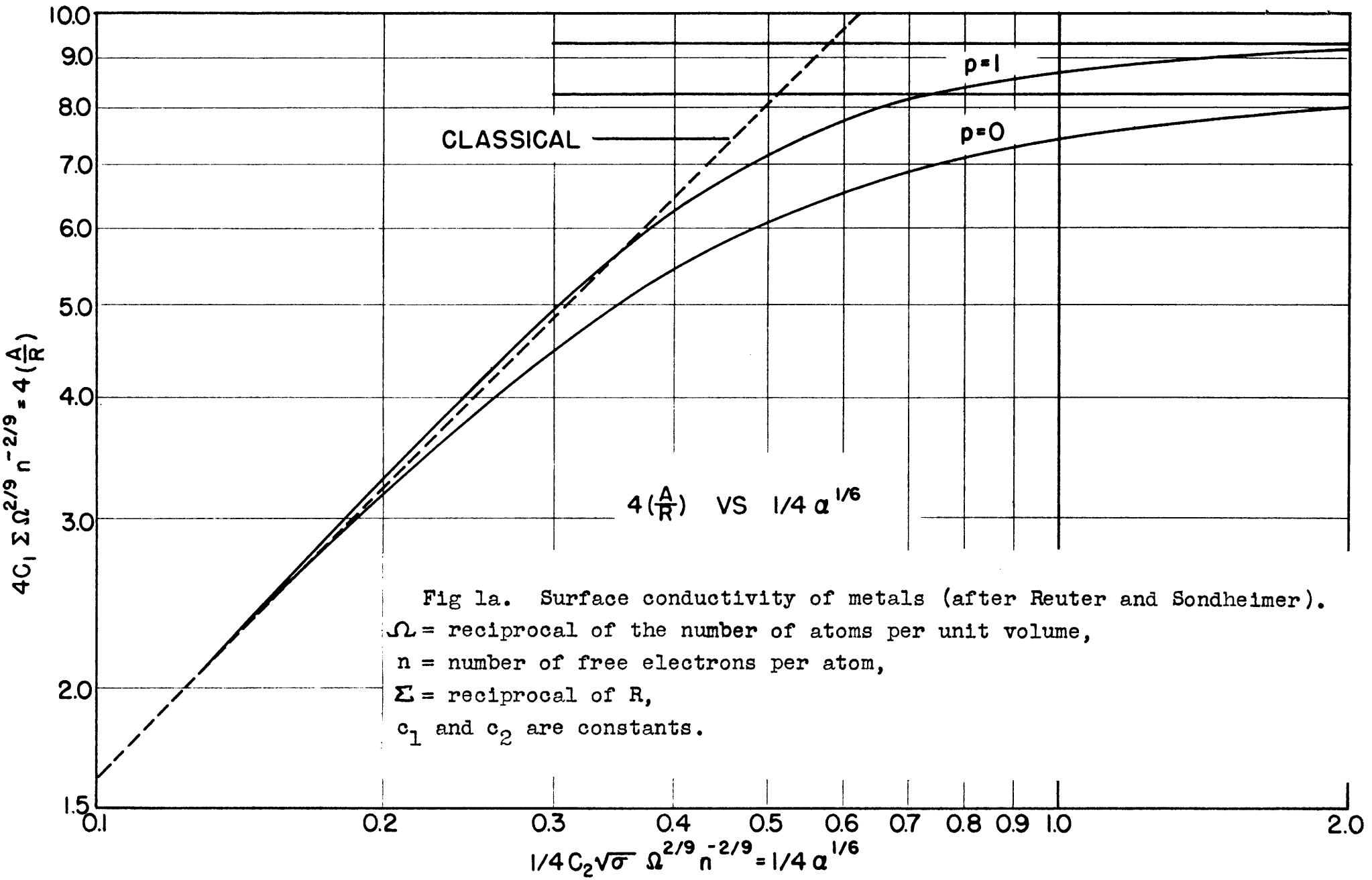

Fig 1a. Surface conductivity of metals (after Reuter and Sondheimer).
Ω = reciprocal of the number of atoms per unit volume,
n = number of free electrons per atom,
Σ = reciprocal of R,
c_1 and c_2 are constants.

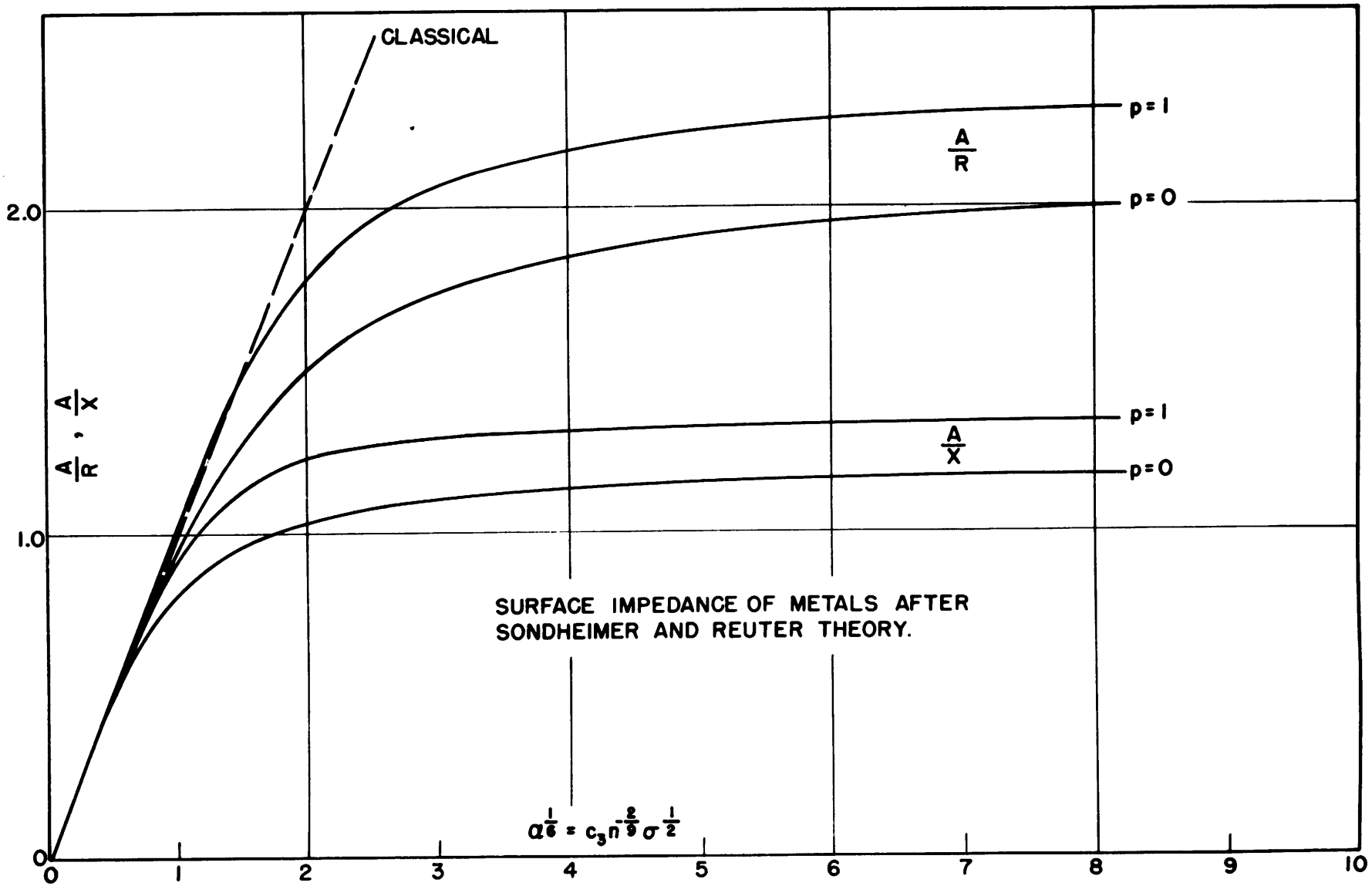
CLASSICAL
p = 1
A/R
p = 0
2.0
A/X , A/R
p = 1
A/X
p = 0
1.0
SURFACE IMPEDANCE OF METALS AFTER
SONDHEIMER AND REUTER THEORY.
$\alpha^{\frac{1}{6}} = c_3 n^{-\frac{2}{9}} \sigma^{\frac{1}{2}}$
0
0
1
2
3
4
5
6
7
8
9
10

FIG 1b.

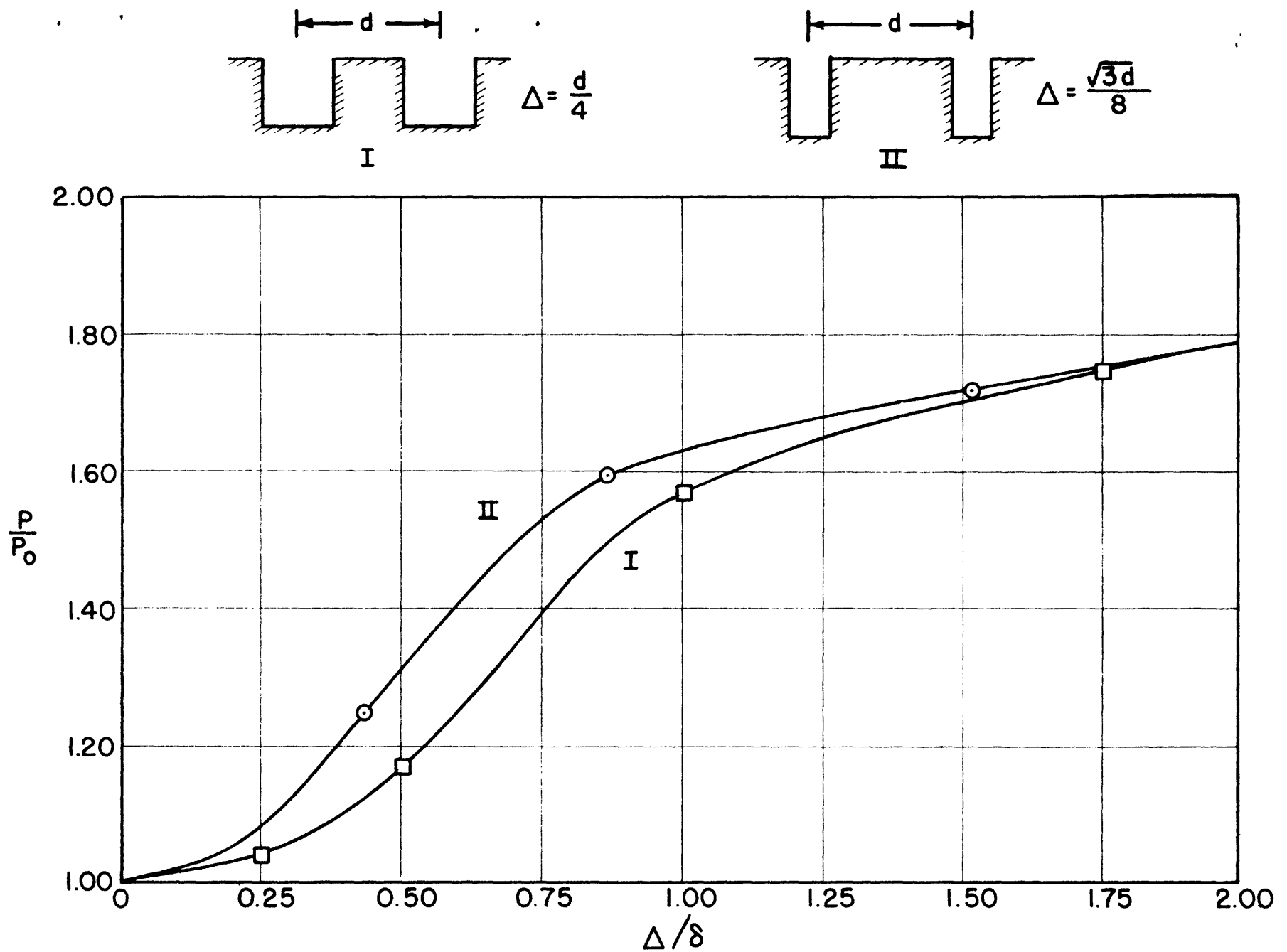

Fig 2. Relative power loss vs (rms roughness)/(skin depth). (after Morgan).

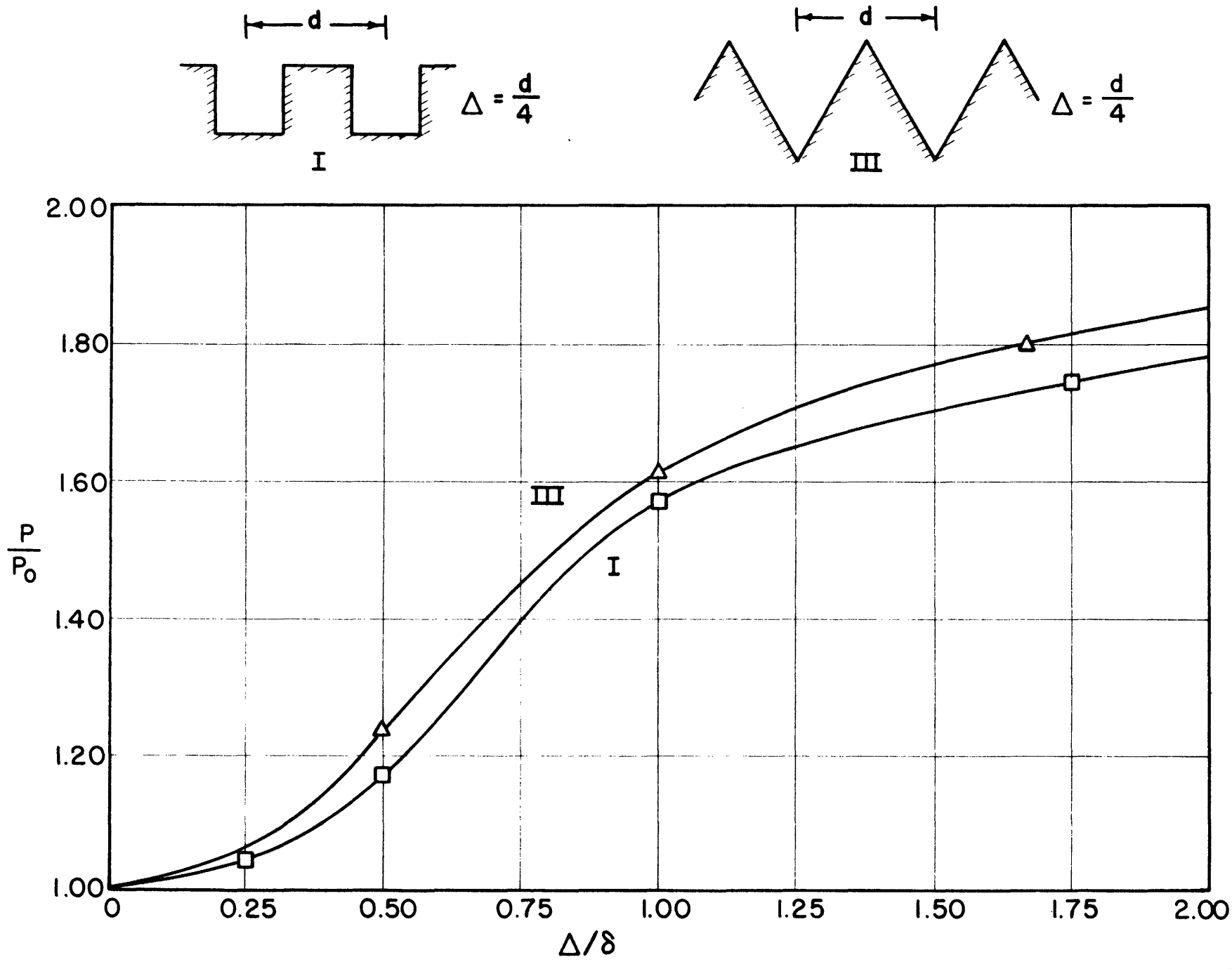

Fig 3. Relative power loss vs (rms roughness)/(skin depth); (after Morgan).

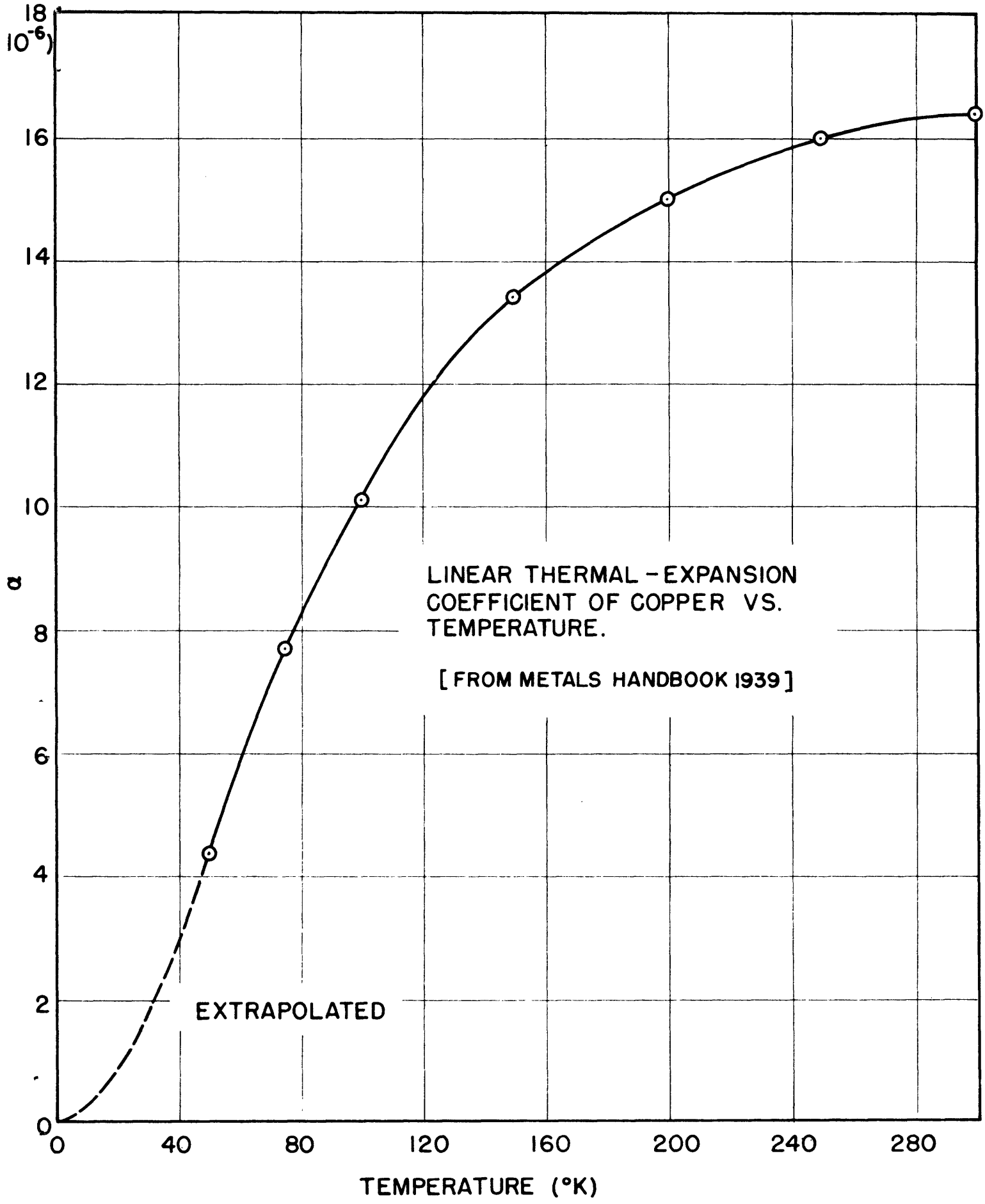
18
10^{-6})
16
14
12
10
α
8
6
4
2
0
0
40
80
120
160
200
240
280
TEMPERATURE (°K)
LINEAR THERMAL-EXPANSION COEFFICIENT OF COPPER VS. TEMPERATURE.
[FROM METALS HANDBOOK 1939]
EXTRAPOLATED

Fig 4.

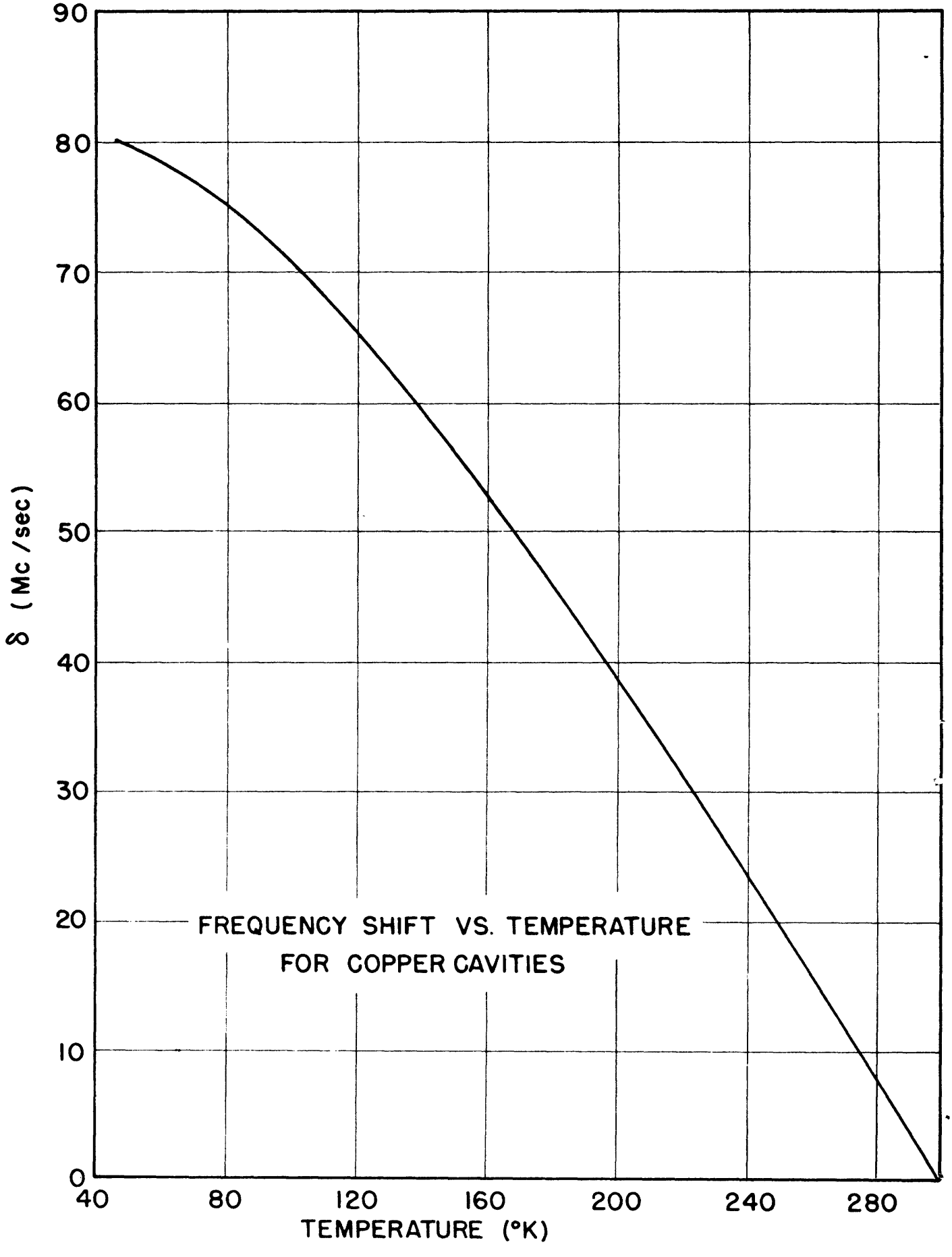
90
80
70
60
50
40
30
20
10
0
δ (Mc/sec)
FREQUENCY SHIFT VS. TEMPERATURE
FOR COPPER CAVITIES
40
80
120
160
200
240
280
TEMPERATURE (°K)

Fig 5.

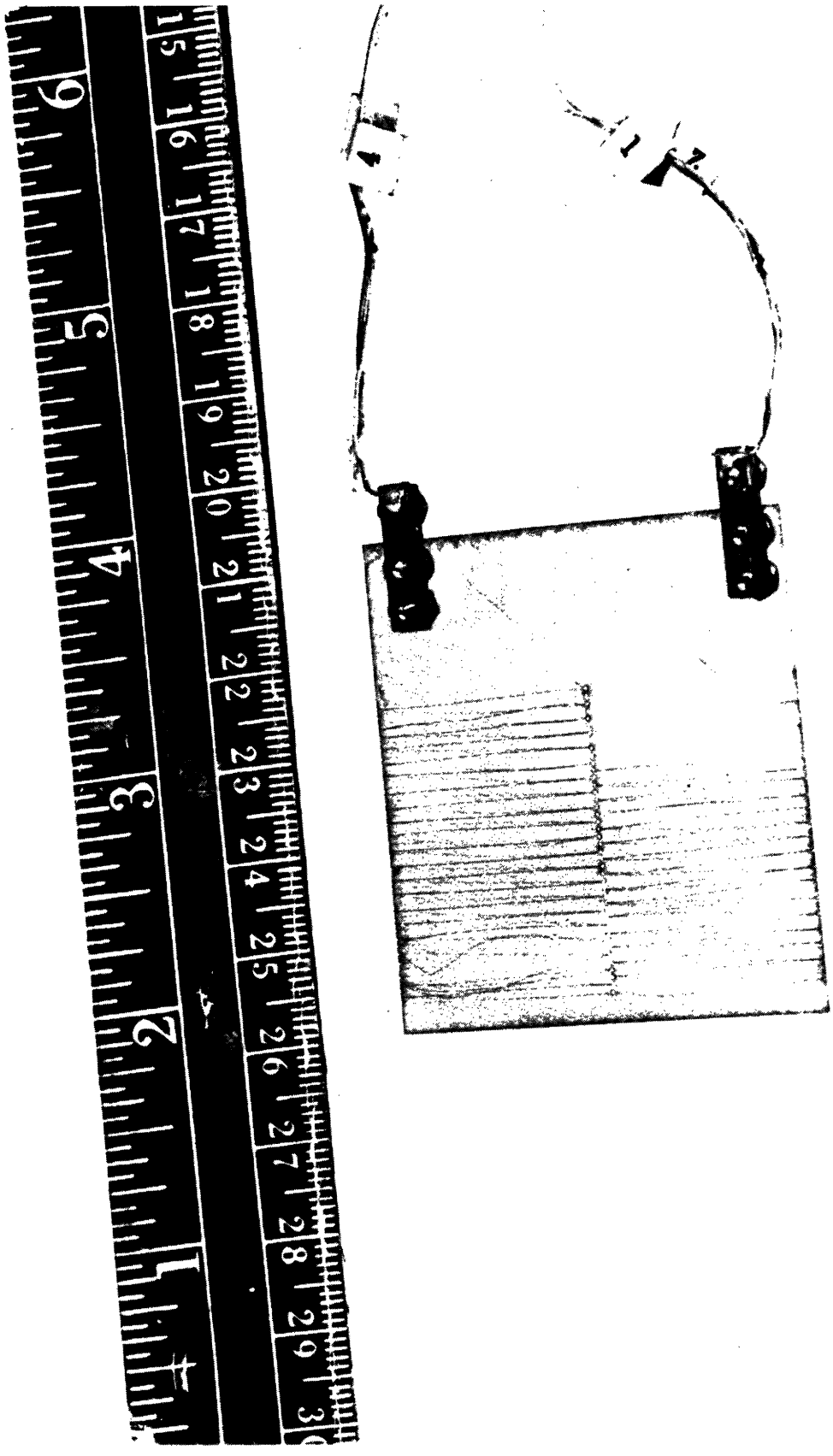

FIG 6. GOLD RESISTANCE THERMOMETER.

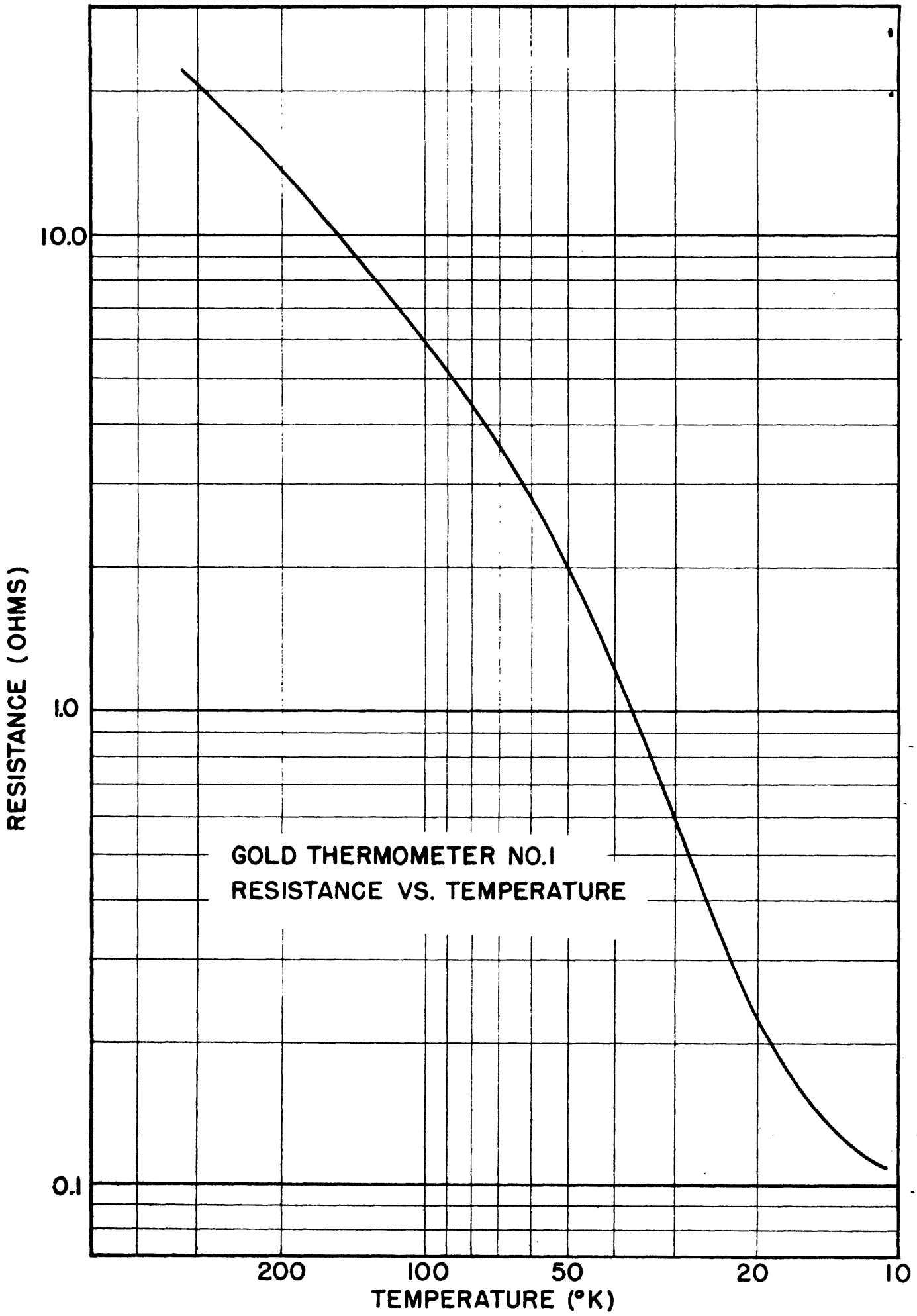
10.0
1.0
0.1
RESISTANCE (OHMS)
GOLD THERMOMETER NO.1
RESISTANCE VS. TEMPERATURE
200
100
50
20
10
TEMPERATURE (°K)

Fig 7.

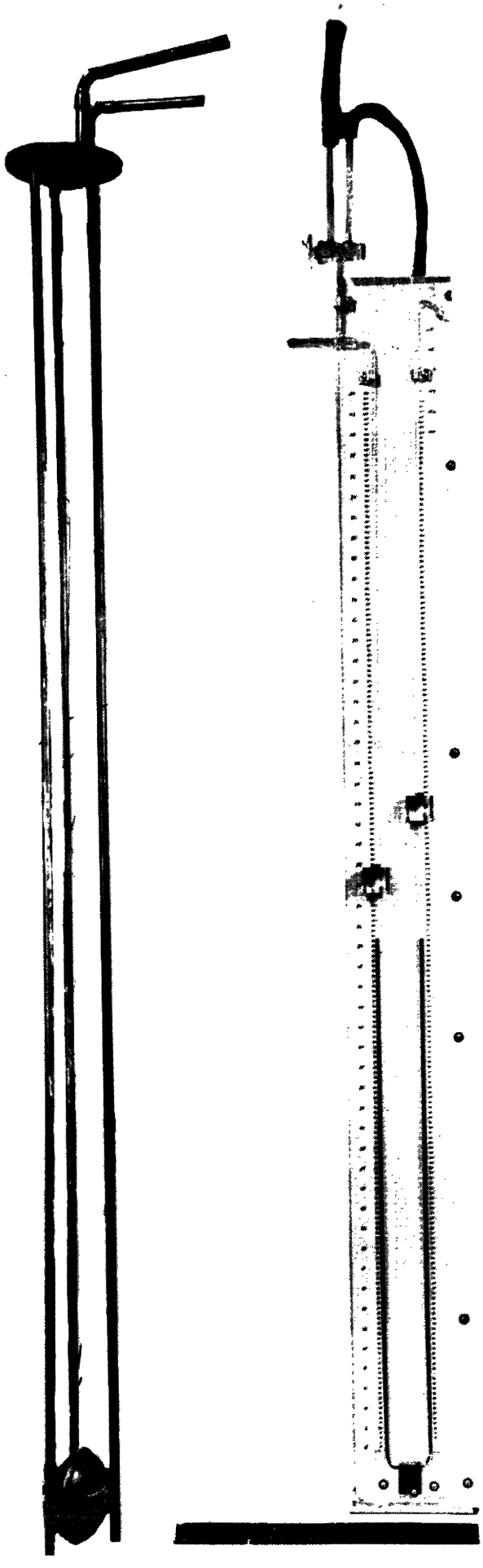

FIG 8. HELIUM-GAS THERMOMETER.

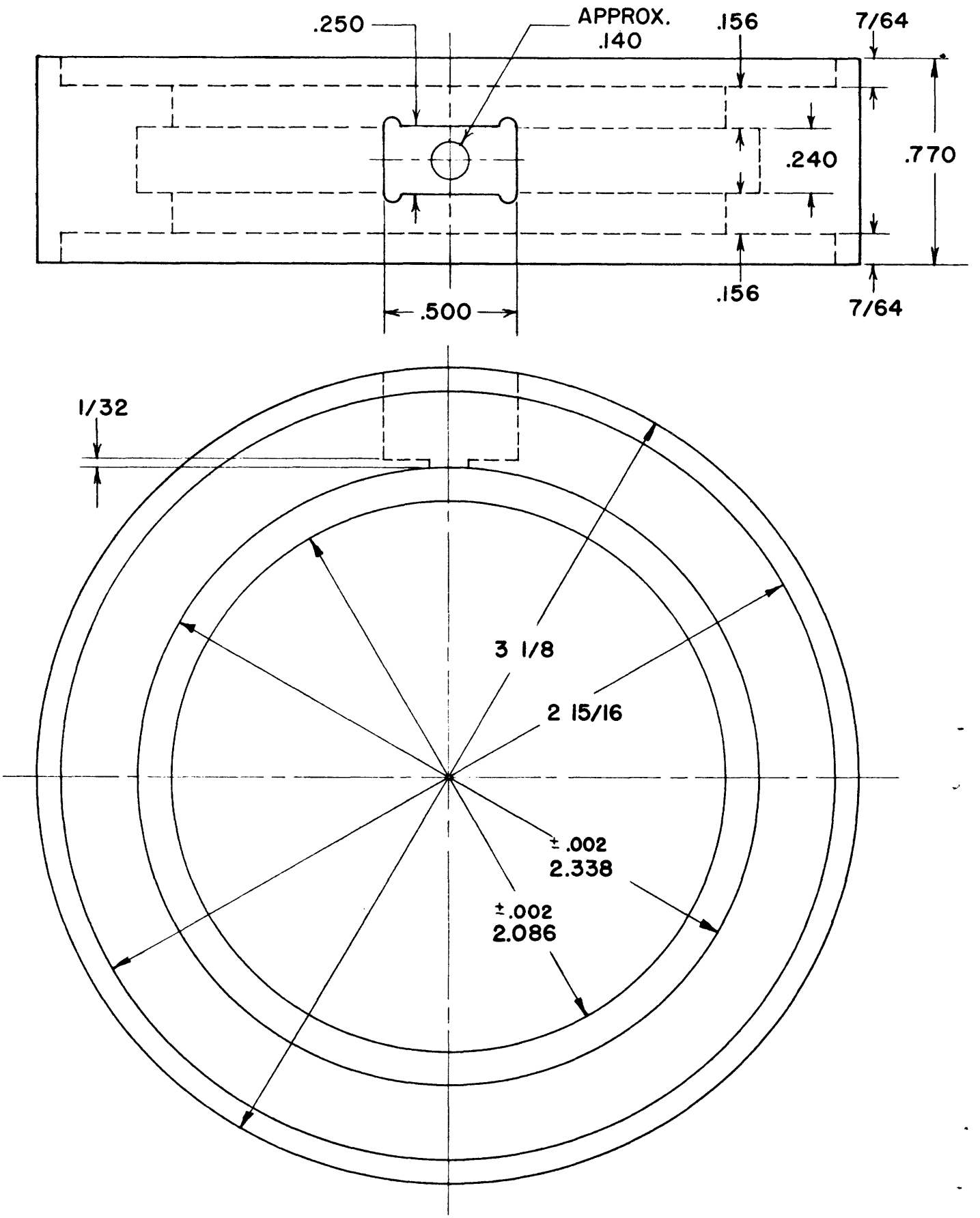

Fig 9. Scale drawing of the microwave cavity.

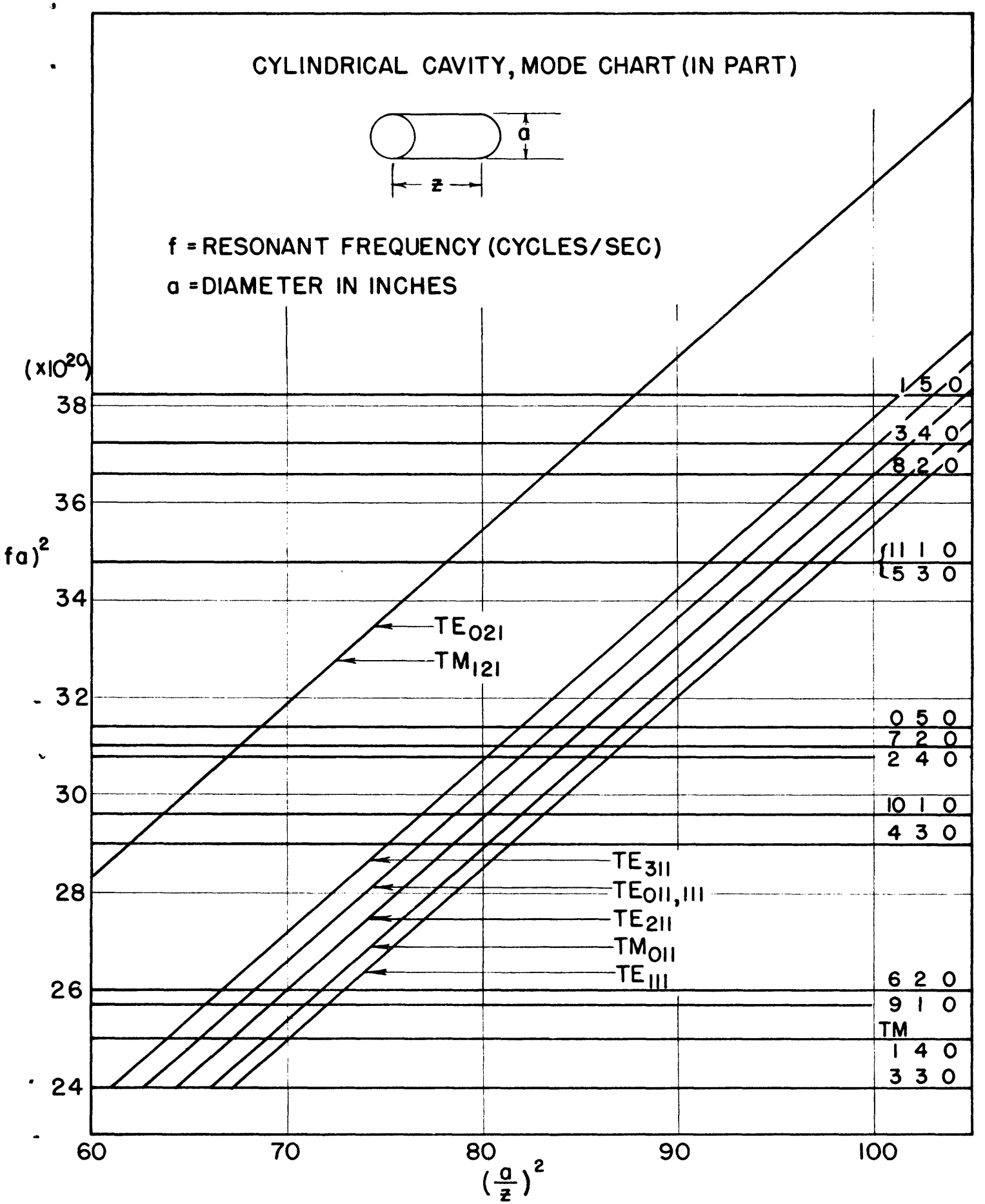

Fig 10. Section of the mode chart for a cylindrical cavity.

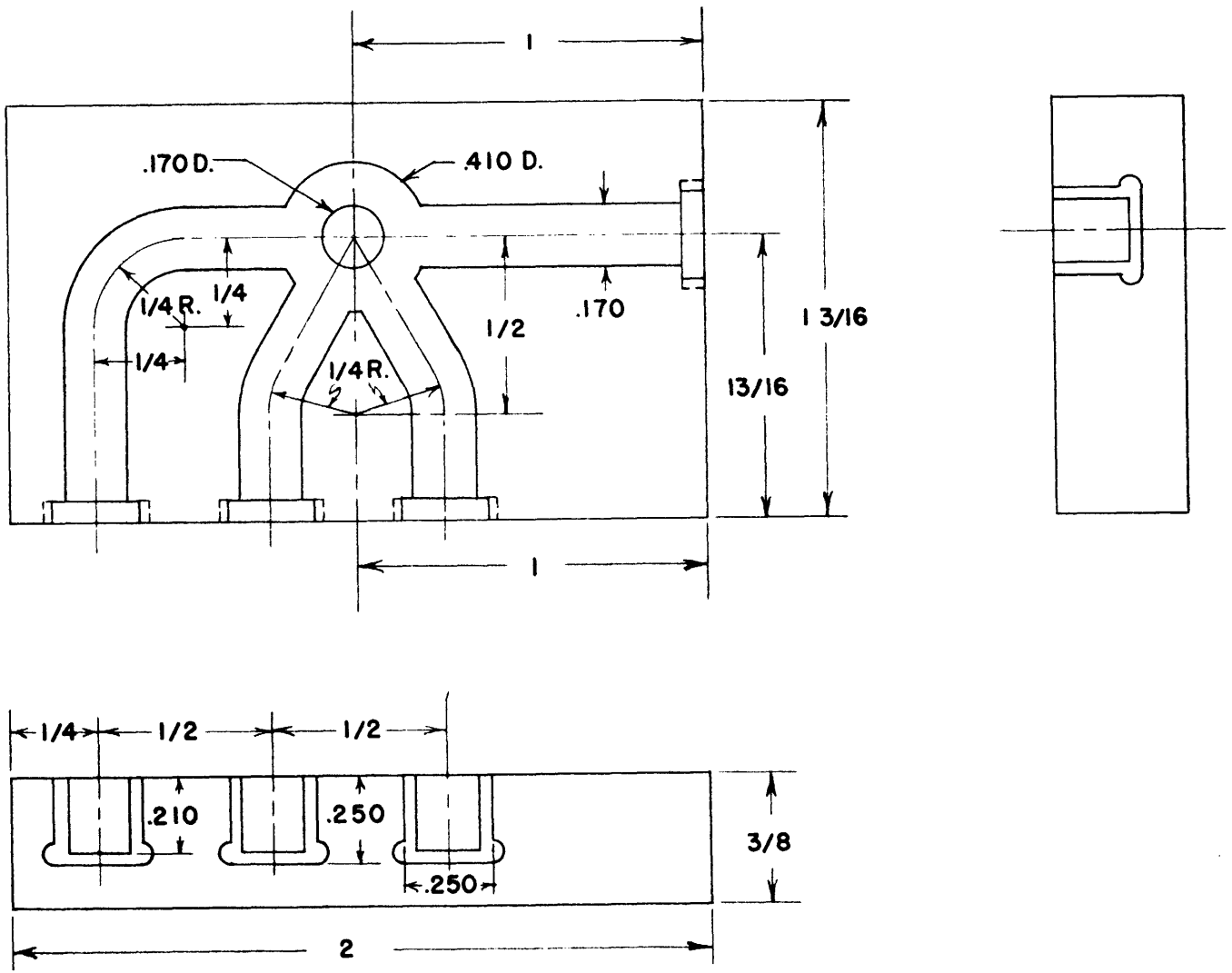

Fig 12. Scale drawing of rat race I.

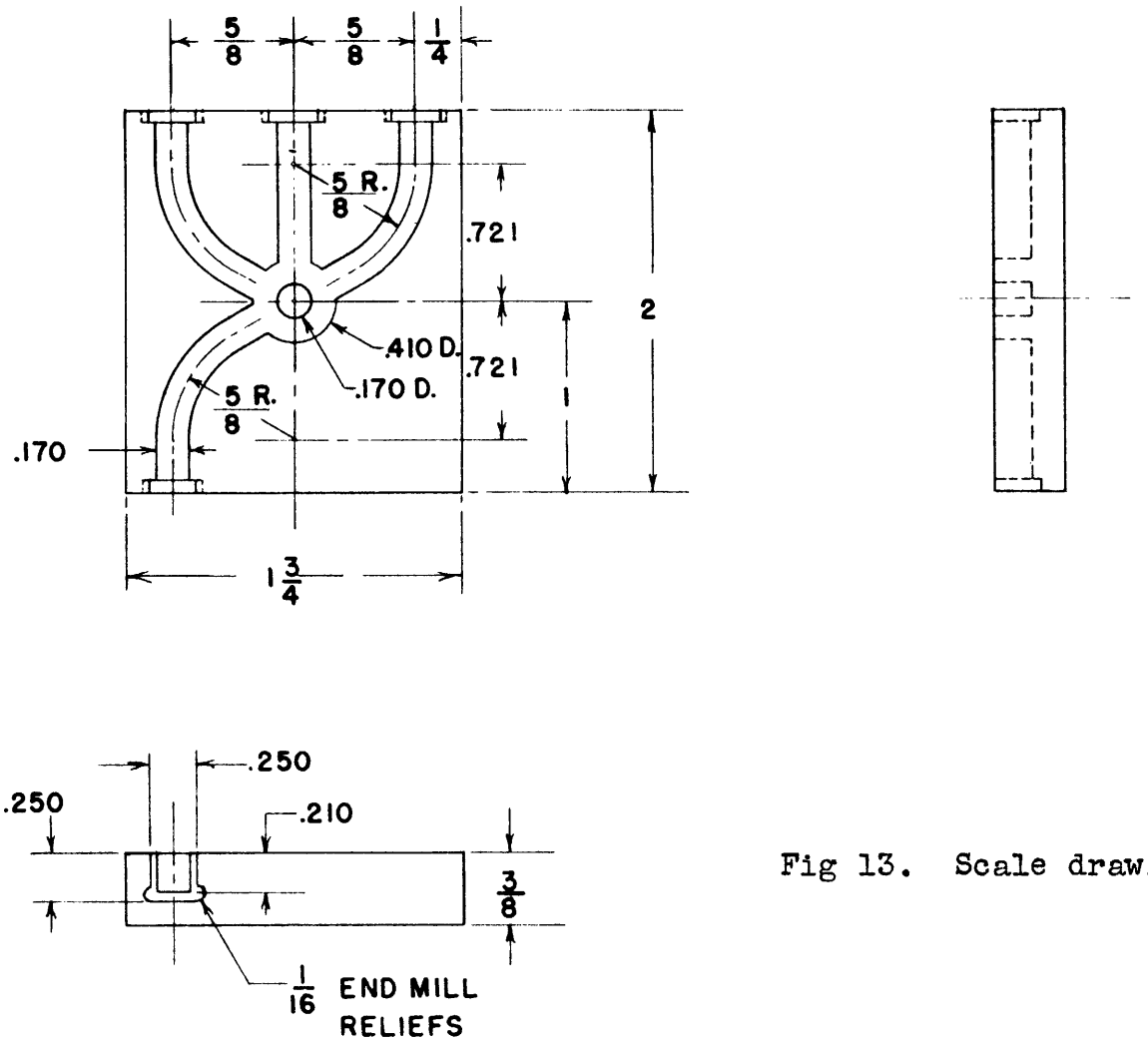

Fig 13. Scale drawing of rat race II.

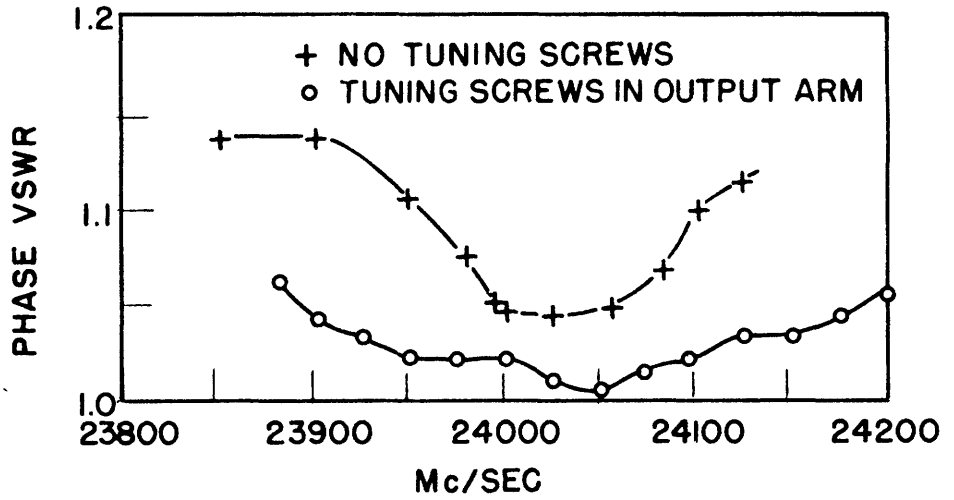

Fig 14a. Phase VSWR vs frequency: Rat race I.

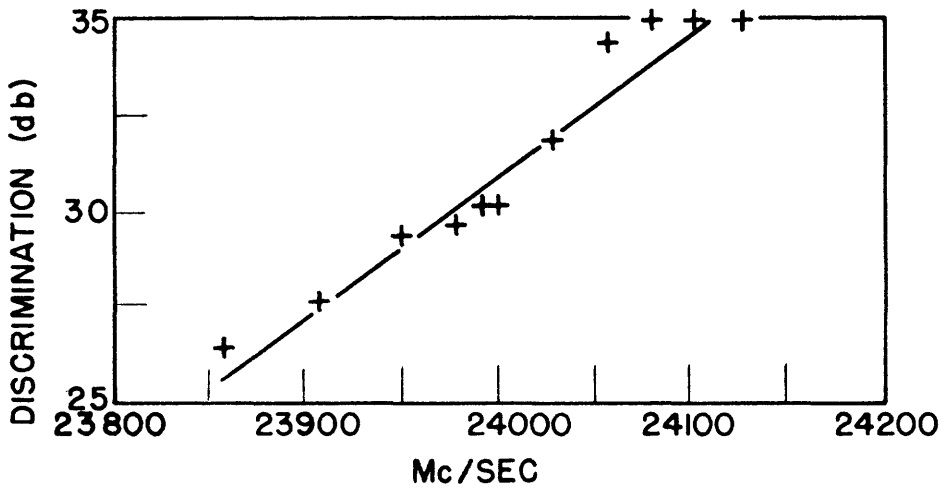

Fig 14b. Discrimination vs frequency: Rat race I, no tuning screws.

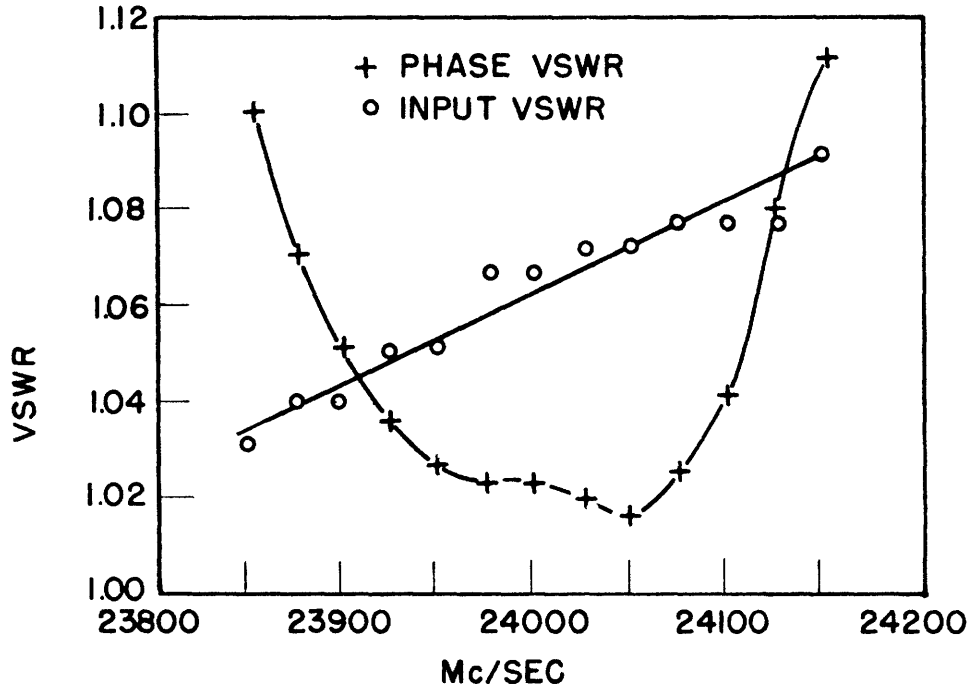

Fig 15a. Phase VSWR vs frequency, and input VSWR vs frequency: Rat race II, no tuning screws.

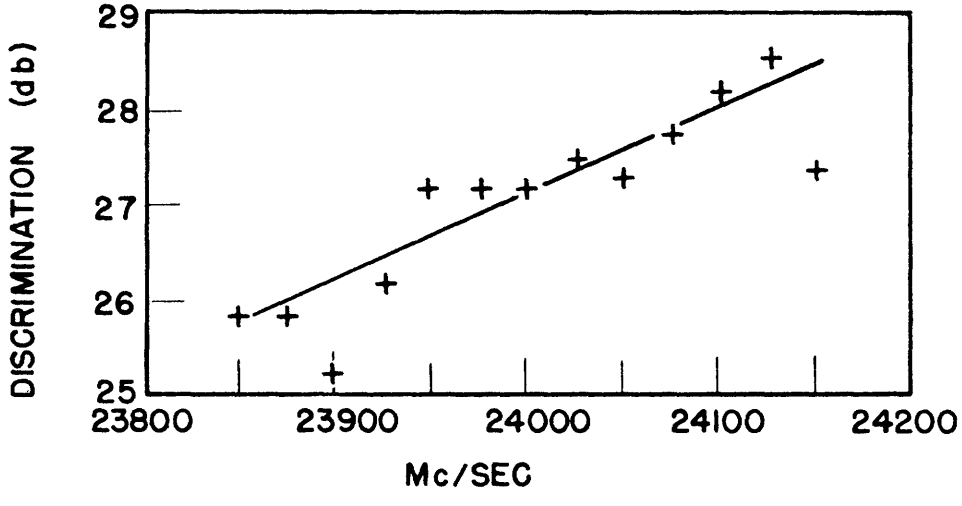

Fig 15b. Discrimination vs frequency: Rat race II, no tuning screws.

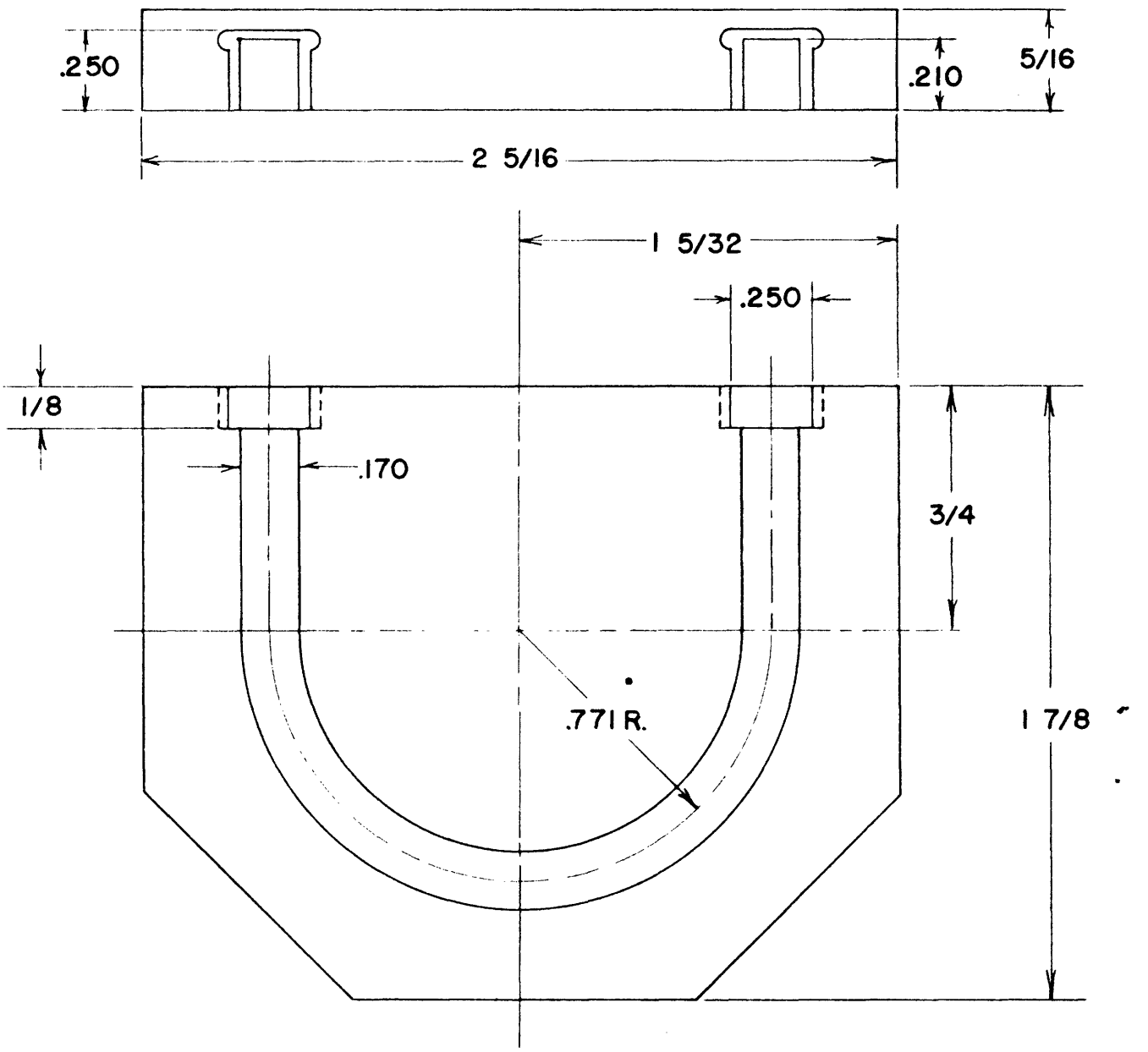

Fig 16. Scale drawing of 180° precision bend.

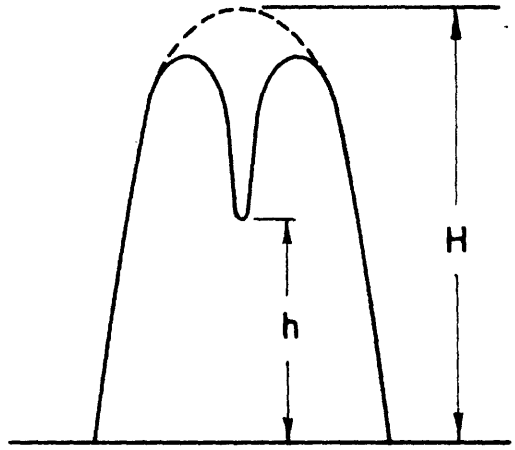

Fig 17. Single-mode oscilloscope presentation.

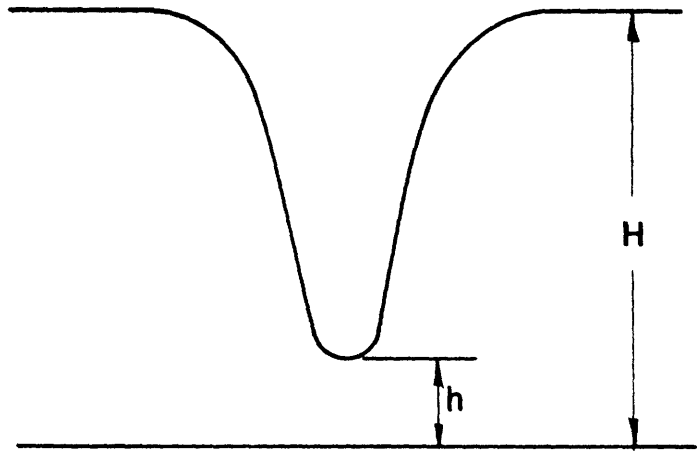

Fig 18. Mechanical-sweep oscilloscope presentation.

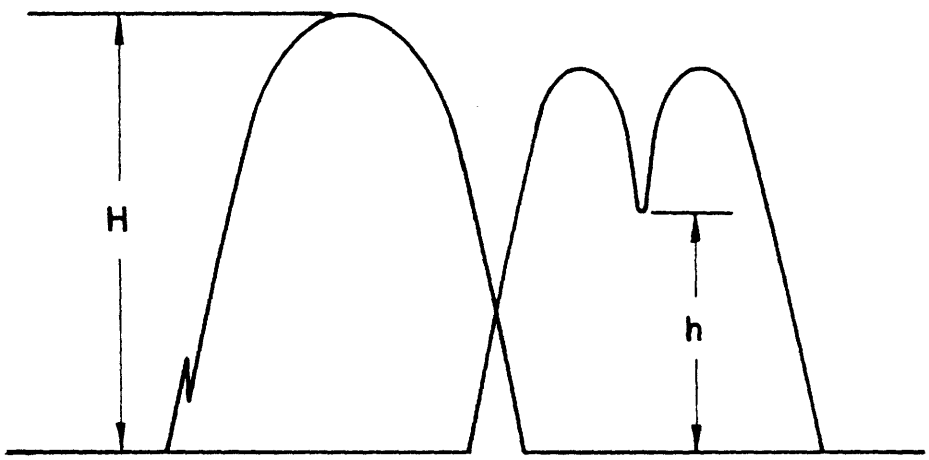

Fig 19. Double-mode oscilloscope presentation.

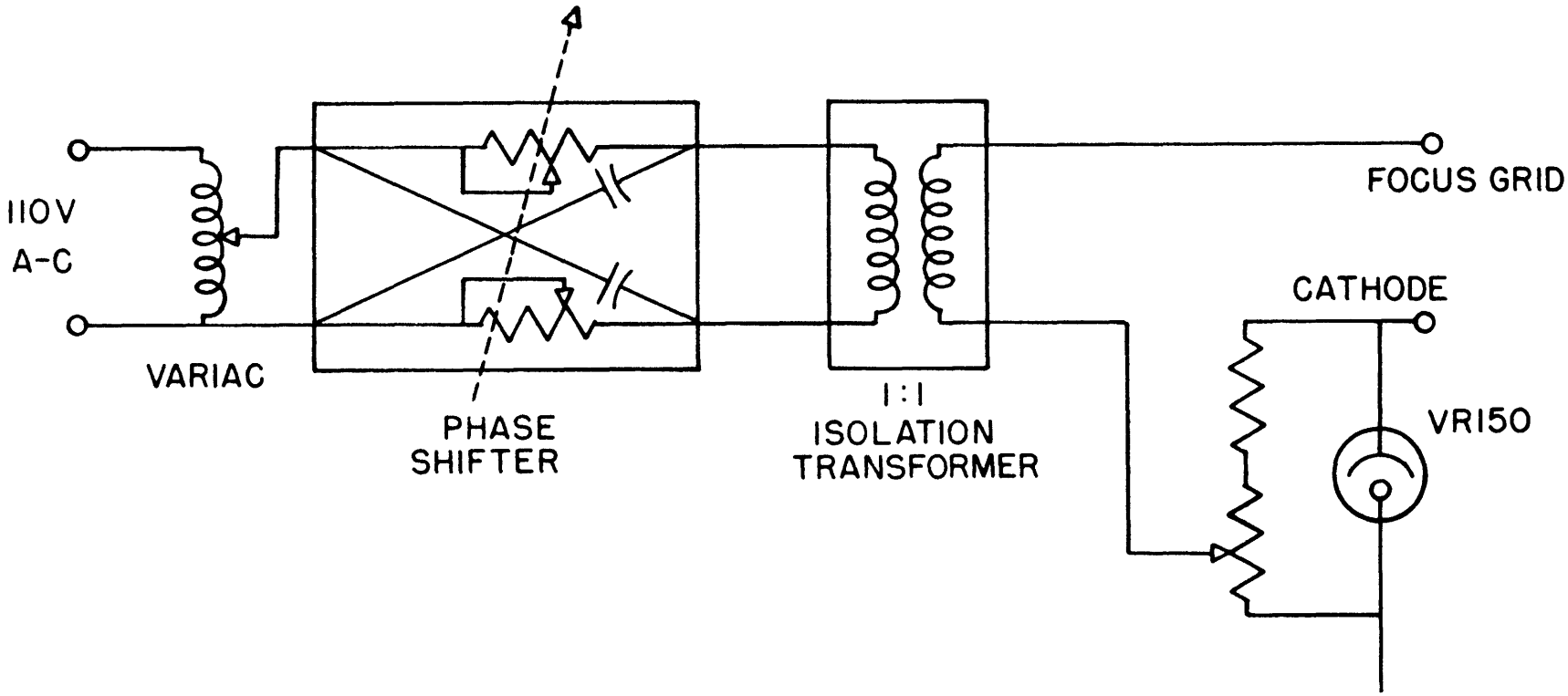

Fig 20. Circuit for modulating the 2K33 focus grid.

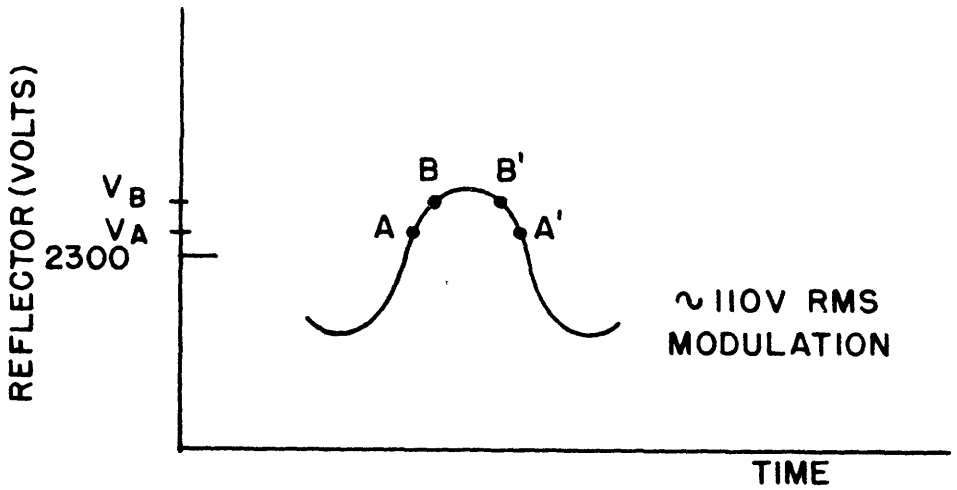

Fig 21. 2K33 reflector voltage vs time.

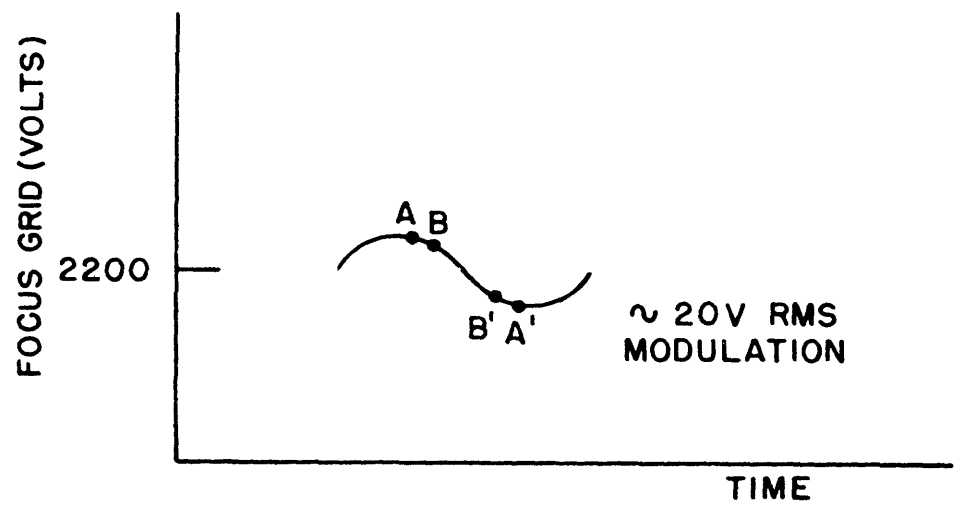

Fig 22. 2K33 focus grid voltage vs time.

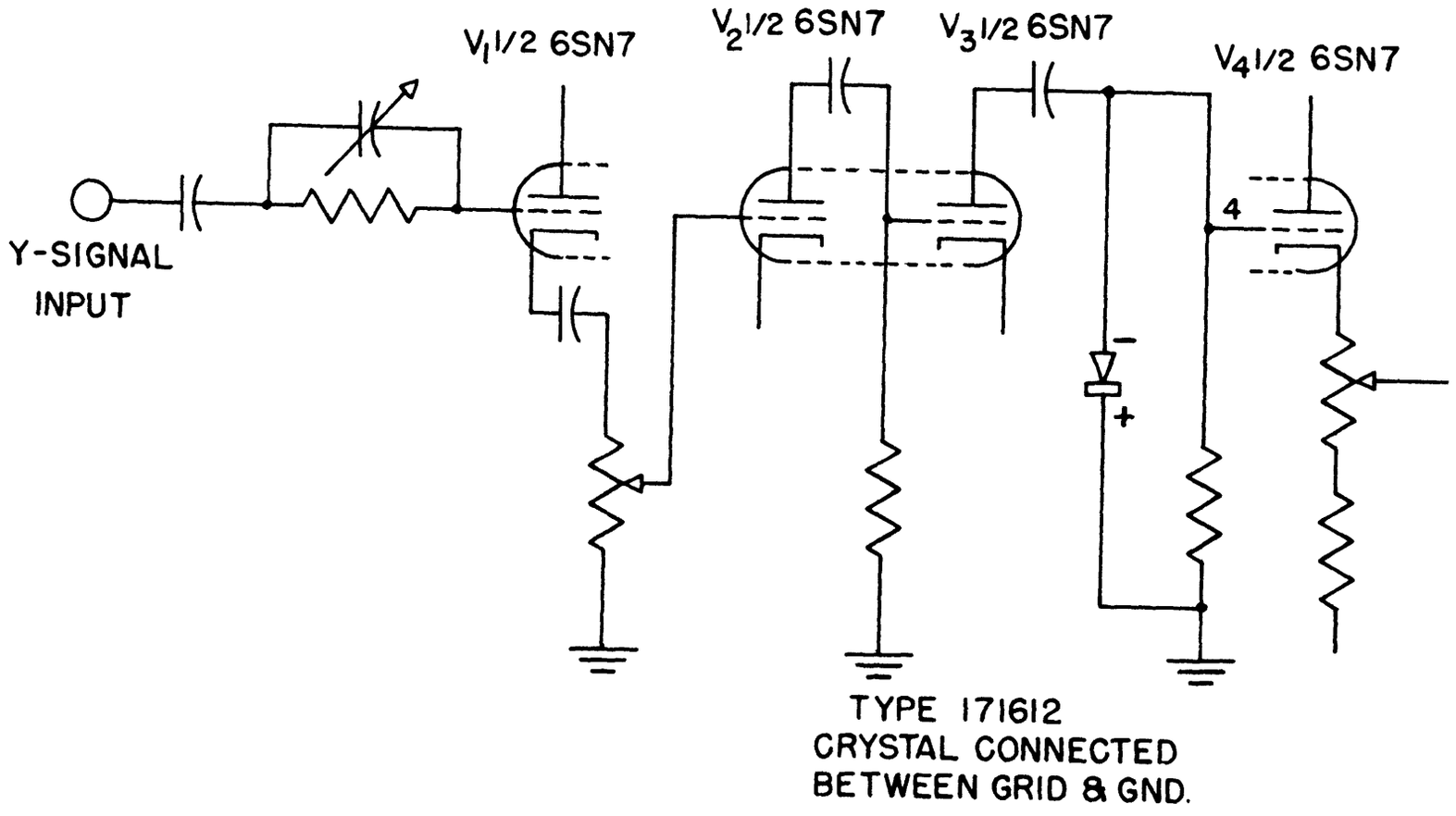

TYPE 208-B DUMONT OSCILLOSCOPE

Fig 23. Circuit showing base-line clamping crystal.

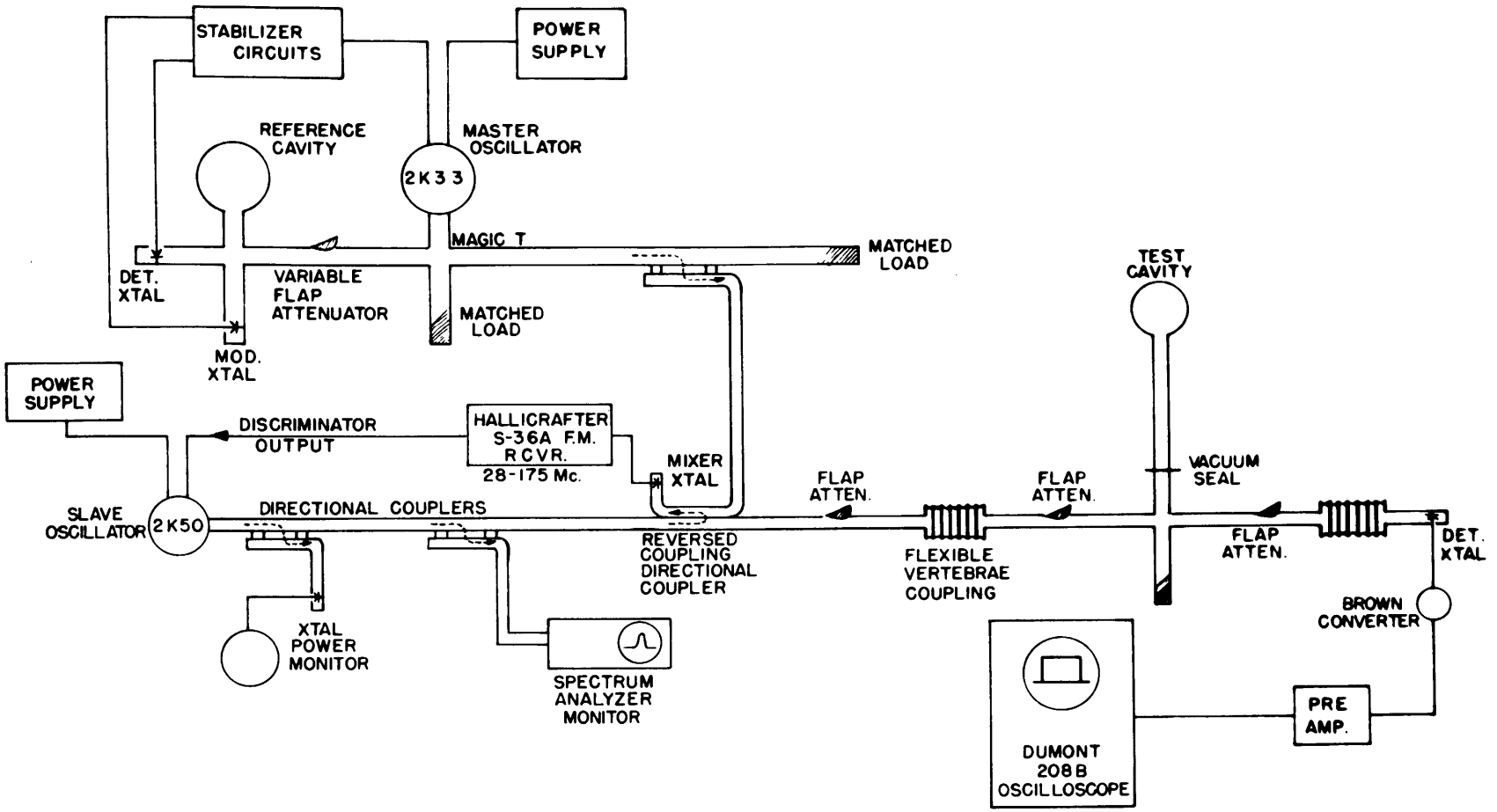

PLUMBING DETAILS OF MASTER AND
SLAVE OSCILLATOR ARRANGEMENT

FIG 24

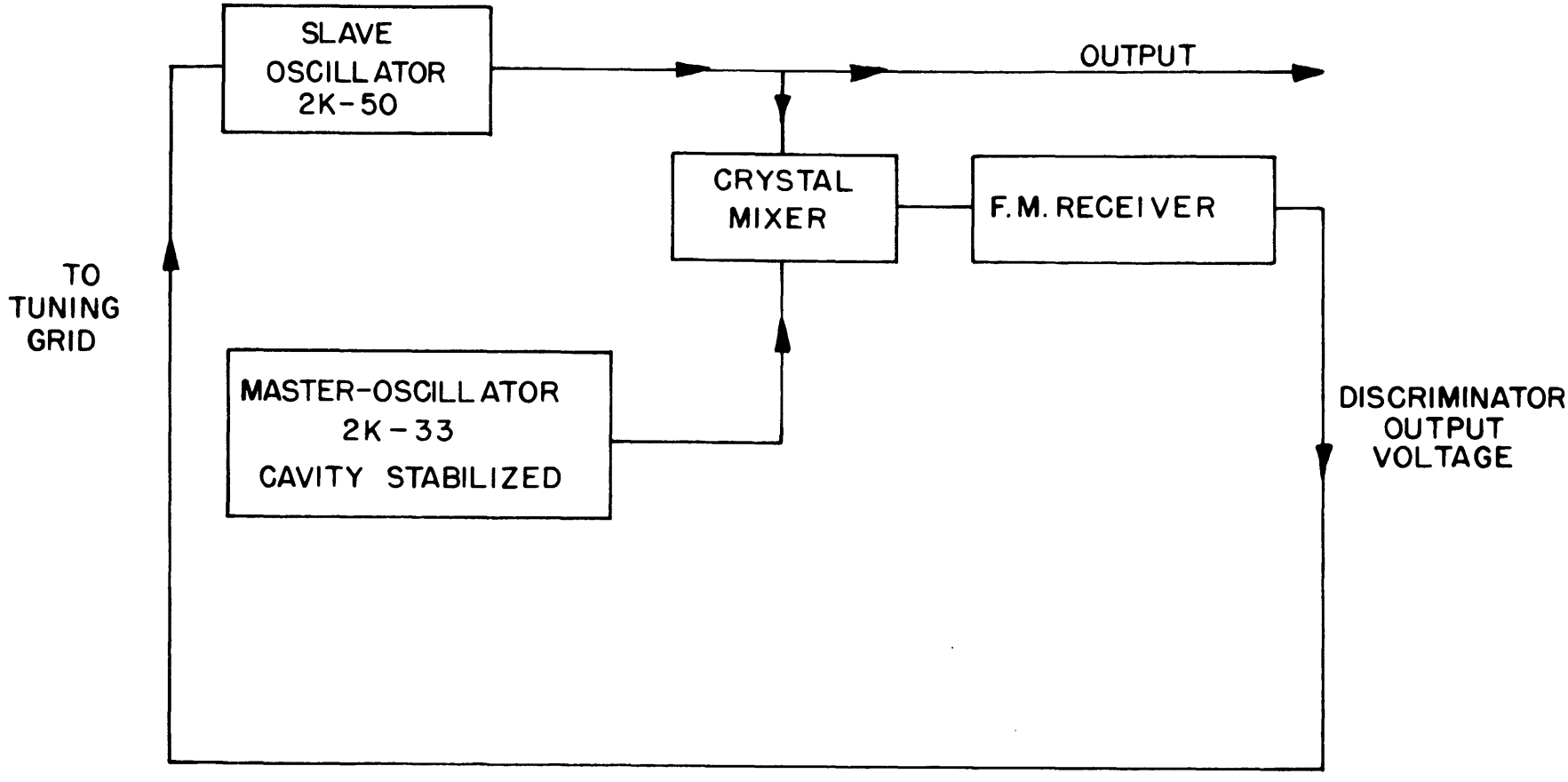

ARRANGEMENT OF MASTER AND SLAVE OSCILLATORS

FIG 25

FIG 26. SEALED CAVITY (VIII).

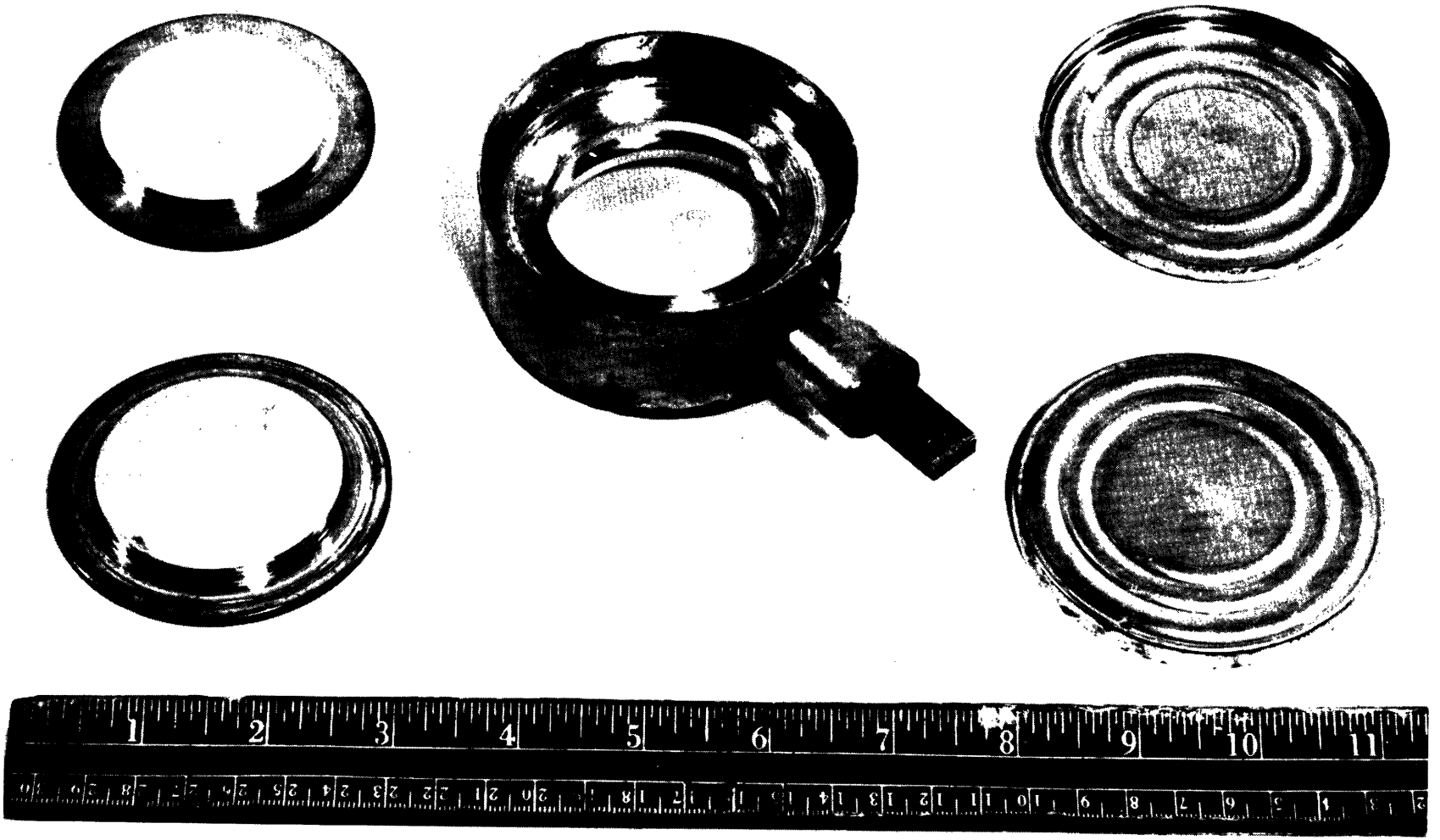

FIG 27. UNSEALED CAVITY (VIII).

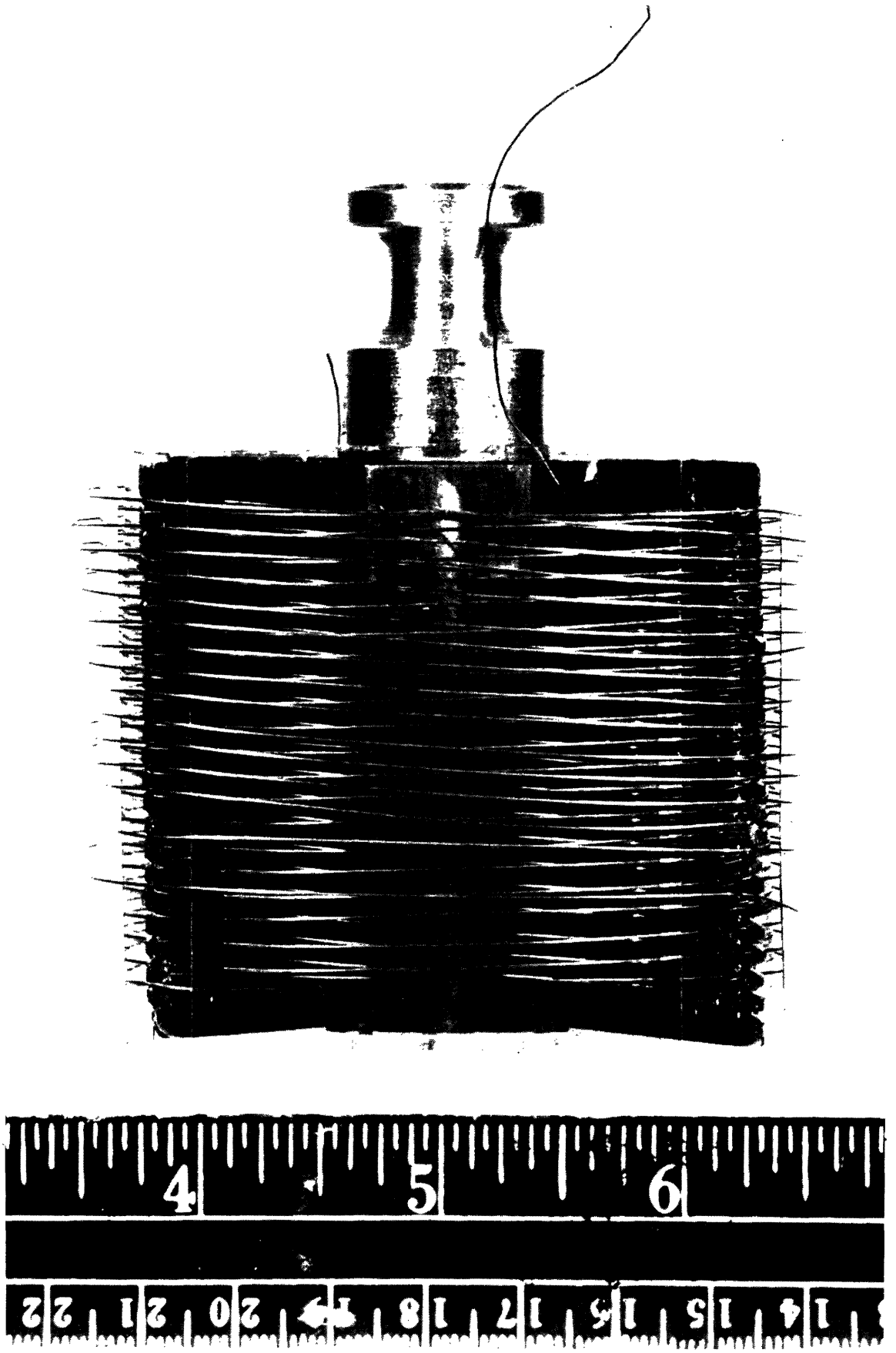

FIG 28A. COPPER COIL, SIDE.

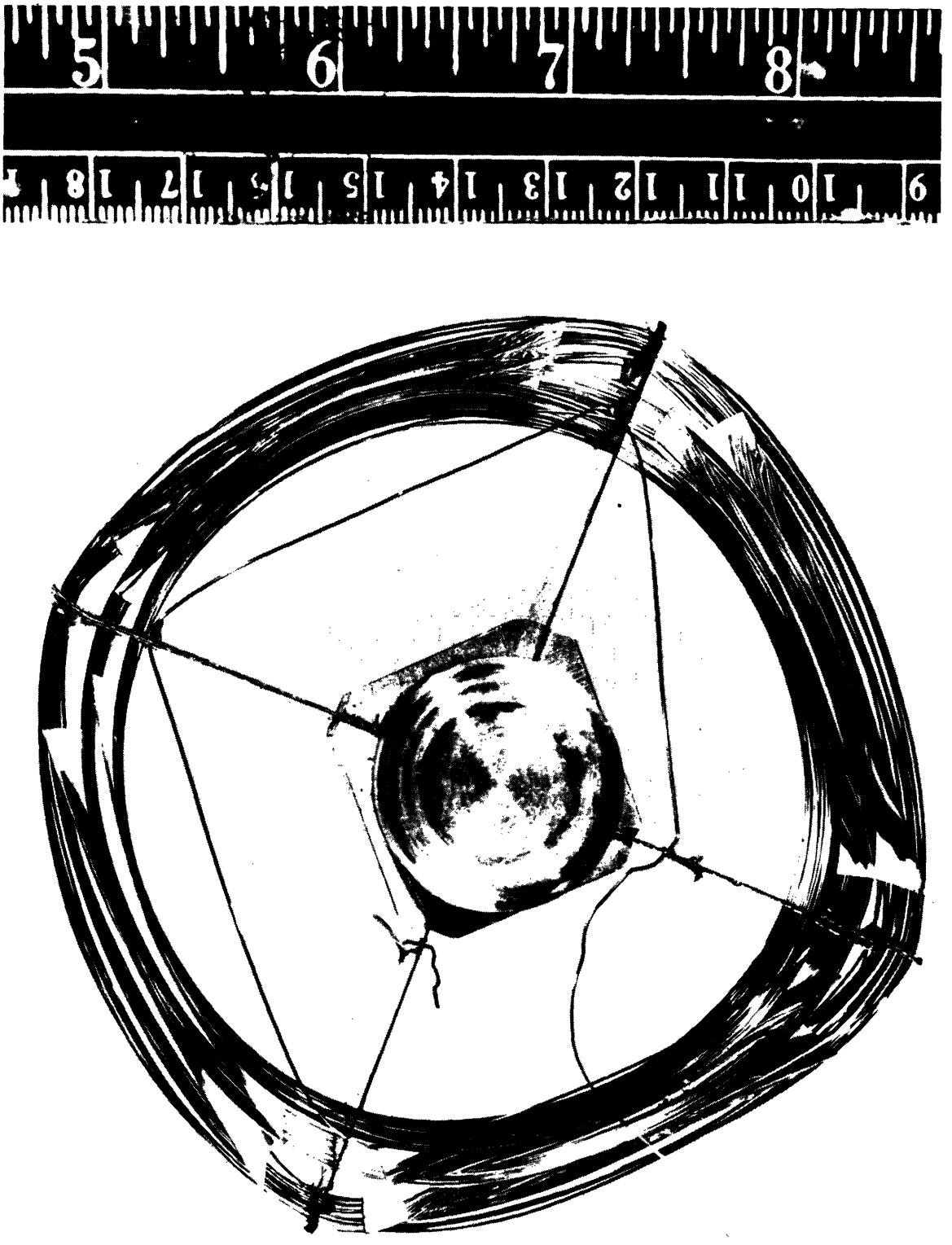

FIG 28B. COPPER COIL, TOP.

(a)

(b)

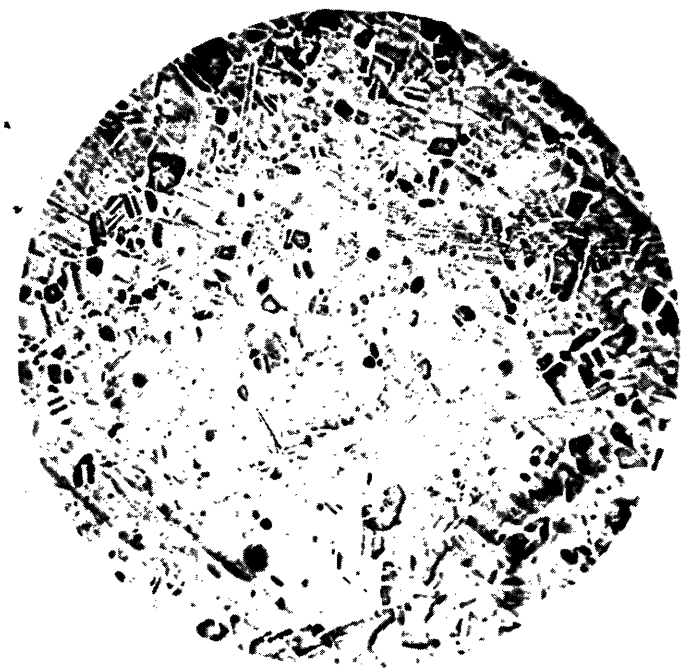

(c)

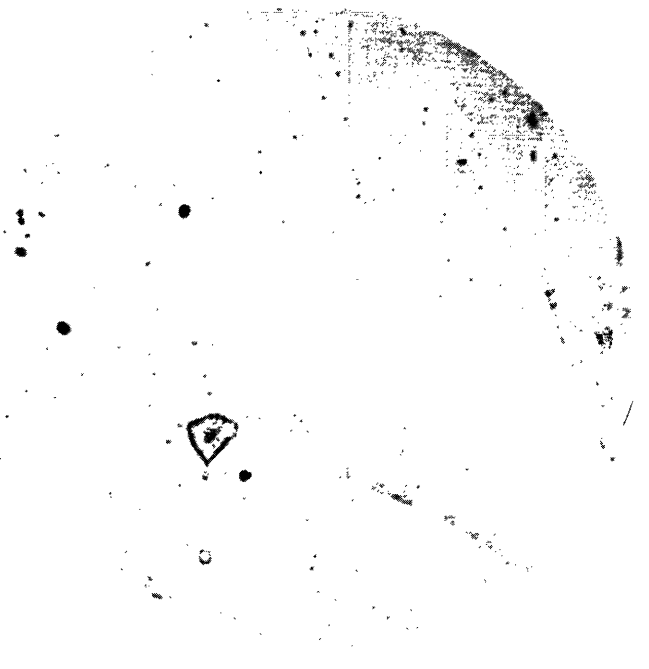

(d)

Fig 29. Photomicrographs of the two electropolished copper lids. (a) 30 X, (b) 500 X, (c) 25 X, (d) 500 X.

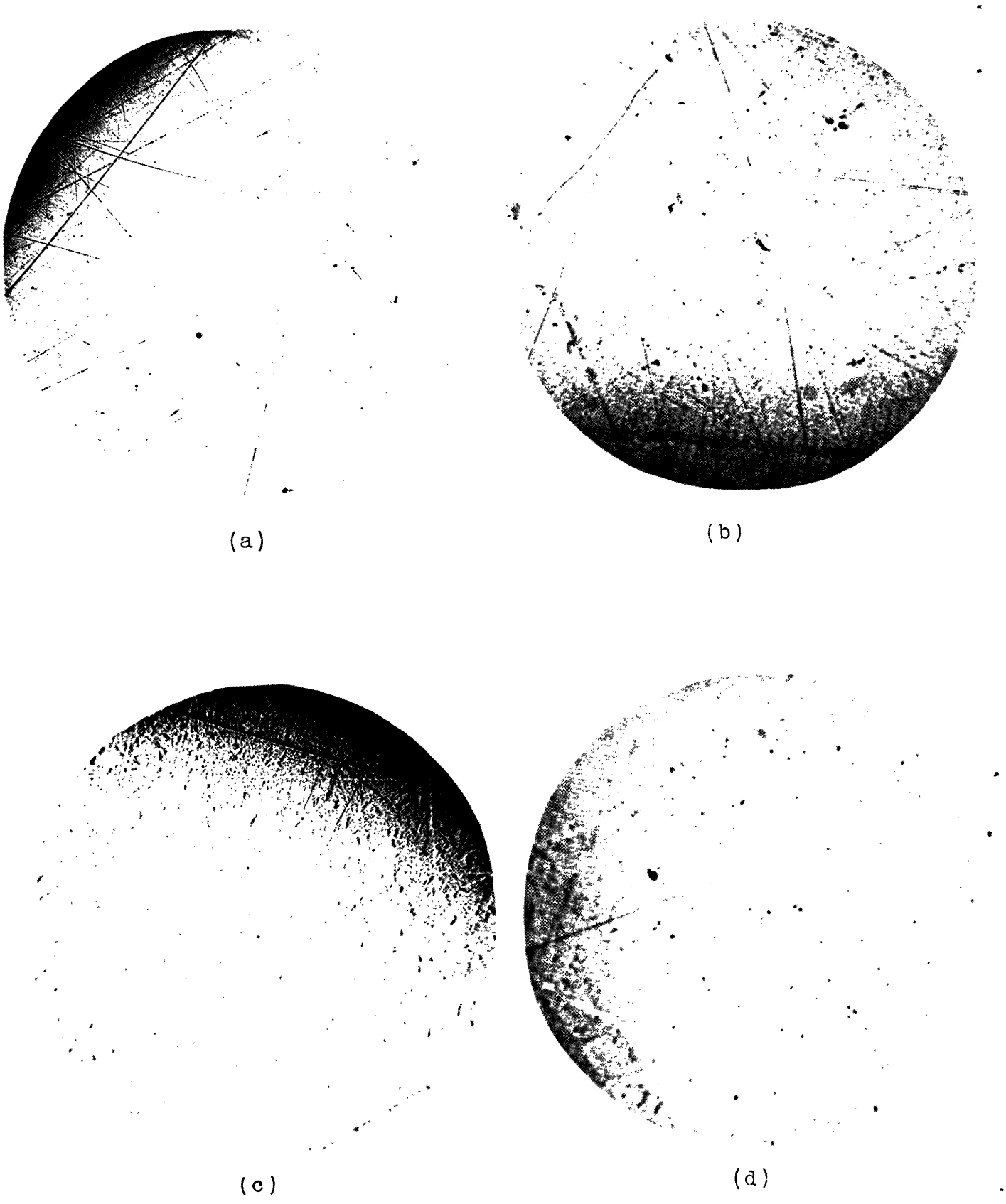

Fig 30. Photomicrographs of the two electropolished silver lids. (a) 25 X, (b) 500 X, (c) 25 X, (d) 500 X.

Fig 32. Photomicrographs of the two cast tin lids.
(a) 30 X, (b) 500 X, (c) 30 X, (d) 500 X.

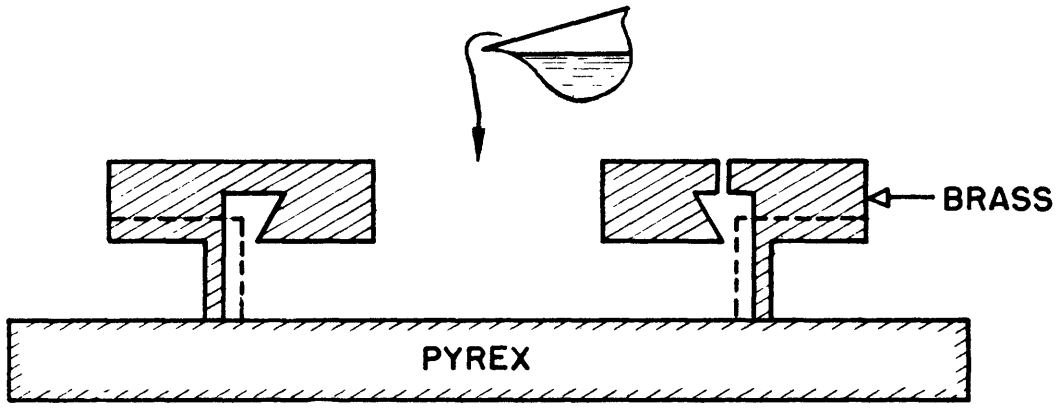

Fig 31. Schematic diagram of method for casting tin cavity lids against glass.

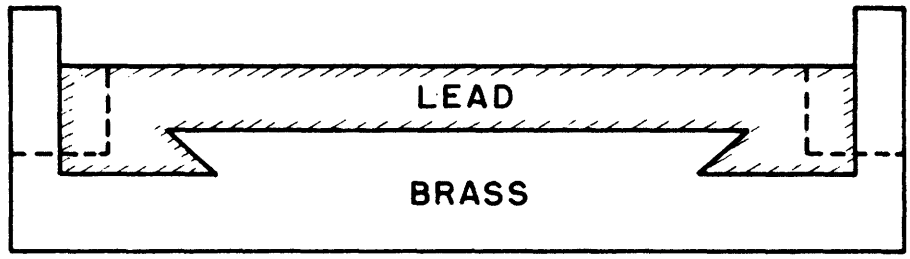

Fig 33. Schematic diagram of method for casting lead cavity lids.

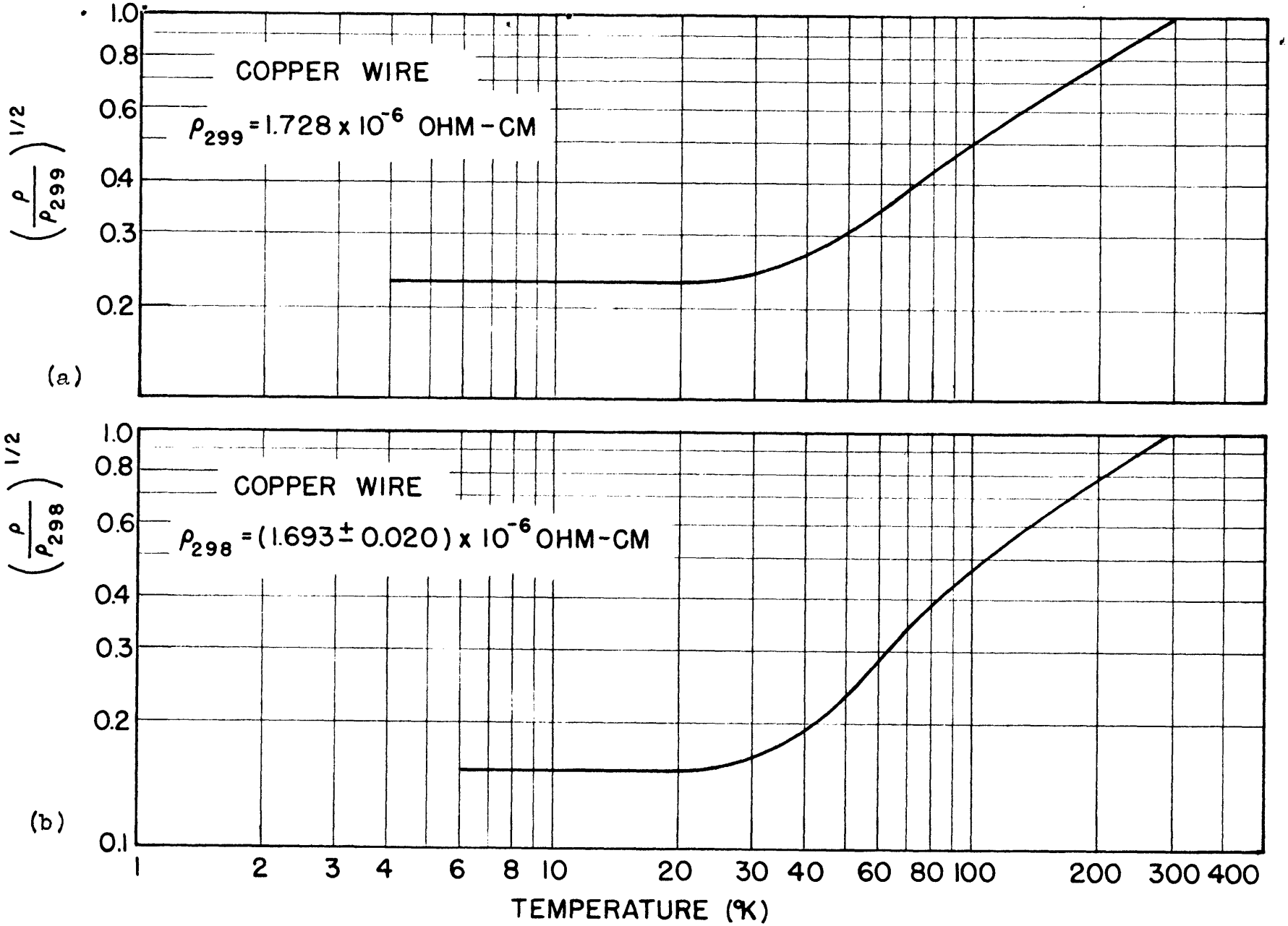

Fig 34. Relative d-c resistivity of copper. (a) stressed wire; (b) same wire annealed $\frac{1}{2}$ hour at 400°C.

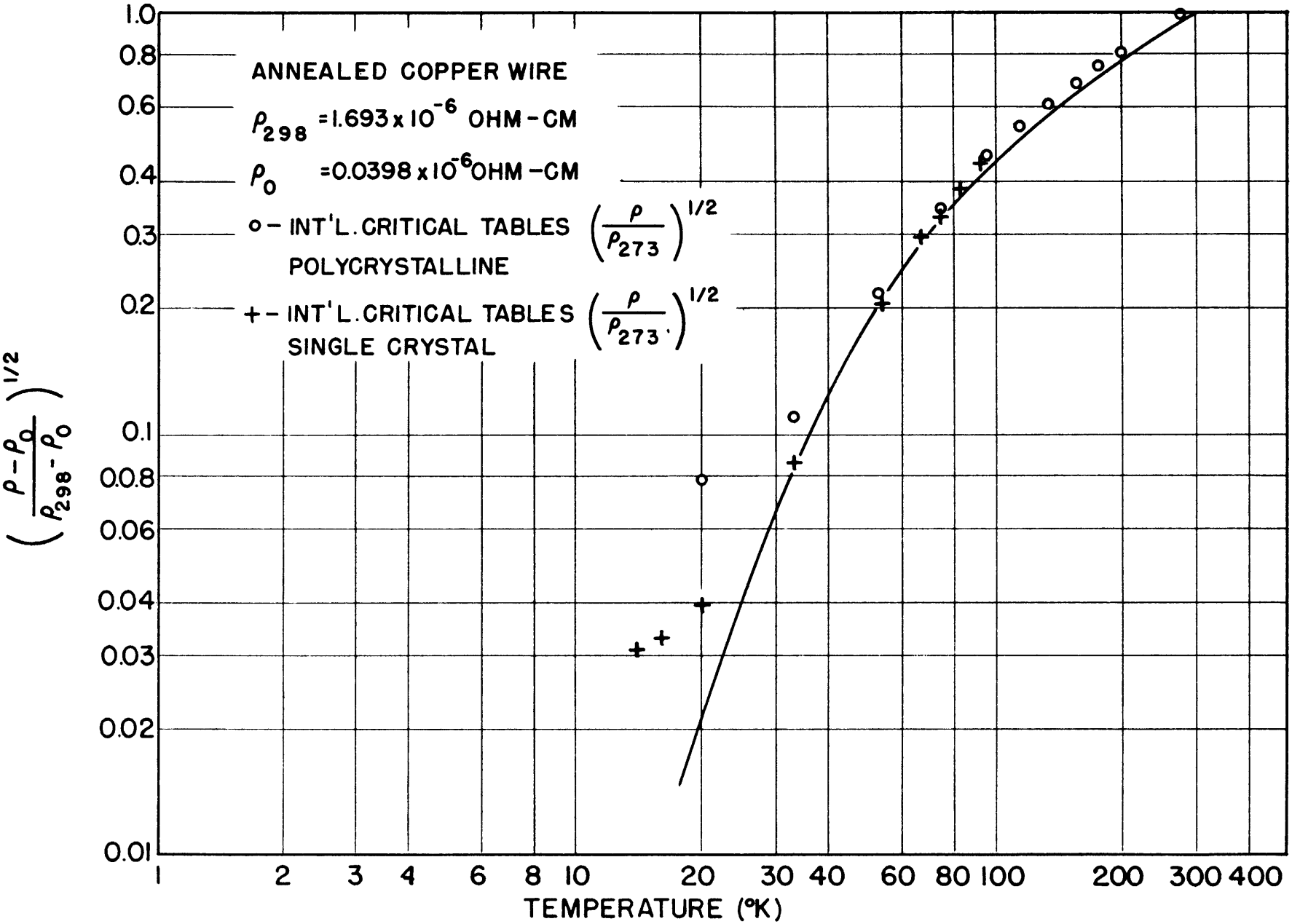

Fig 35. Relative d-c resistivity of "ideal" copper.

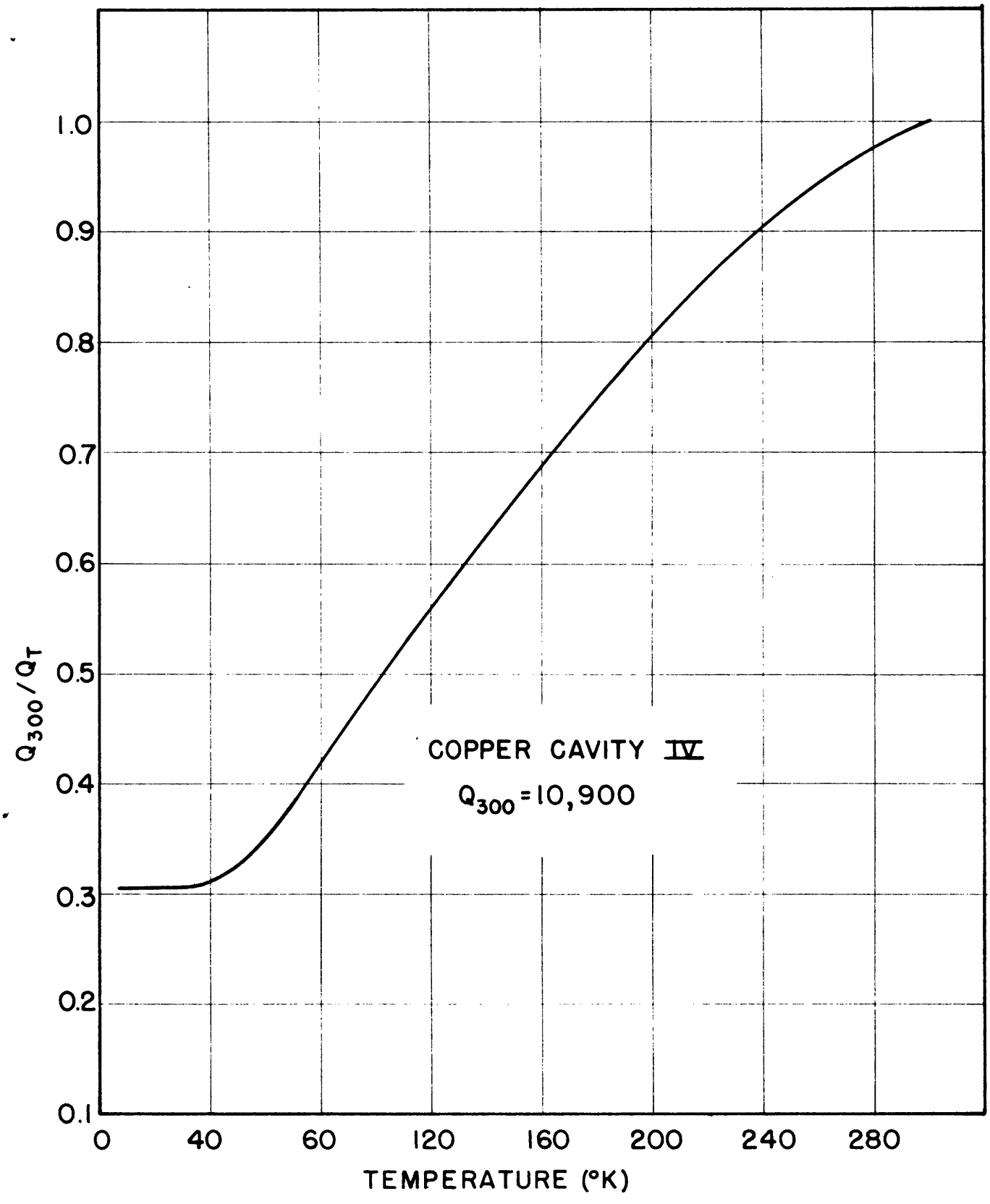

Fig 36. Relative Q_o vs temperature: copper cavity IV.

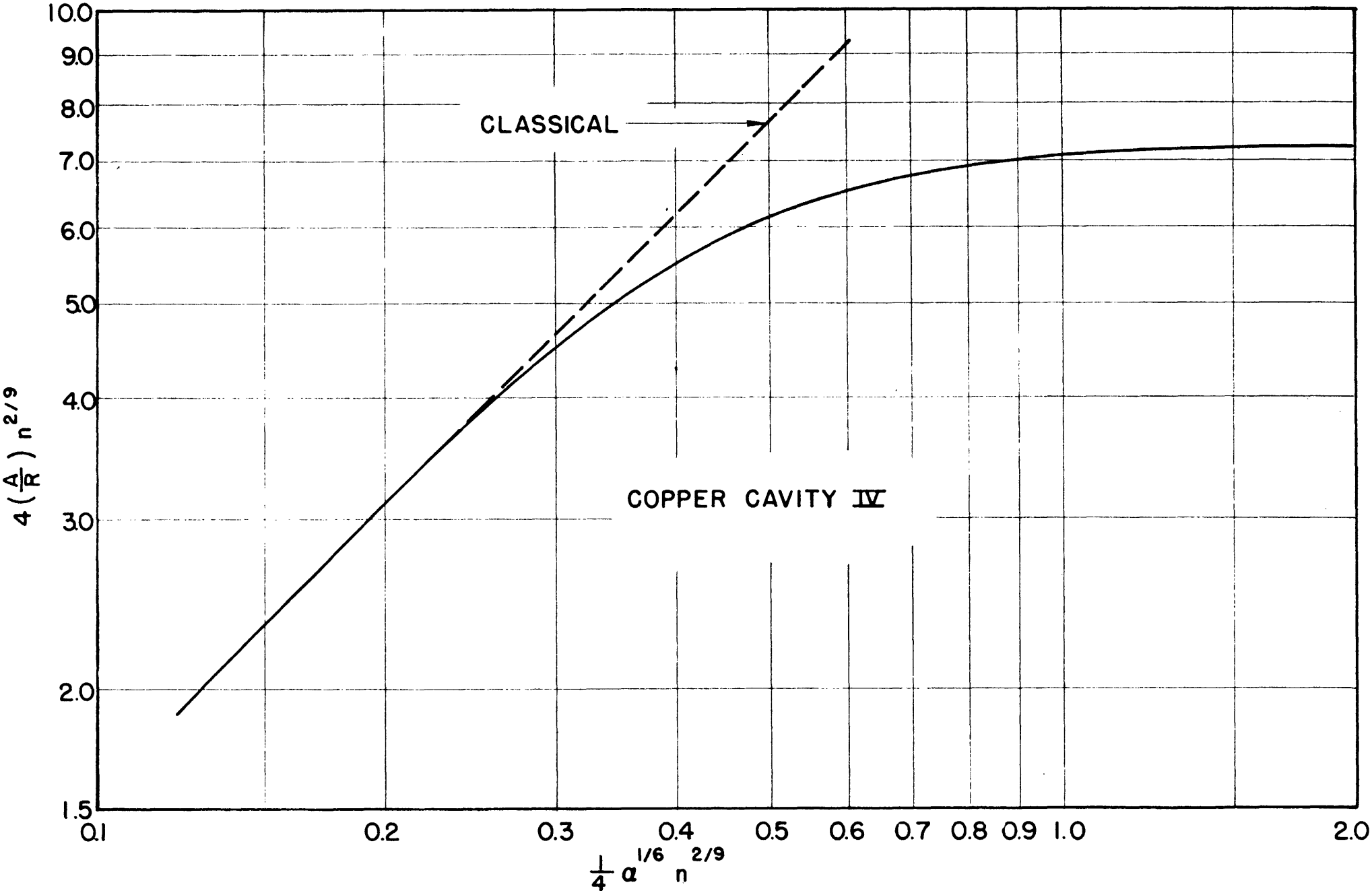

Fig 37. Reuter and Sondheimer plot for copper cavity IV; amended for extra lossy layer, but not "corrected" for surface roughness.

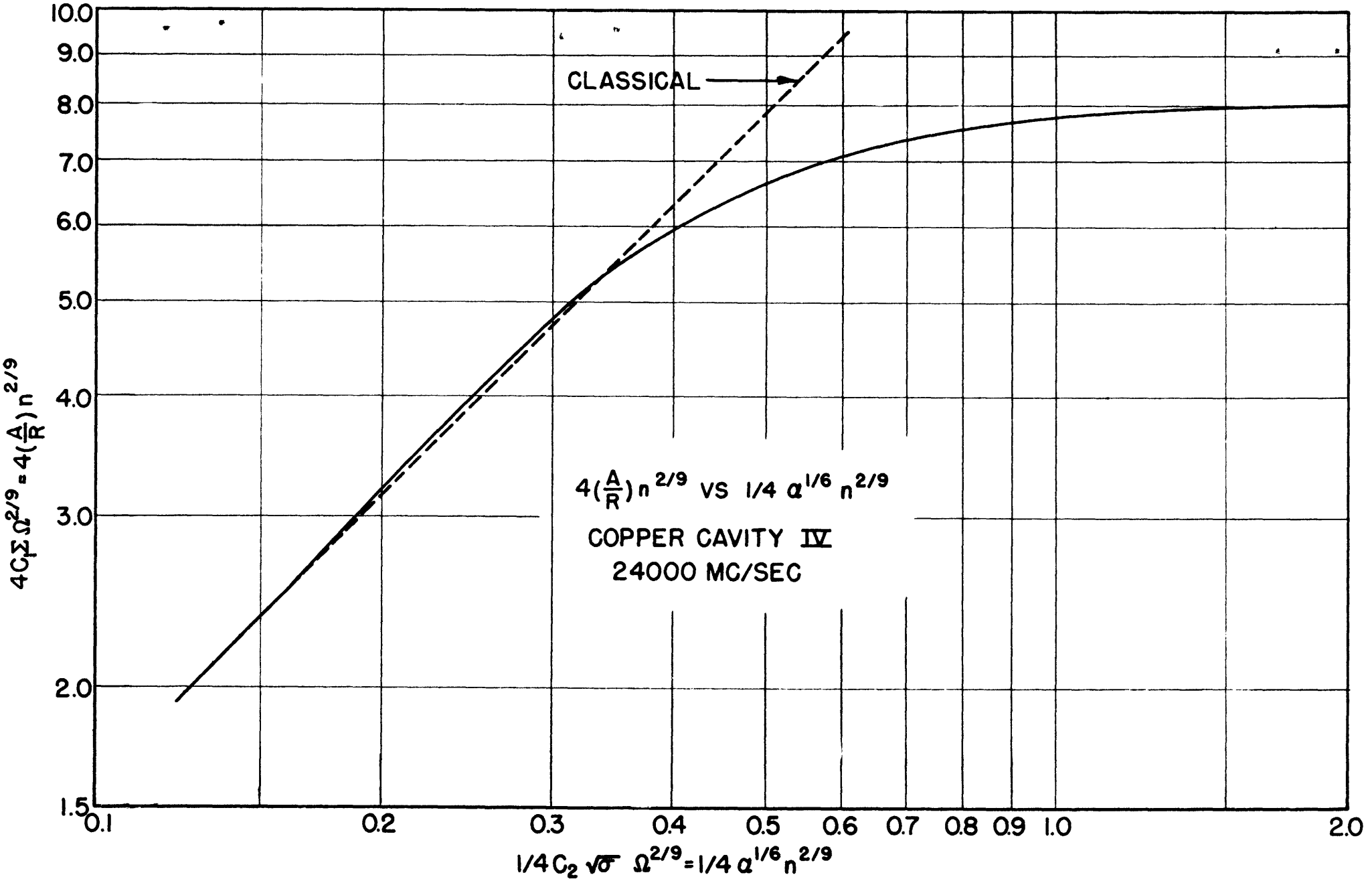

Fig 38. Fig. 37 "corrected" for surface roughness.

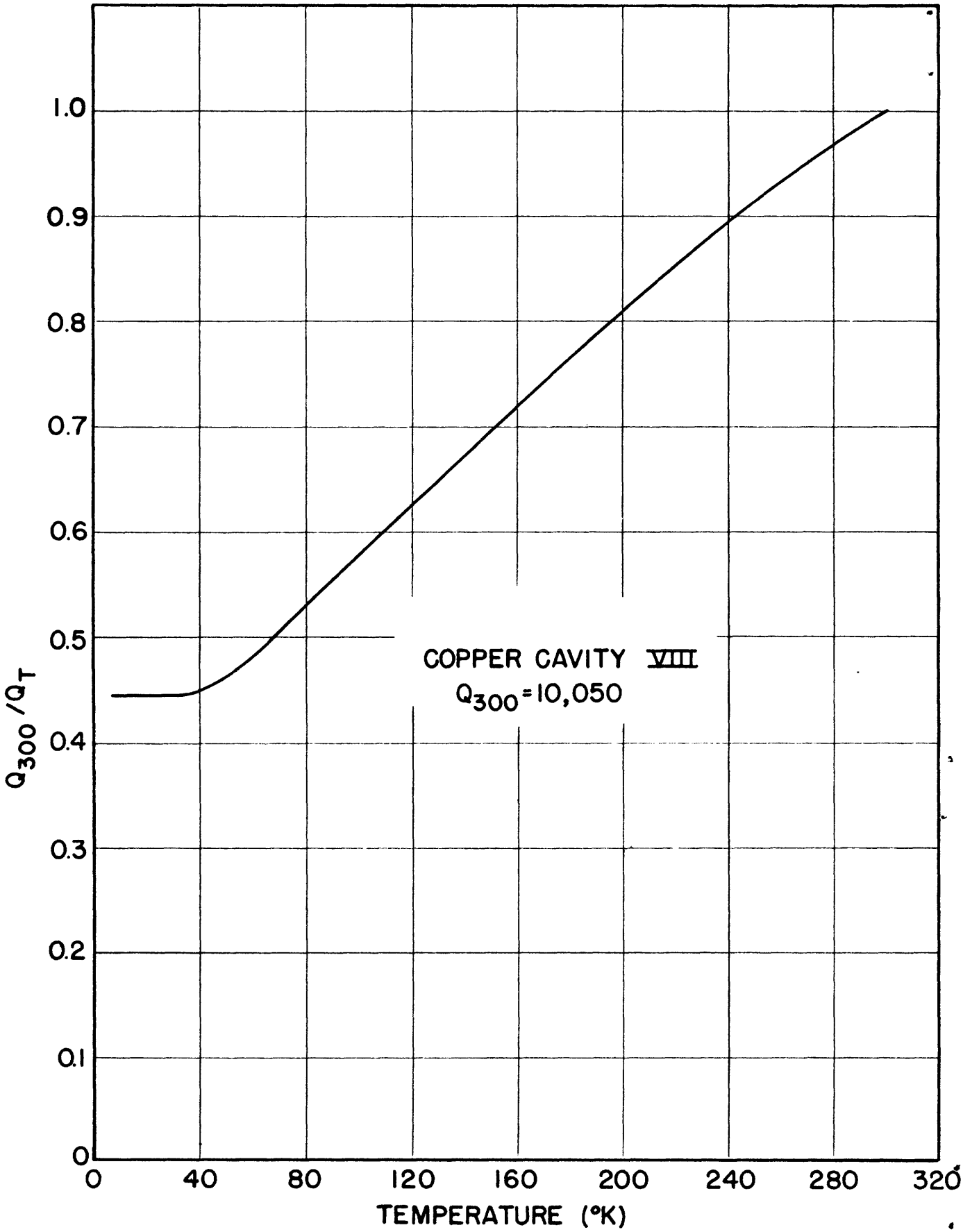

Fig 39. Relative Q_o vs temperature: cavity VIII; stressed copper lids.

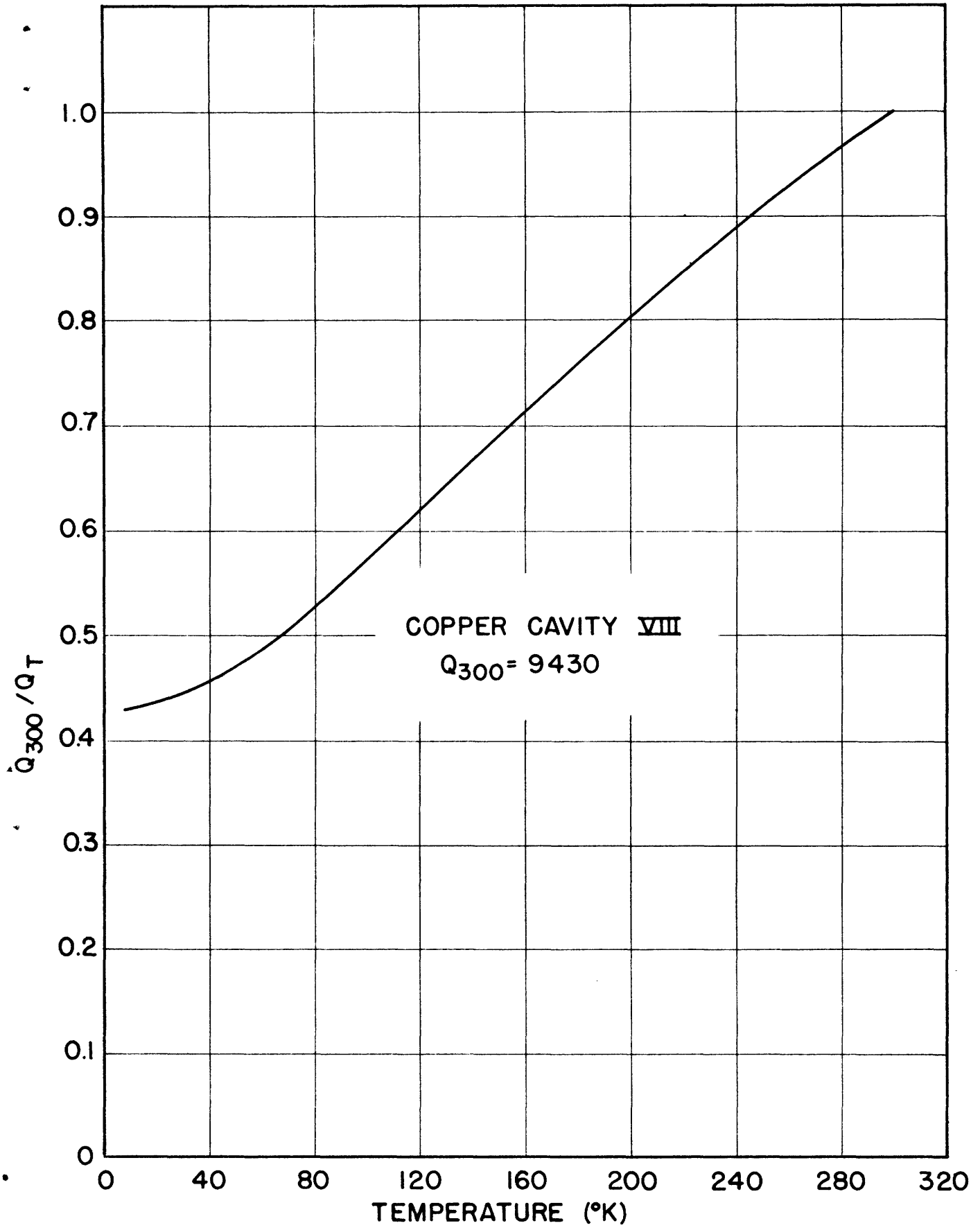

Fig 40. Relative Q_o vs temperature: cavity VIII and copper lids annealed 24 hours at 143°C in vacuo.

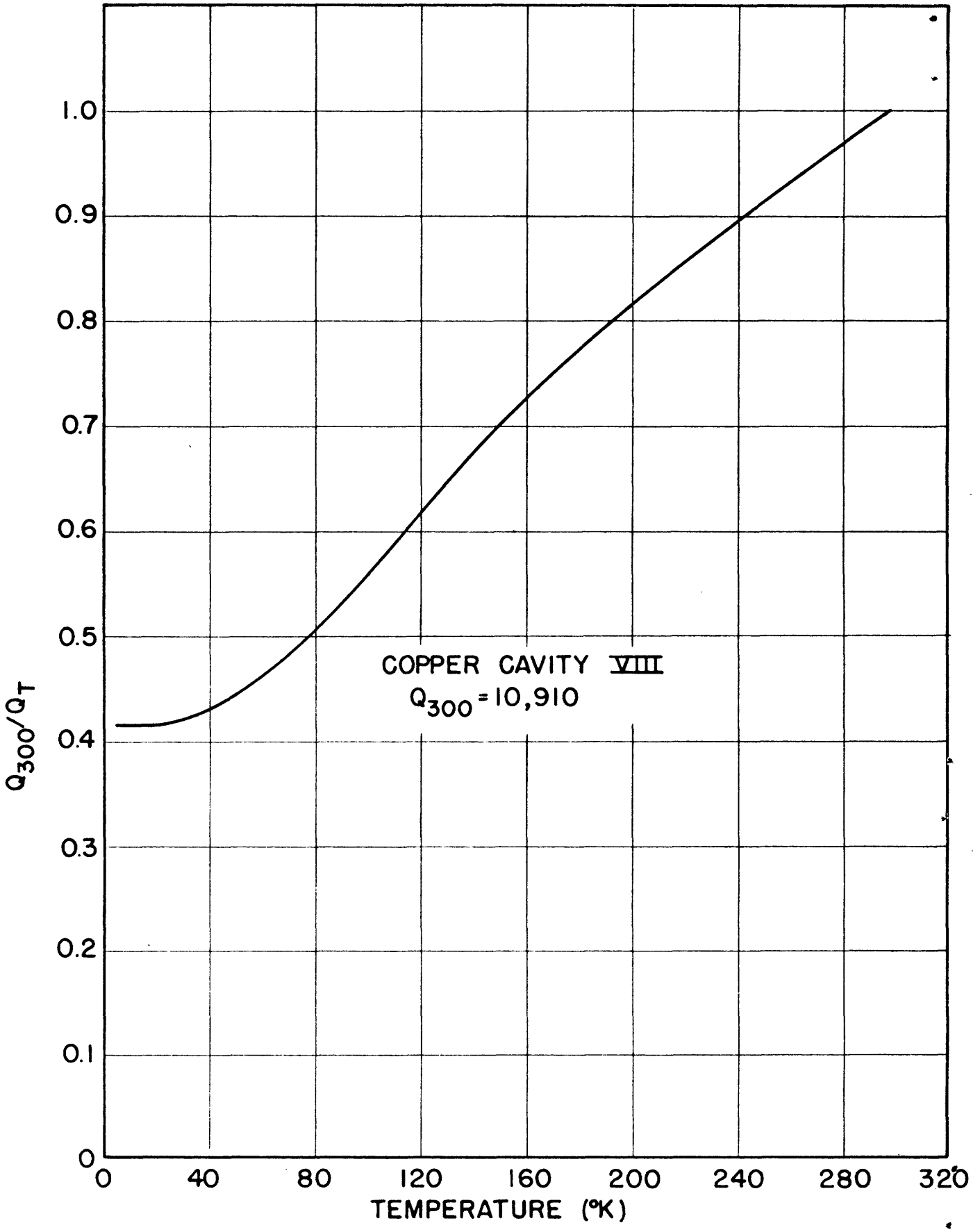

Fig 41. Relative Q_o vs temperature: cavity VIII; copper lids annealed 15 minutes at 900°C in H_2.

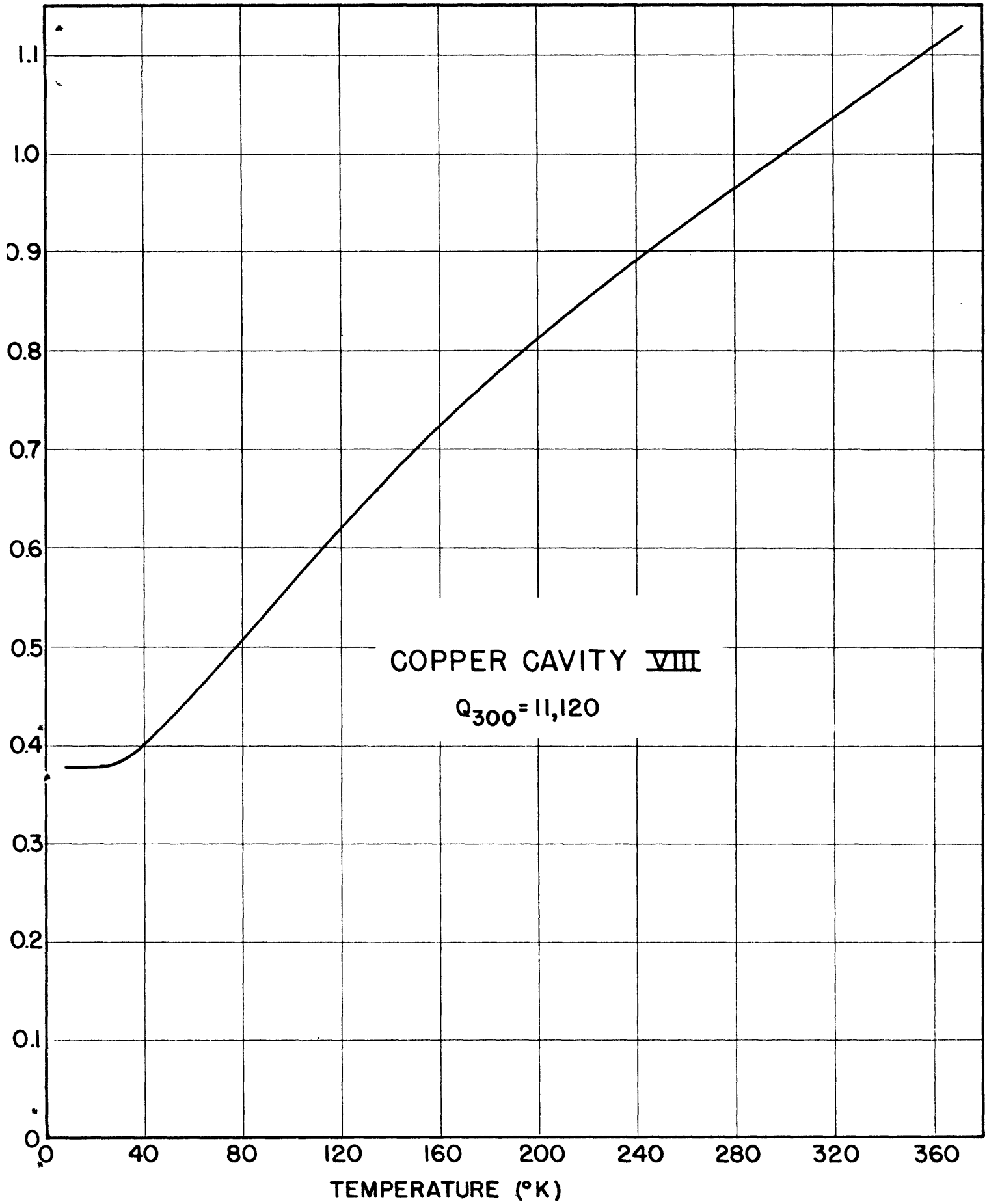

Fig 42. Relative Q_o vs temperature: cavity VIII; copper lids electropolished.

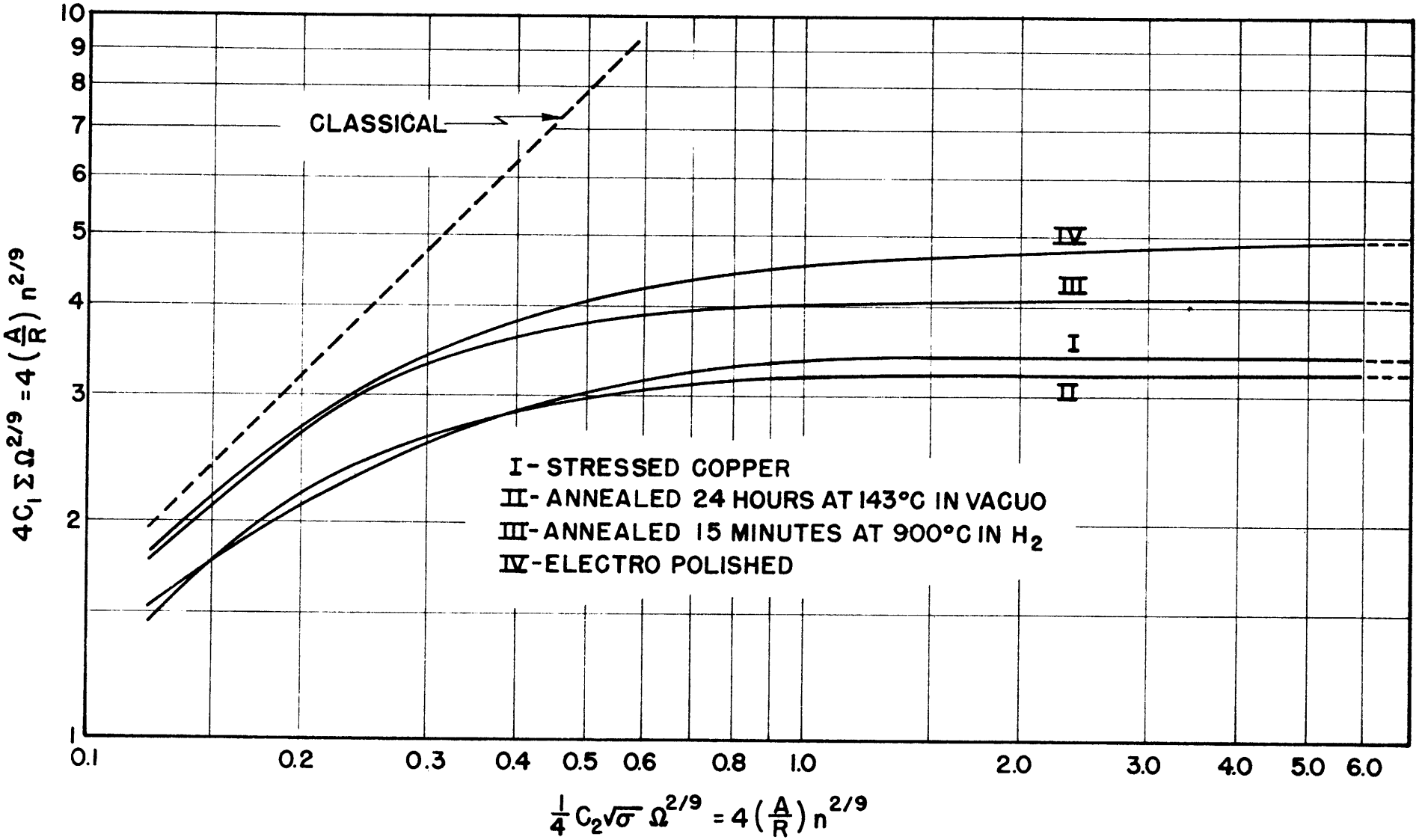

Fig 43. Reuter and Sondheimer plots for: I, stressed copper; II, same sample annealed 24 hours at 143°C in vacuo; III, same sample annealed 15 minutes at 900°C in H_2; IV, same sample electropolished.

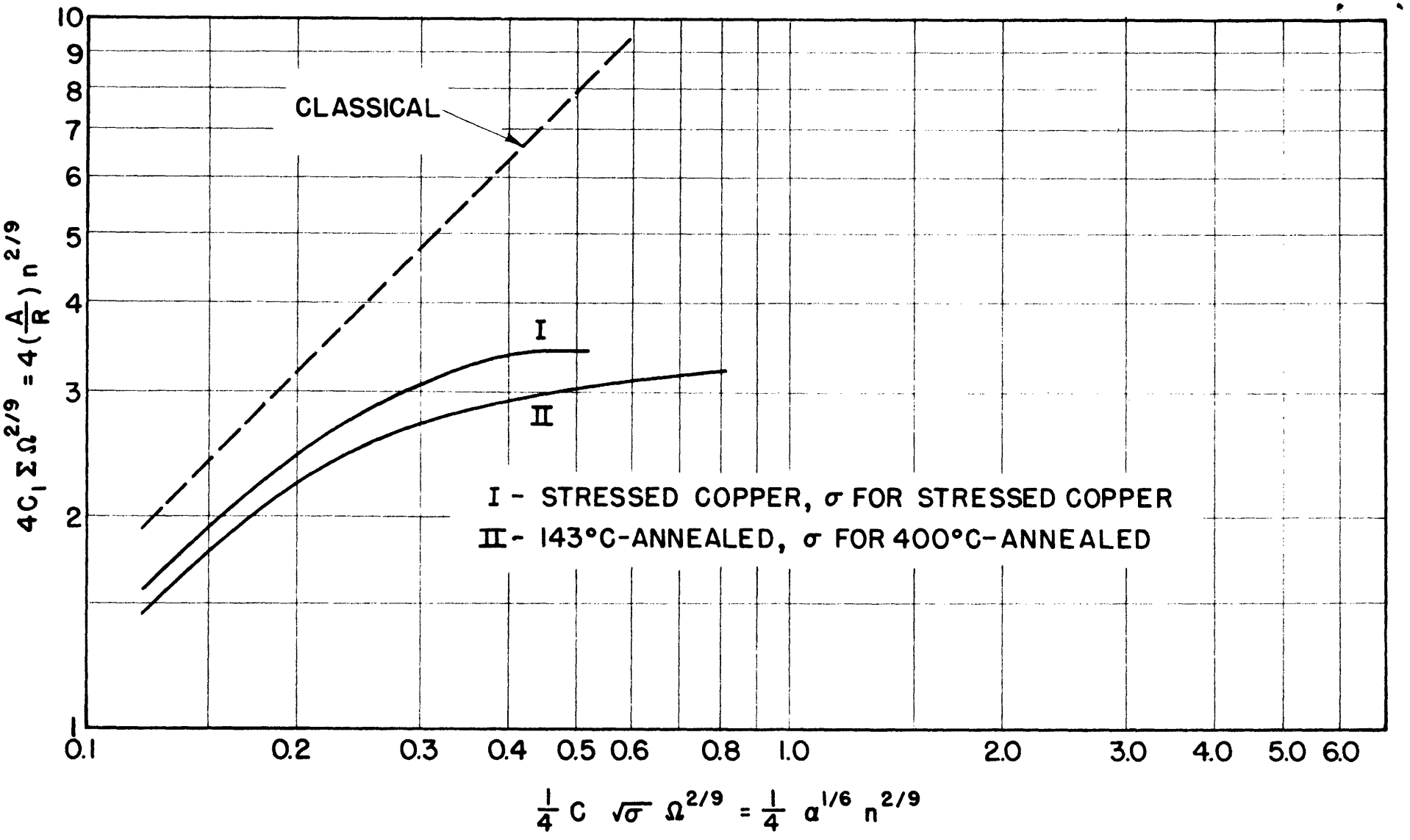

Fig 44. Reuter and Sondheimer plots for: I, stressed copper lids, using values of σ for stressed copper; II, 143°C-annealed copper lids, using values of σ for 400°C-annealed copper.

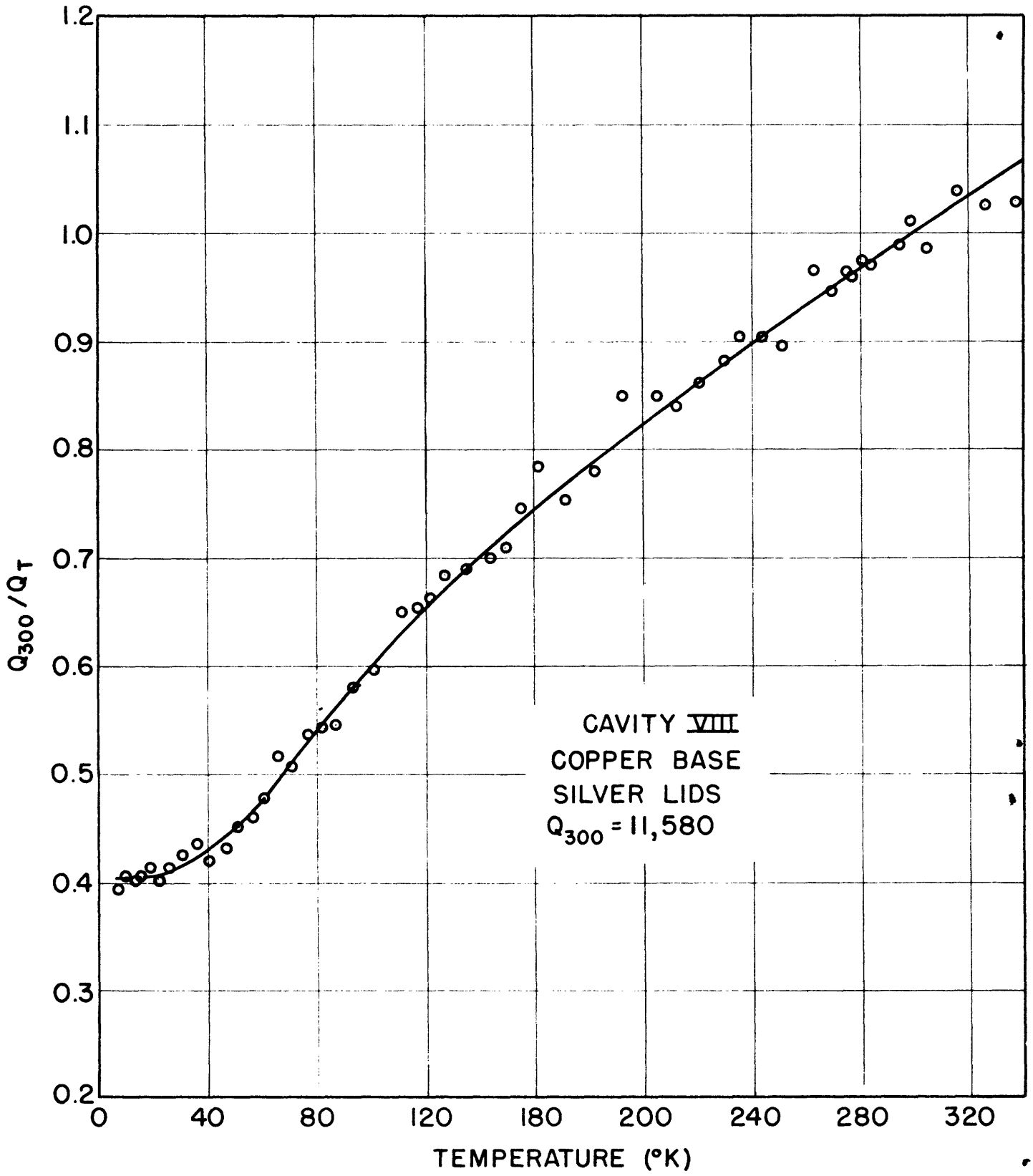

Fig 45. Relative Q_o vs temperature: cavity VIII; electropolished silver lids.

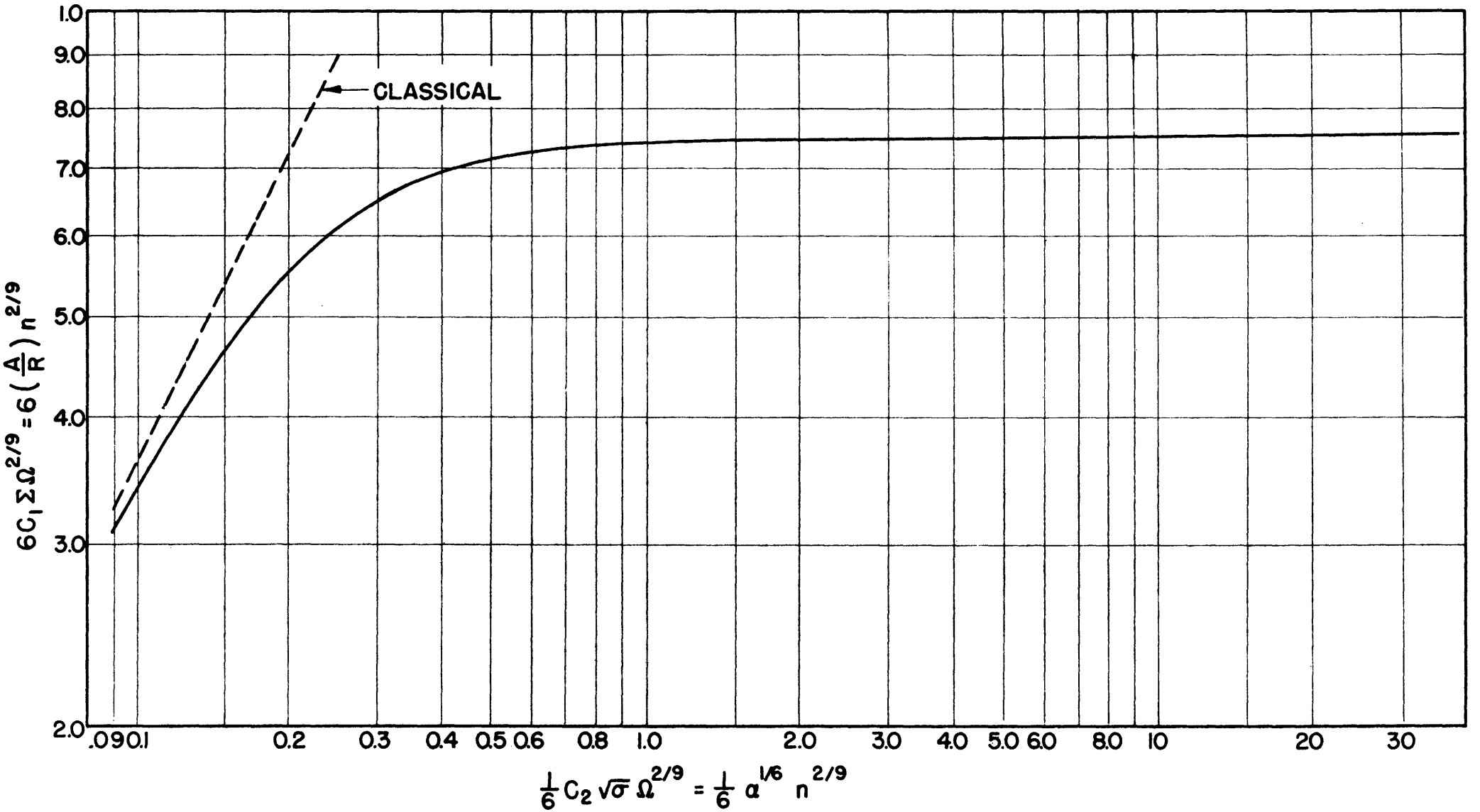

Fig 46. Reuter and Sondheimer plot for electropolished silver.

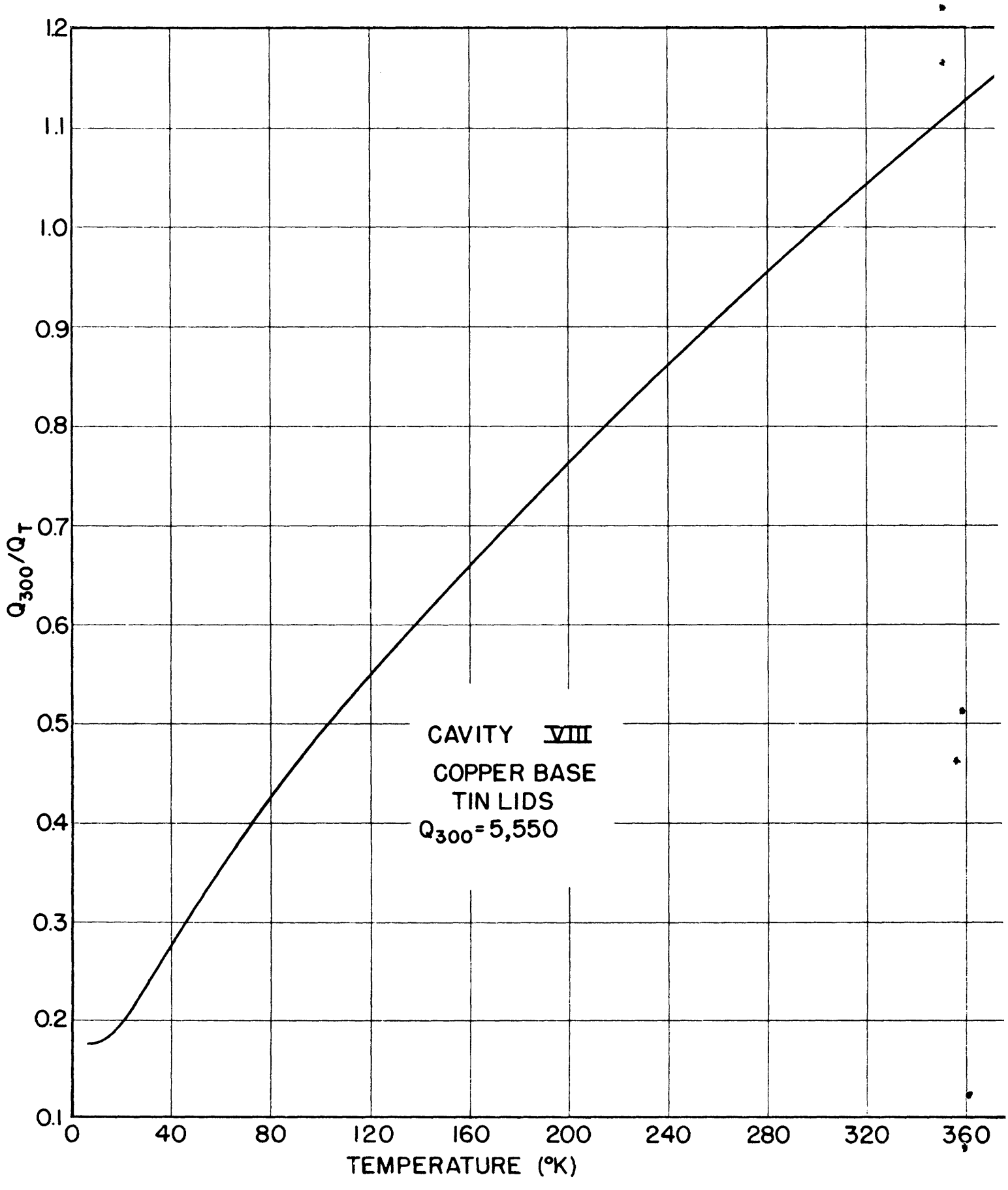

Fig 47. Relative Q_0 vs temperature: cavity VIII; cast tin lids.

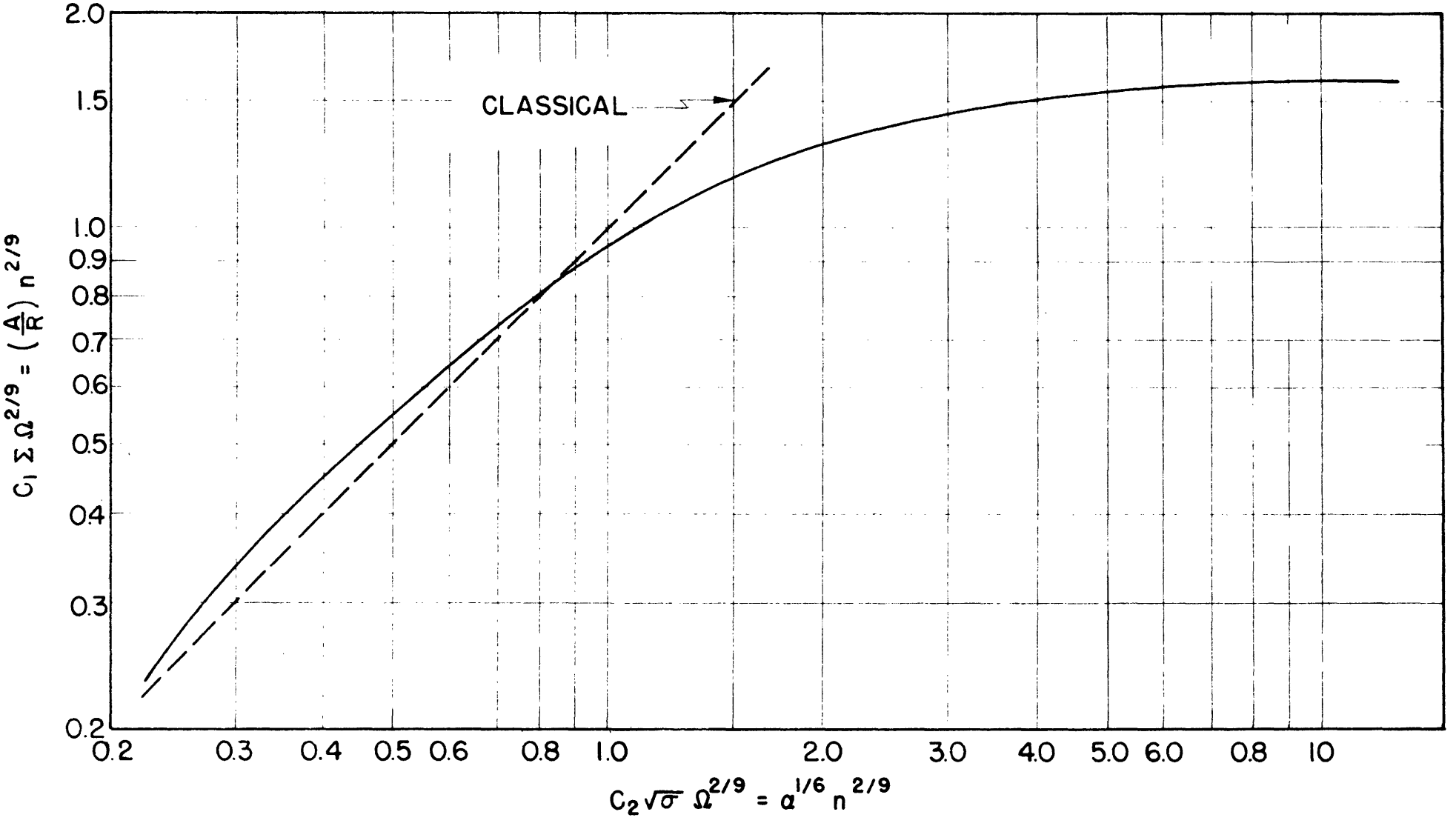

Fig 48. Reuter and Sondheimer plot for tin cast against glass.

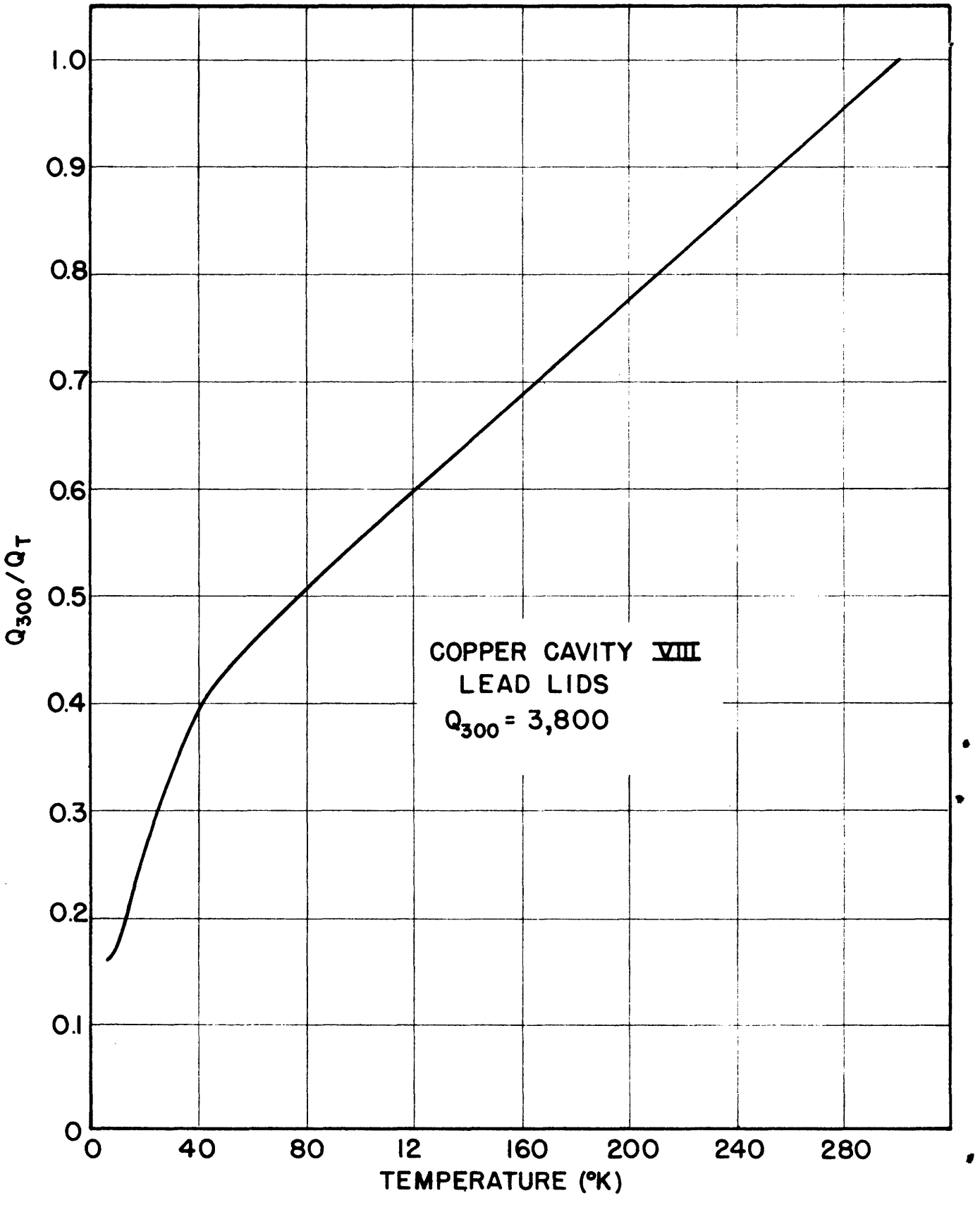

Fig 49. Relative Q_o vs temperature: cavity VIII; finely machined lead lids.

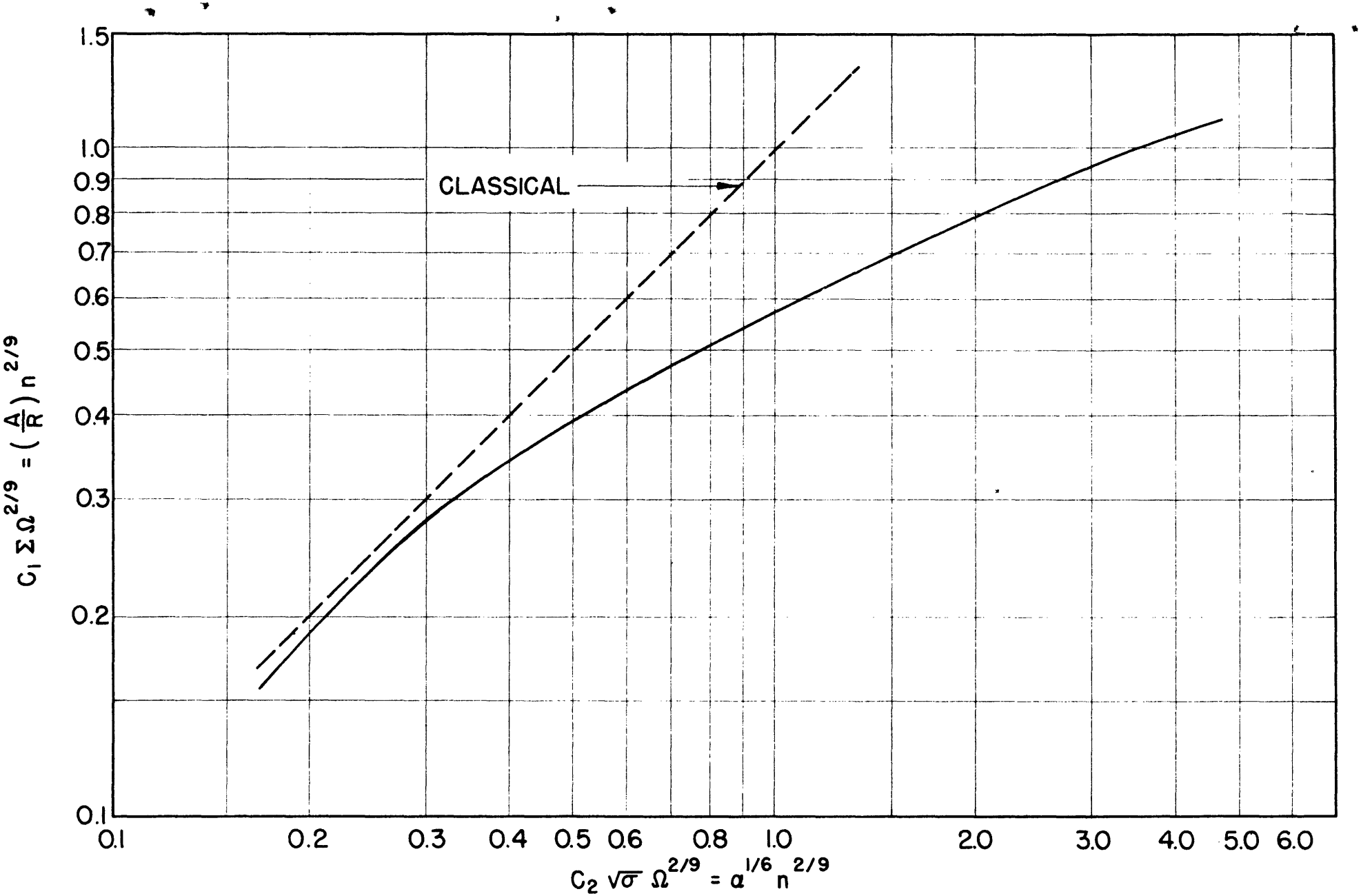

Fig 50. Reuter and Sondheimer plot for finely machined lead.

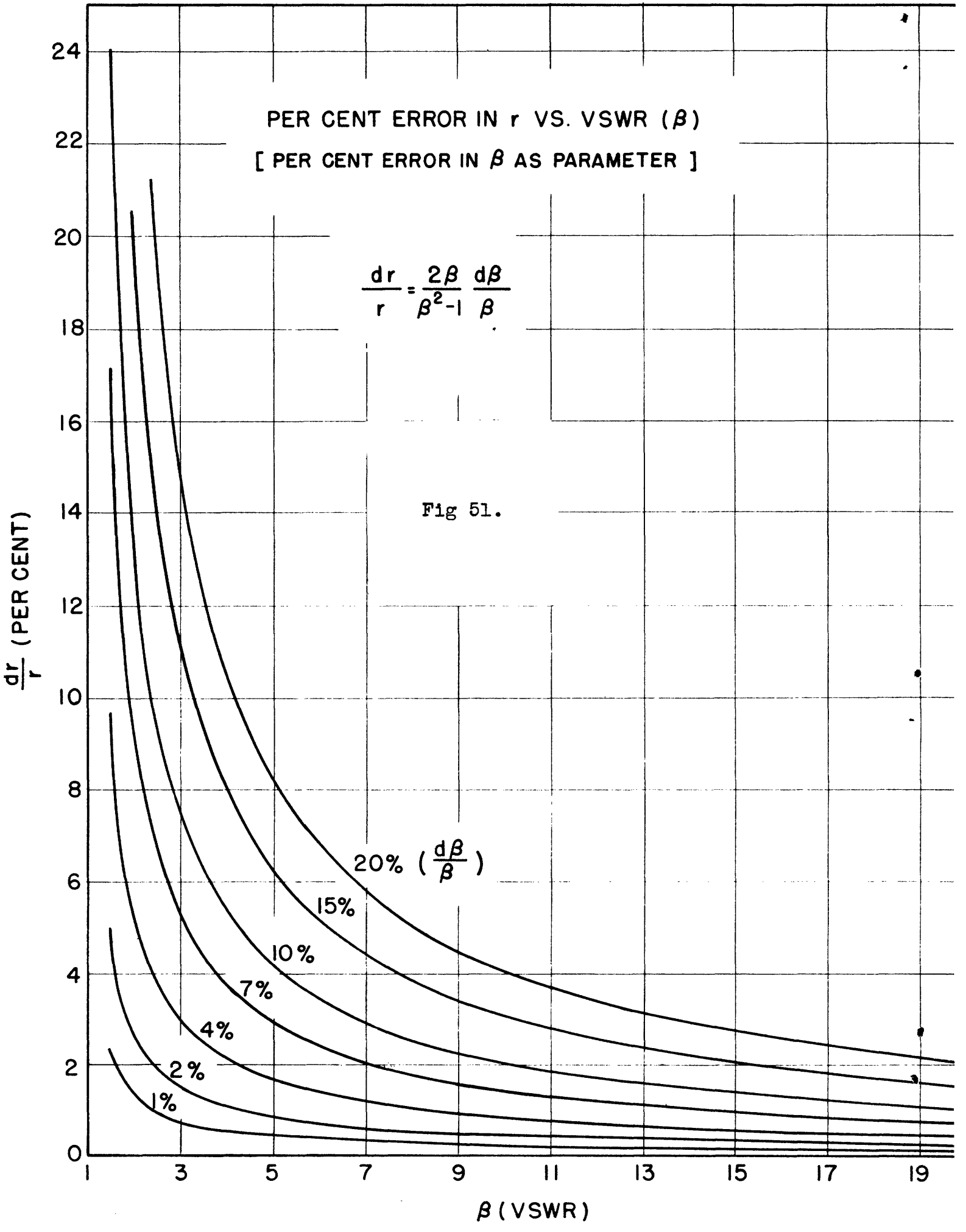
PER CENT ERROR IN r VS. VSWR (β)
[PER CENT ERROR IN β AS PARAMETER]
$\frac{dr}{r} = \frac{2\beta}{\beta^2-1}\frac{d\beta}{\beta}$
Fig 51.
$\frac{dr}{r}$ (PER CENT)
β (VSWR)
20% ($\frac{d\beta}{\beta}$)
15%
10%
7%
4%
2%
1%
0
2
4
6
8
10
12
14
16
18
20
22
24
1
3
5
7
9
11
13
15
17
19

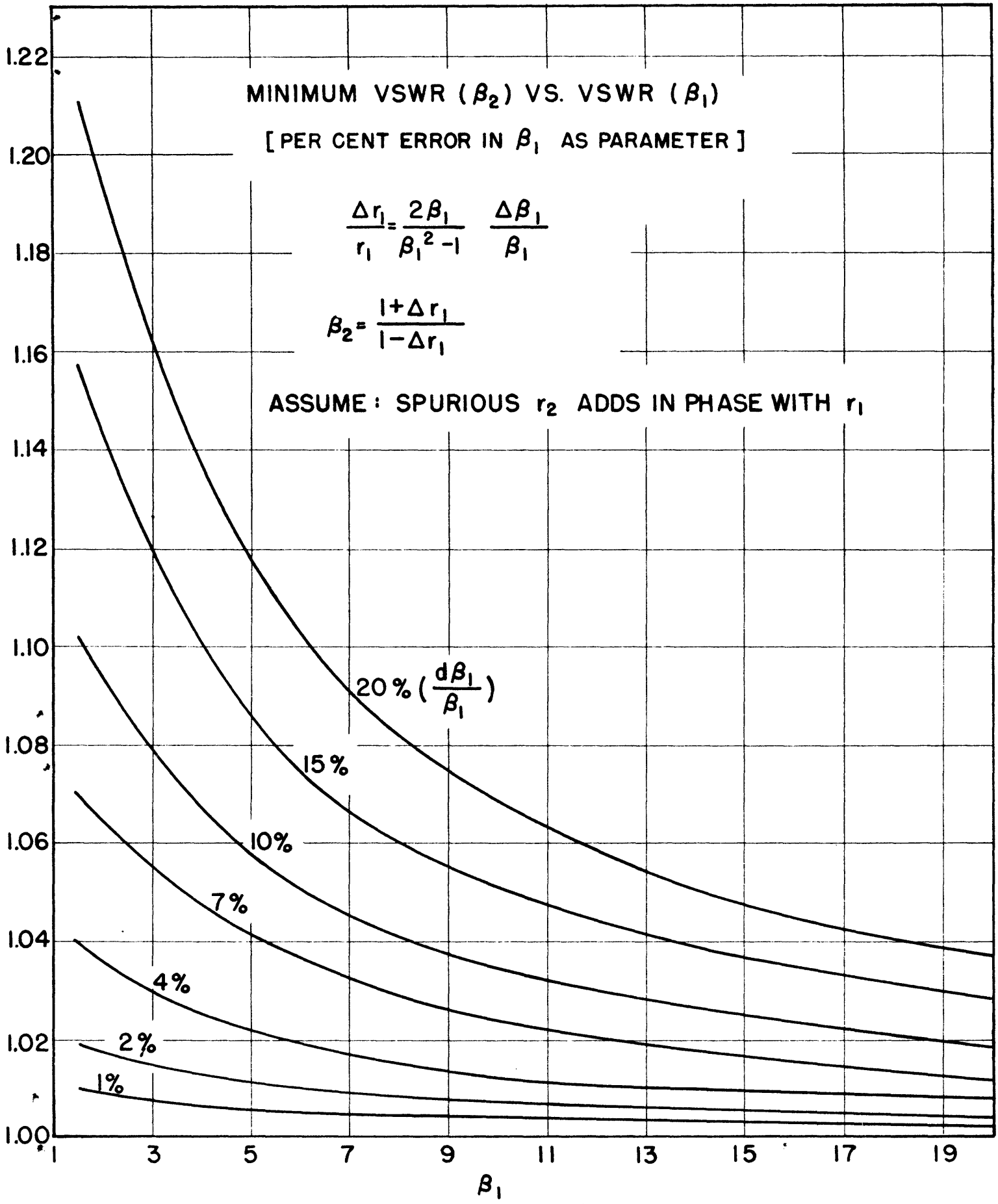
MINIMUM VSWR (β_2) VS. VSWR (β_1)
[PER CENT ERROR IN β_1 AS PARAMETER]
$\frac{\Delta r_1}{r_1} = \frac{2\beta_1}{\beta_1^2 - 1} \frac{\Delta \beta_1}{\beta_1}$
$\beta_2 = \frac{1+\Delta r_1}{1-\Delta r_1}$
ASSUME: SPURIOUS r_2 ADDS IN PHASE WITH r_1
20% ($\frac{d\beta_1}{\beta_1}$)
15%
10%
7%
4%
2%
1%
1.22
1.20
1.18
1.16
1.14
1.12
1.10
1.08
1.06
1.04
1.02
1.00
1
3
5
7
9
11
13
15
17
19
β_1

Fig 52.

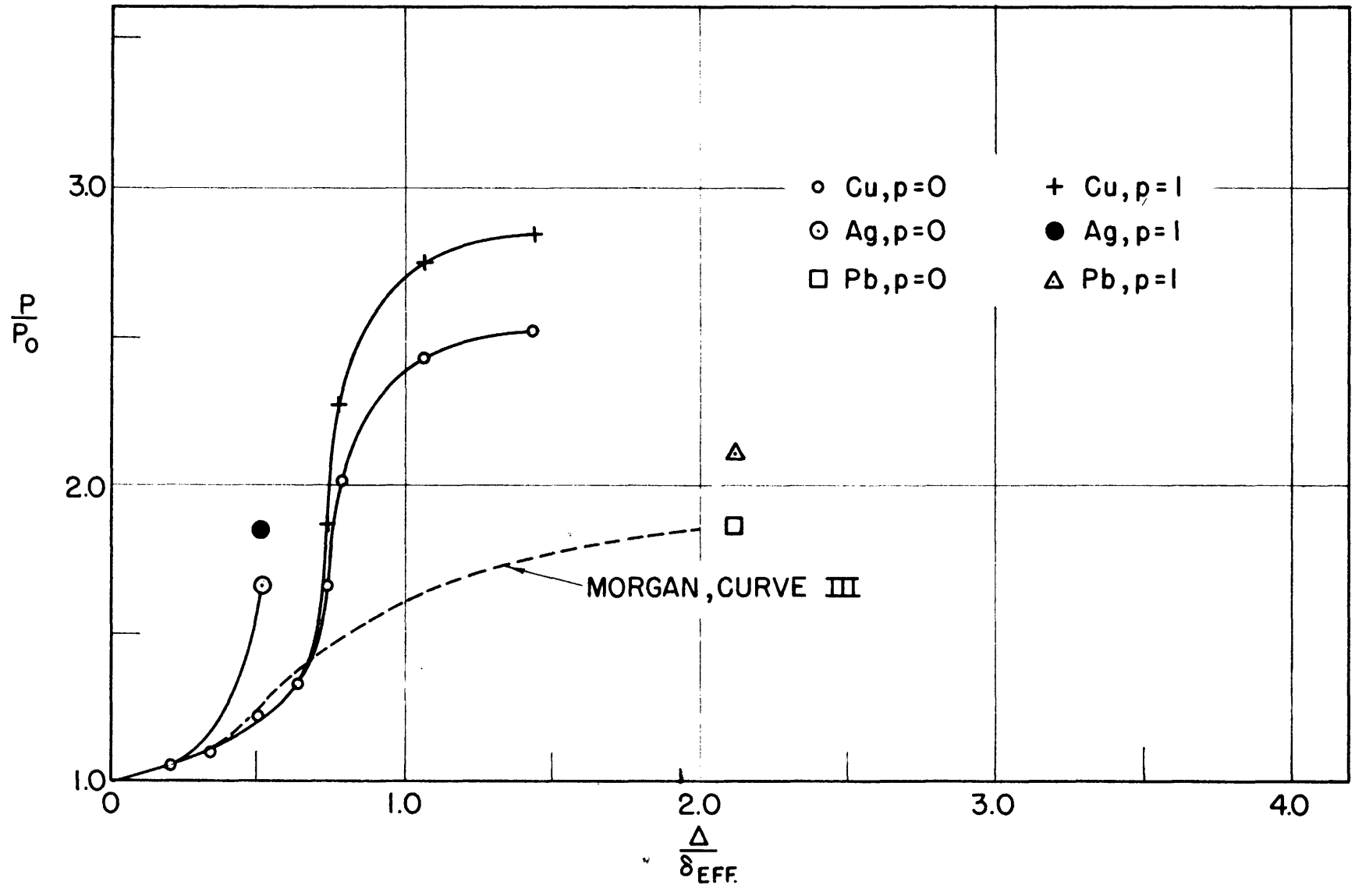

Fig 53. Relative power loss vs (rms roughness)/(effective skin depth). Computed from data, assuming n = 1.0 , and using the asymptotic Σ of Reuter and Sondheimer.

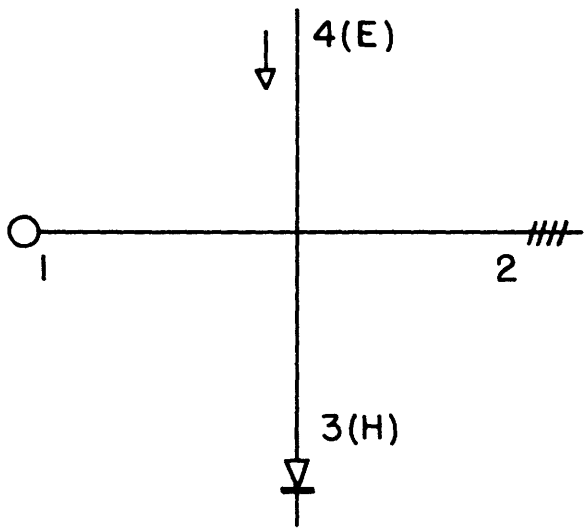

Fig 55. Schematic diagram of impedance bridge.

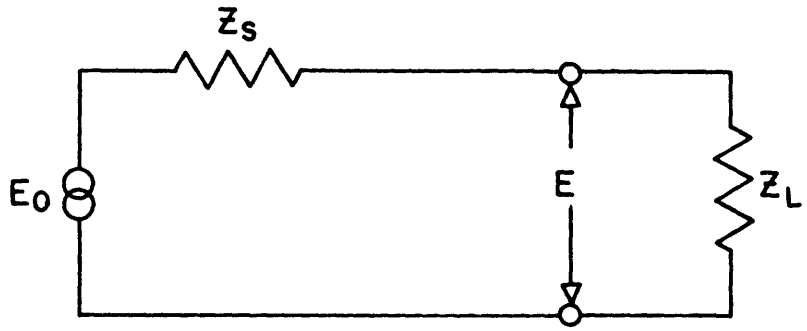

Fig 56. Equivalent circuit of generator and impedance bridge load.

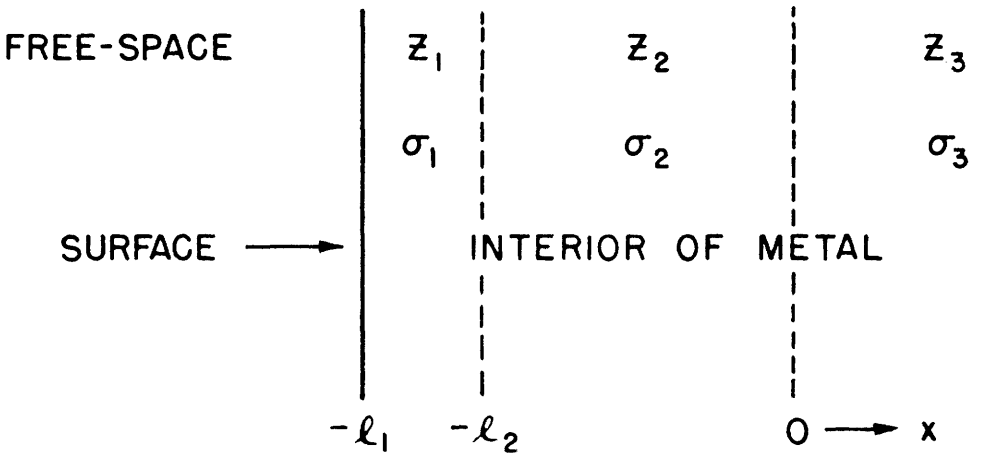

Fig 57. Schematic diagram of a metal showing resemblance to a transmission line.

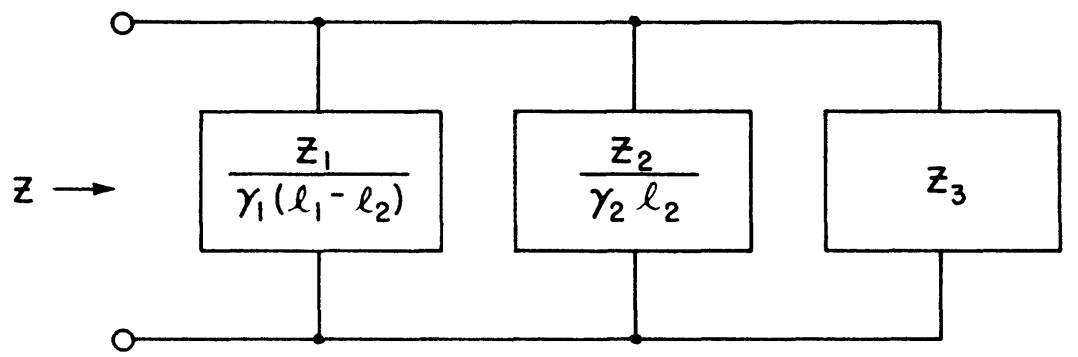

Fig 58. Transmission line equivalent of Fig. 57 .

ACKNOWLEDGMENTS

The author wishes to express his appreciation to Professor J. C. Slater for his guidance and interest in this work. Many thanks are due to Mr. R. J. Harrison, Dr. E. Maxwell, and Dr. I. Simon for clarifying and stimulating discussions, to Messrs. R. P. Cavileer and J. W. Toomey for very efficient helium cryostat operation, and to Mr. P. L. Nicholas for assistance with electronic equipment. Thanks are also due to Mr. E. C. Ingraham for his valuable suggestions and fine work in the construction of the cavities and in the vacuum sealing procedures. Mr. T. Eaton, of Arthur D. Little, Inc., is thanked for his courtesy in electropolishing the silver specimen.

BIBLIOGRAPHY

(1) Garrison, J. B., An Investigation of Superconductivity at a Wavelength of 1.25 Cm., Ph.D. Thesis, M.I.T., 1947.

(2) Maxwell, E., The Surface Impedance of Tin at 24,000 Mc/sec in the Superconducting and Normal States, Ph.D. Thesis, M.I.T., 1948.

(3) London, H., Proc. Roy. Soc. A, 176, 522 (1940).

(4) Pippard, A. B., Proc. Roy. Soc. A, 191, 370 (1947).

(5) Reuter, G. E. H. and Sondheimer, E. H., Proc. Roy. Soc. A, 195, 336 (1948).

(6) Maxwell, E., Jour. App. Phys., 18, 629 (1947).

(7) Morgan, S. P., Jr., Jour. App. Phys., 20, 352 (1949).

(8) Stratton, J. A., Electromagnetic Theory, McGraw-Hill Book Co., New York, 1941.

(9) Hagen, E. and Rubens, H., Ann. Physik, 14, 936 (1904).

(10) Mott, N. F. and Jones, H., The Theory of the Properties of Metals and Alloys, Oxford University Press, 1936.

(11) Slater, J. C., Rev. Mod. Phys., 18, 441 (1946).

(12) Lees, C. S., Trans. Farad. Soc., 31, 1102 (1935).

(13) Collins, S. C., R.S.I., 18, 157 (1947)

(14) Kintzer, J. P., Bell Sys. Tech. Jour., July, 1947.

(15) Slater, J. C., M.I.T. Research Laboratory of Electronics Technical Report No. 37.

(16) Montgomery, C. G., Techniques of Microwave Measurements, McGraw-Hill Book Co., New York, 1948.

(17) Handbk d. Exp. Phys. 11/2, 50 (1935).

(18) Simon, I., M.I.T. Research Laboratory of Electronics Laboratory Report, January 15, 1949.

(19) Morgan, S. P., Jr., Private Communication.